FINAL REPORT

Evaluation of Target Picking Methods for Magnetic Data

ESTCP Project MM-0502

March 2008

Tom Furuya,
SAIC

Environmental Security Technology Certification Program

Distribution Statement A: Approved for Public Release, Distribution is Unlimited

Table of Contents

Table of Contents i
List of Figures iii
List of Tables vii
List of Acronyms viii
Acknowledgements viii
1. Introduction 1
1.1 Background 1
1.2 Objectives of the Demonstration 2
1.3 Regulatory Drivers 2
1.4 Stakeholder/End-User Issues 3
2. Technology Description 4
2.1 Technology Developments and Application 4
2.2 Previous Testing of the Technology 6
2.2.1 Wavelet-based Algorithm 7
2.2.1.1 Segmentation Algorithm 8
2.2.1.2 Integration with Oasis Montaj™ 9
2.2.1.3 Synthetic Magnetic Data Test 11
2.2.2 Rule-based Clusters 12
2.2.3 Dipole based Matched Filter 14
2.2.4 Analytic Signal 16
2.3 Factors Affecting Cost and Performance 18
2.4 Advantages and Limitations of the Technology 19
3. Demonstration Design 20
3.1 Performance Objectives 20
3.2 Selecting Test Sites 22
3.3 Test Site History/Characteristics 33
3.4 Present Operations 34
3.5 Pre-Demonstration Testing and Analysis 34
3.6 Testing and Evaluation Plan 35
3.6.1 Demonstration Set-up and Start-up 35
3.6.2 Period of Operation 35
3.6.3 Area Characterized or Remediated 35
3.6.4 Residuals Handling 36
3.6.5 Operational Parameters 36
3.6.6 Demobilization 37
3.7 Selection of Analytical/Testing Methods 38
3.8 Selection of Analytical/Testing Laboratory 38
4. Performance Assessment 39
4.1 Performance Criteria 39
4.2 Performance Confirmation Methods 40
4.3 Data Analysis, Interpretation, and Evaluation 41

4.3.1 Phase 1 – Synthetic Magnetic data 41
4.3.1.1 Automated Wavelet Detection algorithm 42
4.3.1.2 Clustering algorithm 44
4.3.1.3 Analytic signal 46
4.3.1.4 Matched Filter Algorithm 47
4.3.2 Phase 2 – Live Site data 49
4.3.2.1 USACE GPO 52
4.3.2.2 Pueblo of Isleta, NM 59
4.3.2.3 Seaside, CA 66
4.3.2.4 Jefferson Proving Ground, IN 73
4.3.2.5 Aberdeen Proving Ground, MD 81
4.3.2.6 WAA Airborne survey – Pueblo Precision Bombing Range #2, CO 89
4.3.2.7 WAA Transect survey – Pueblo Precision Bombing Range #2, CO 98
4.3.3 Target Picking Time 102
4.3.4 Qualitative Metrics 103
4.3.5 Discussion 104
5. Cost Assessment 106
5.1 Cost Reporting 106
5.2 Cost Analysis 106
6. Implementation Issues 108
6.1 Environmental Checklist 108
6.2 Other Regulatory Issues 108
6.3 End-User Issues 108
7. References 109
8. Points of Contact 110
ESTCP 110
SAIC 110
Sky Research 110

List of Figures

Figure 1. Synthetic magnetic data set with 60 targets. 7
Figure 2. Segmentation algorithm applied to a large HeliMag dataset. The solid blue lines delineate the boundaries between adjacent sub-regions. The dashed lines delineate the buffer regions. 8
Figure 3. Schematic of the SkyNet architecture. 9
Figure 4. Screen-capture of the AWD algorithm being used directly from within Oasis montaj™. 11
Figure 5. Results of AWD algorithm on the synthetic magnetic data. The 60 true locations are marked as white circles and the wavelet picks as black crosses. 12
Figure 6. Results of clustering algorithm on the synthetic magnetic data. The true locations are plotted as circles and the automatic picker detections are plotted as "+". 14
Figure 7. Color contour map of the match filter output calculated from the synthetic magnetic data. The true locations are plotted as circles and the automatic picker detections are plotted as "+". 15
Figure 8. Color contour map of the analytic signal grid calculated from the synthetic magnetic data. The calculated footprint of selected anomalies using the polygon (red) and circle (black) options are shown. 17
Figure 9. Color contour map of the analytic signal grid calculated from the synthetic magnetic data. The true locations are plotted as circles and the automatic picker detections are plotted as "+". 18
Figure 10. NRL MTADS magnetic data collected at APG Open field. The red box outlines the area evaluated by the target pickers. The crosses show publicly released ground truth. 26
Figure 11. USACE magnetic data collected at Jefferson Proving Ground. The crosses show known ground truth. 27
Figure 12. USACE-supplied magnetic data over GPO. The crosses show known ground truth. . 28
Figure 13. Airborne magnetic data from near BT4 at the Pueblo Precision Bombing Range in Colorado. 29
Figure 14. Vehicular magnetic data from Isleta South. The crosses show known ground truth. . 30
Figure 15. Magnetic data from Seaside. The crosses show known ground truth. 31
Figure 16. This map shows the location of the vehicle based magnetic transect data near BT4 at the Pueblo Precision Bombing Range in Colorado. The red lines show the transects included in this demonstration. 32
Figure 17. Parameter dialog box for AWD algorithm 36
Figure 18. Parameter dialog boxes for clustering algorithm. 37
Figure 19. Receiver Operating Characteristic (ROC) curve of the different target pickers for the synthetic 60 dipole data. The symbols along each line represent the analyst's threshold value. 42
Figure 20. Results of AWD algorithm on the synthetic magnetic data. The true locations are plotted as circles and the automatic picker detections are plotted as "+" 44
Figure 21. Results of clustering algorithm on the synthetic magnetic data. The true locations are plotted as circles and the automatic picker detections are plotted as "+". 46

Figure 22..ROC curve of the analytic signal algorithm applied to the 60 dipole synthetic data set using different number of 3x3 Hanning filters. 47
Figure 23. Results of matched filter algorithm on the synthetic magnetic data. The color coded map shows the ratio (Matched filter output/Chi square). The true locations are plotted as circles and the automatic picker detections are plotted as "+" 49
Figure 24. Graph showing the number of ground truth objects detected by each method as a function of signal amplitude; USACE GPO. 53
Figure 25. Color-coded map showing the analytic signal data overlain by the ground truth, manual picks and anomalies identified by the analytic signal method; USACE GPO..... 54
Figure 26. Color-coded map showing the total field magnetic data overlain by the ground truth, manual picks and anomalies identified by the clustering method; USACE GPO. 55
Figure 27. Color-coded map showing the (Matched filter output / Chi square) data overlain by the ground truth, manual picks and anomalies identified by the matched filter method; USACE GPO. 56
Figure 28. Color-coded map showing the total field magnetic data overlain by the ground truth, manual picks and anomalies identified by the AWD method; USACE GPO. 57
Figure 29. Color-coded map showing the total field magnetic data overlain by the ground truth and anomalies identified manually; USACE GPO. 58
Figure 30. Graph showing the number of ground truth objects detected by each method as a function of signal amplitude; Isleta..... 60
Figure 31. Color-coded map showing the analytic signal data overlain by the ground truth, manual picks and anomalies identified by the analytic signal method; Isleta. 61
Figure 32. Color-coded map showing the total field magnetic data overlain by the ground truth, manual picks and anomalies identified by the clustering method; Isleta..... 62
Figure 33. Color-coded map showing the (Matched filter output / Chi square) data overlain by the ground truth, manual picks and anomalies identified by the matched filter method; Isleta. 63
Figure 34. Color-coded map showing the total field magnetic data overlain by the ground truth, manual picks and anomalies identified by the AWD method; Isleta. 64
Figure 35. Color-coded map showing the total field magnetic data overlain by the ground truth and anomalies identified manually; Isleta..... 65
Figure 36. Graph showing the number of ground truth objects detected by each method as a function of signal amplitude; Seaside. 67
Figure 37. Color-coded map showing the analytic signal data overlain by the ground truth, manual picks and anomalies identified by the analytic signal method; Seaside..... 68
Figure 38. Color-coded map showing the total field magnetic data overlain by the ground truth, manual picks and anomalies identified by the clustering method; Seaside. 69
Figure 39. Color-coded map showing the (Matched filter output / Chi square) data overlain by the ground truth, manual picks and anomalies identified by the matched filter method; Seaside. 70
Figure 40. Color-coded map showing the total field magnetic data overlain by the ground truth, manual picks and anomalies identified by the AWD method; Seaside. The larger circle in the center of the figure is an example of an object with questionable ground truth. 71

Figure 41. Color-coded map showing the total field magnetic data overlain by the ground truth and anomalies identified manually; Seaside. 72
Figure 42. Graph showing the number of ground truth objects detected by each method as a function of signal amplitude; JPG. 74
Figure 43. Color-coded map showing the analytic signal data overlain by the ground truth, manual picks and anomalies identified by the analytic signal method; JPG. 75
Figure 44. Color-coded map showing the total field magnetic data overlain by the ground truth, manual picks and anomalies identified by the clustering method; JPG. 76
Figure 45. Color-coded map showing the (Matched filter output / Chi square) data overlain by the ground truth, manual picks and anomalies identified by the matched filter method; JPG. 77
Figure 46. Color-coded map showing the total field magnetic data overlain by the ground truth, manual picks and anomalies identified by the AWD method; JPG. 78
Figure 47. Color-coded map showing the total field magnetic data overlain by the ground truth and anomalies identified manually; JPG. 79
Figure 48. Total field magnetic data over a portion of the eastern edge of the JPG survey area. The X's show the multiple wavelet picks caused by positioning problems. The color scale is the same as in Figure 46. 80
Figure 49. Receiver operating curve showing the number of ground truth objects detected by each method versus Background alarm rate; APG. 82
Figure 50. Graph showing the average miss for Easting and Northing (in meters). The range bars are symmetrical standard deviations. 83
Figure 51. Comparison of the location accuracy of the positions output directly from the different picking methods (left) and the locations output after passing the selected data to the magnetic fitting algorithm in UX-Analyze (right). 84
Figure 52. Depth fit accuracy of the different picking methods. Data extracted from each picking method were passed to a magnetic inversion algorithm to estimate the target's depth. 84
Figure 53. Color-coded map showing the analytic signal data overlain by the manual picks and anomalies identified by the analytic signal method; APG. 85
Figure 54. Color-coded map showing the total field magnetic data overlain by the manual picks and anomalies identified by the clustering method; APG. 86
Figure 55. Color-coded map showing the (Matched filter output / Chi square) data overlain by the manual picks and anomalies identified by the matched filter method; APG. 87
Figure 56. Color-coded map showing the total field magnetic data overlain by the manual picks and anomalies identified by the AWD method; APG. 88
Figure 57. Graph showing Pd versus the number of false alarms (automatic picks not matching a manual picks); Pueblo airborne. 90
Figure 58. Graph showing the number of manual picks detected by each method as a function of signal amplitude; Pueblo airborne. 91
Figure 59. Color-coded map showing the analytic signal data overlain by the manual picks and anomalies identified by the analytic signal method; Pueblo airborne. 92
Figure 60. Color-coded map showing the total field magnetic data overlain by the manual picks and anomalies identified by the clustering method; Pueblo airborne. 93

Figure 61. Color-coded map showing the (Matched filter output / Chi square) data overlain by the manual picks and anomalies identified by the matched filter method; Pueblo airborne. 94
Figure 62. Color-coded map showing the total field magnetic data overlain by the manual picks and anomalies identified by the AWD method; Pueblo airborne. 95
Figure 63. Color coded map of the total field magnetic showing the noise at various locations. The noise was estimated by calculating the standard deviation of the data contained within each box. 96
Figure 64. Color coded map of the total field magnetic data showing the numerous picks due to geology by the different target pickers in the northern portion of the Pueblo airborne survey area 97
Figure 65. Color coded map of the total field magnetic data showing some targets missed by the manual picker but detected by all the automatic methods. 97
Figure 66. Graph showing the number of ground truth objects detected by each method as a function of signal amplitude; Pueblo transects. 99
Figure 67. Graph showing the number of ground truth objects detected by each method as a function of signal amplitude; Pueblo transects. 99
Figure 68. Color-coded map showing the total field magnetic data overlain by the manual picks and anomalies identified by the clustering method; Pueblo transects. 100
Figure 69. Section of transect magnetic data showing some low amplitude declaration by the different picking methods. The analytic signal, clustering, wavelet and manual picks are plotted as black plus sign, red box, black cross and black circle, respectively. 101
Figure 70. Graph showing the total time to analyze the data sets for the different target picking methods 102
Figure 71. Graph showing the processing time to analyze the data sets for each of the target picking methods 103

List of Tables

Table 1. Performance Objectives for production surveys 21
Table 2. Performance Objectives for WAA surveys 22
Table 3. Criteria and Data sets 25
Table 4. Target Picking Demonstration Schedule 35
Table 5. Performance Criteria for this Demonstration 39
Table 6. Best Parameter Set for AWD Algorithm for All Surveys. 51
Table 7. Best Parameter Set for Clustering Algorithm for All Surveys. 51
Table 8. Best Parameter Set for Matched Filter Algorithm for All Surveys. 52
Table 9. Best Parameter Set for Analytic Signal Method for All Surveys. 52
Table 10. USACE GPO - Detection and location accuracy 53
Table 11. Isleta - Detection and location accuracy 59
Table 12. Seaside - Detection and location accuracy 66
Table 13. Seaside - Weight of targets missed 67
Table 14. JPG - Detection and location accuracy 73
Table 15. APG - Detection and location accuracy 82
Table 16 APG - Location and size accuracy of the 80 targets selected for inversion. 83
Table 17. WAA Pueblo Airborne - Detection and location accuracy 90
Table 18. WAA Pueblo Transects - Detection and location accuracy 98
Table 19. Cost categories and details 106

List of Acronyms

ACRONYM	DEFINITION
APG	Aberdeen Proving Ground
AS	Analytic Signal
AWD	Automated Wavelet Detection
BBR	Badlands Bombing Range
BRAC	Base Realignment and Closure
Chisq	Chi Square Error
COE	Corps of Engineers
DLL	Dynamic Link Library
Dod	Department of Defense
ERDC	Engineer Research and Development Center
ESTCP	Environmental Security Technology Program
FUDS	Formerly Used Defense Sites
GPO	Geophysical Proveout
GPS	Global Positioning System
GUI	Graphical User Interface
GX	Geosoft Executable
IDL	Interactive Data Language
JPG	Jefferson Proving Ground
MTADS	Multi-sensor Towed Array System
NAVEODTECHDIV	Naval Explosive Ordnance Disposal Technology Division
NRL	Naval Research Laboratory
Pd	Probability of detection
Pfa	Probability of false alarm
rBAR	Background alarm rate
RTK	Real Time Kinematic
SERDP	Strategic Environmental Research and Development Program
SGI	Silicon Graphics Incorporated
SNR	Signal to Noise Ratio
UpC	Upward Continuation
USACE	US Army Corp of Engineers
UXO	Unexploded Ordnance
WAA	Wide Area Assessment

Acknowledgements

Contributing firms to this demonstration include SAIC, formally AETC Incorporated (lead), Sky Research and NAEVA Geophysics. We thank Bob Selfridge and others at the USACE for supplying data for this demonstration. This research was supported wholly by the U.S. Department of Defense, through the Environmental Security Technology Certification Program (ESTCP) through Project MM-0502, under Contract W912HQ-05-C-0015.

Abstract

Due to the large numbers (up to tens of thousands) of possible targets identified in nominal UXO surveys, efficient and reliable machine-aided target pickers should be used to identify targets for subsequent characterization. When selecting anomalies, the goal is to identify all anomalous features that may be caused by UXO while minimizing operator time and eliminating operator bias. To facilitate advanced physics-based modeling, however, the target pickers should also be able to select data appropriate to the target, i.e., to outline or estimate the anomalies spatial extent. The current approach to target selection is either manual identification or amplitude thresholding. The former is time intensive, not clearly defined, and prone to operator bias. The latter is sensitive to noise and is prone to over- or under-picking unless judicious oversight is exercised. Neither approach provides measures for estimating the footprint of the anomaly. The impact to the DoD is obvious. Systematic, fast, and robust target pickers can save money and produce a defensible target list compared to the current methods.

This project evaluated four automatic target pickers against the manual method and transitioned them to the user community via Oasis montaj™ by building custom Geosoft Executables (GX). Oasis montaj™ is a geophysical data processing and visualization package developed and marketed by Geosoft Incorporated. The four automatic target pickers were: (1) a wavelet-based detection algorithm, (2) clustering positive and negative peaks, (3) a dipole-based matched filter, and (4) analytic signal.

The demonstration was broken up into two phases. The first phase used a 60 dipole synthetic data set to explore the parameter space and optimize the algorithms for the four automatic target pickers. The result of phase one was a set of starting parameters that was used in phase two. The second phase applied the target pickers to seven magnetic data sets using the parameters output from phase one as a starting point. The seven data sets possessed different signal and noise characteristics and anomaly densities. Three datasets provided from the Corps of Engineers (COE), a helicopter-towed Wide Area Assessment (WAA) dataset, a vehicle-towed transect WAA dataset, and vehicle-towed Multi-sensor Towed Array System (MTADS) datasets from the Aberdeen Proving Ground (APG) standardized test site and Target S1 at Isleta Pueblo in New Mexico were used for the evaluation. Because each data set has its own unique data characteristics the starting parameters were adjusted iteratively to achieve the best performance. The knowledge gained from phase one was used to guide these adjustments.

Overall, the manual method proved to be the best at picking valid targets especially in areas with varying amounts of geology and background noise. In general, the manual picker was able to set a lower threshold for each data set than the automatic methods because he can screen out the anomalies with signal amplitudes above a threshold that are caused by noisy data or geology and pick the small amplitude anomalies located in the quieter areas. This ability is also useful when dealing with poor quality data. The manual picker was able to interpret positioning problems that caused some large anomalies to appear to be several small anomalies and only make one declaration whereas some of the automatic pickers had multiple declarations. The main drawbacks to the manual method are time, operator bias and operator error.

Of the automatic methods the analytic signal and wavelet method gave the best results overall but each of the methods had their own strengths and weaknesses and the best method to use was very data dependent. A general observation for all the automatic pickers is that they should not be run blindly. The analyst should carefully choose their parameters and analyze the results. The process of iteratively changing parameters and visual review of the results was essential in selecting the best parameters.

The wavelet method worked well on a range of target sizes and densities. It performed better than the other methods at picking targets that were clustered. It was fairly quick to run on total coverage surveys but much less efficient when run on transect data. Its main weaknesses were the complexity of the parameters and over picking in areas with geology, noise or poor data quality.

The clustering method performed well detecting isolated targets with similar sizes. When a range of target sizes were encountered and the parameters were set to detect the large anomalies any small anomaly close to the large anomaly tended to be missed. The clustering algorithm also had problems picking anomalies in areas with high geology and noise. Overall, it ran slower than the analytic signal on total survey areas but was more efficient on transect data because it works on the profile data and not a grid. It also took longer to setup because there were multiple parameters that need to be tuned.

The matched filter method performed the worst. It was hindered by its requirement to have total data coverage within the filter box. This would increase geophysical data collection costs because additional data would need to be collected around the perimeter of the survey area. It ran the slowest of the automatic methods but the limited number of parameters helped reduce its complexity. It had difficulty with overlapping targets, range of target sizes and poor data quality. The one area it excelled at was picking targets in areas with a variety of geology.

Implementation of the automatic picking methods used in this demonstration should considerably reduce the time and thus cost required to pick anomalies when compared to the manual method. The amount of cost savings will depend on the data. In areas with isolated anomalies and low background noise or geology the cost savings will be maximized because the automatic pickers are able to detect over 90% of the anomalies in a fraction of the time compared to the manual method. As the geologic noise increases or data quality decreases the cost savings will diminish but still should be significant.

In conclusion, the best use of the automatic target pickers may be to quickly and consistently select all the strong isolated targets by setting the picking parameters to minimize false alarms. The remaining anomalies can then be selected using the manual method. This combines the strengths of each method and will result in a better product than using only the automatic methods and cost savings compared to using only the manual method.

MM-0502 Final Report
Target Picking Methods for Magnetic Data

1. Introduction

1.1 Background

Buried Unexploded Ordnance (UXO) is arguably one of the most serious and prevalent environmental problems currently facing Department of Defense (DoD) facility managers. Not limited to active sites and test ranges, these problems also occur at DoD sites that are currently inactive and in areas adjacent to military ranges that belong to the civilian sector or are under control of other government agencies. The exact amount of land affected is uncertain, but it is generally agreed to be in excess of 10 million acres in the continental United States. UXO mitigation and remediation requirements assume even more compelling proportions when the DoD lands involve Formerly Used Defense Sites (FUDS) or Base Realignment and Closure (BRAC) sites. These sites must be certified as suitable for the end use depending on the pending disposition. Oversight and evaluation of these processes involve non-DoD agencies including the EPA; state, county, and local governments; and the civilian community.

Due to the large numbers (up to tens of thousands) of possible targets identified in nominal UXO surveys, efficient and reliable machine-aided target pickers should be used to identify targets for subsequent characterization. When selecting anomalies, the goal is to identify all anomalous features that may be caused by UXO while minimizing operator time and eliminating operator bias. To facilitate advanced physics-based modeling, however, the target pickers should also be able to select data appropriate to the target, i.e., to outline or estimate the anomalies spatial extent.

The current approach to target selection is either manual identification or amplitude thresholding. The former is time intensive, not clearly defined, and prone to operator bias. The latter is sensitive to noise and is prone to over- or under-picking unless judicious oversight is exercised. Neither approach provides measures for estimating the footprint of the anomaly. The impact to the DoD is obvious. Systematic, fast, and robust target pickers save money and produce a defensible target list – the alternatives do not.

This project evaluated four automatic target pickers and transitioned them to the user community via Oasis montaj™ by building custom Geosoft Executables (GX). Oasis montaj™ is a geophysical data processing and visualization package developed and marketed by Geosoft Incorporated. It has a large capacity database, a professional graphic interface, and an established client base. We decided to transition research algorithms via Oasis montaj™ in order to leverage its significant capabilities, marketing channels, and customer support services.

1.2 Objectives of the Demonstration

This ESTCP project is aimed at evaluating four automatic target-picking algorithms for total field magnetometer data and comparing the detection results with ground truth when available or to anomalies chosen manually by a commercial expert. The four picking methods included in the study are (1) a wavelet-based detection algorithm, (2) a rule-based, clustering approach, (3) a dipole-based matched filter, and (4) a thresholded analytic signal algorithm. Our goal is to identify all anomalous features that may be caused by UXO while minimizing operator time and eliminating operator bias. Simply identifying geophysical anomalies is not enough, however to facilitate advanced physics-based modeling, the target picking routines should also be able to identify the anomalies spatial extent.

The project ran each target picking routine on demonstration data sets that possessed different signal and noise characteristics and anomaly densities. Three datasets provided from the Corps of Engineers (COE), a helicopter-towed Wide Area Assessment (WAA) dataset, a vehicle-towed transect WAA dataset, and vehicle-towed Multi-sensor Towed Array System (MTADS) datasets from the Aberdeen Proving Ground (APG) standardized test site and Target S1 at Isleta Pueblo in New Mexico were used for the evaluation.

1.3 Regulatory Drivers

The Senate Report (Report 106-50), pages 291–293, accompanying the *National Defense Authorization Act for Fiscal Year 2000* (Public Law 106-65), included a provision entitled "Research and development to support unexploded ordnance clearance, active range unexploded ordnance clearance, and explosive ordnance disposal." This provision requires the Secretary of Defense to submit to the Congressional Defense Committees a report that gives a complete estimate of the current and projected costs, including funding shortfalls, for UXO response at active facilities and installations subject to BRAC, and FUDS.

The following statements are taken verbatim out of the DoDs 2001 Report to Congress:

> *"Decades of military training, exercises, and testing of weapons systems has required that we begin to focus our response on the challenges of UXO. Land acreage potentially containing UXO has grown to include active military sites and land transferring or transferred for private use, such as Base Realignment and Closure (BRAC) sites and Formerly Used Defense Sites (FUDS). DoD responsibilities include protecting personnel and the public from explosive safety hazards; UXO site cleanup project management; ensuring compliance with federal, state, and local laws and environmental regulations; assumption of liability; and appropriate interactions with the public.*
>
> *…Through limited experience gained in executing these activities, it has become increasingly clear that the full size and extent of the impact of sites containing UXO*

is yet to be realized. … DoD has completed an initial baseline estimate for UXO remediation cost. This report provides a UXO response estimate in a range between $106.9 billion and $391 billion in current year [2001] dollars. …Technology discovery, development, and commercialization offers some hope that the cost range can be decreased. …

*… **Objective**: **Develop standards and protocols** for navigation, geo-location, data acquisition and **processing**, and performance of UXO technologies.*

- *Standard, high quality archived data are needed for optimal data processing of geophysical data, re-acquisition for response activities, quality assurance, quality control, and review by all stakeholders. In addition standards and protocols are required for evaluating UXO technology performance to aid in selecting the most effective technologies for individual sites.*
- ***Standard software and visualization tools are needed to provide regulatory and public visibility to and understanding of the analysis and decision process made in response activities**."*

1.4 Stakeholder/End-User Issues

The stakeholders and end-users of this data processing and analysis technology include private contractors that conduct geophysical investigations in support of UXO clean up programs and governmental employees that provide technical oversight. This demonstration will introduce the stakeholders and end-users to data products associated with this analysis approach, and to the inherent transparency of the target picking process. This basic information will help to improve the results of future geophysical investigations conducted by others. The market for this type of guidance document includes all practicing geophysical service firms currently working in the UXO industry.

2. Technology Description

2.1 Technology Developments and Application

The user community would benefit from an algorithm that accurately identifies and locates magnetic anomalies using quantifiable decision criteria and limited user interactions. The underlying aim is to reduce analysts' bias because it is not predictable, consistent, or correctable. This project made and compared anomaly declarations for each dataset chosen using the following five approaches: (1) a wavelet-based detection algorithm, (2) clustering positive and negative peaks, (3) a dipole-based matched filter, (4) analytic signal, and (5) manual selection. Each approach is described below. We will also evaluate how each method can be used to identify the anomalies spatial extent.

Wavelet-based Algorithm: Billings and Herrmann (2003) developed a magnetic target picking method called the Automated Wavelet Detection (AWD) algorithm. In that method, individual peaks in the magnetic data are followed across multiple scales, with the decay in peak amplitude related to the depth to the source. Nearby positive and negative peaks in the image are only joined together if they satisfy two conditions: (i) the peaks must have comparable depth estimates and (ii) the peaks must move towards each other as the wavelet scale becomes finer. In this way, one can avoid incorrectly joining the peaks from nearby dipoles. In the last stage of the algorithm, the amplitudes of the peaks and their relative position are used to provide an initial estimate of the dipole parameters including a good initial estimate of the size of the region to invert about each anomaly.

The AWD method has a solid theoretical basis by using the Poisson wavelet (Moreau, et al., 1999). This wavelet has been extensively studied and applied to interpretation of potential fields (see Moreau, et al., 1999 and references therein), particularly for locating and characterizing edges in the data (Hornby et al., 1999). A very useful property of this class of wavelets is that the wavelet transform can be simply obtained by upward continuation followed by horizontal differentiation. This means that the wavelet coefficients at multiple scales can be easily and rapidly computed.

The algorithm consists of the following five steps:

1. Follow local maxima and minima as the image is zoomed to different scales with a wavelet transform;
2. Estimate the depth to the source of each peak by analyzing how the amplitude of the peak changes with scale;
3. Join nearby positive and negative peaks of comparable depth; and
4. Use the amplitudes and distance between adjacent peaks to provide an initial estimate of dipole parameters.
5. Using the initial estimate of dipole parameters, delineate the region that comprises 97.5% of the dipole energy, and resolve any issues of overlapping anomalies.

Rule-based Clusters: Rule-based clustering approaches threshold the magnetic data to identify positive and negative groups and then associate positive and negative clusters using codified rules to form anomalies. The degree to which they work depends on the noise and signal characteristics of the data and on details of the rules that associate negative and positive clusters. We have identified two rule-based schemes that have been developed and codified under previous research efforts.

The first is an automatic target picker developed during SERDP CU-1092 by Blackhawk Geometrics, Inc. In this version, thresholds for positive and negative data are set by the user. The negative and positive clusters are then identified, and each negative anomaly is associated with the most plausible nearby positive anomaly. The most plausible positive anomaly is determined by a formula that reflects the distance, magnitude of both anomalies, and degree of consistency with the local magnetic declination. Isolated negative anomalies are discarded as noise. As detailed in the CU-1092 project report, there are issues with regard to matching positive and negative lobes in cases where the anomalies are tightly packed and/or overlapping. There are also issues with regard to the picker dividing one anomaly into two if there are minor amplitude sags (due perhaps to inter-sensor difference, heading errors, or gridding). Additionally, the Blackhawk formula-based codes were written for the Silicon Graphics Incorporated (SGI) IRIX operating system or the LINUX operating system.

The second rule-based scheme was developed and codified by AETC Incorporated under funding from Naval Explosive Ordnance Disposal Technology Division (NAVEODTECHDIV) in 1995. Similar to the code developed under CU-1092, it asks the user to identify thresholds, uses the thresholds to create positive and negative clusters, and then associates the clusters in favor of combinations with the least distance between centers.

Dipole based Matched Filter: AETC developed, under ESTCP Project 199918, a Matched Filter AutoProcessor (MFAP) for magnetometer data. This algorithm implements a matched filter based on a magnetic dipole signal. After the magnetometer data is interpolated onto a regular x-y grid, it is automatically convolved with a magnetic dipole signal model for a target accompanied by a search over the unknown parameters in the signal model (target orientation, moment, etc.) to maximize the filter output. The output of the matched filter routine is a surface (grid) that peaks directly over the target location. Because of this, it can be thresholded to identify targets. The Matched Filter approach was developed in the Interactive Data Language (IDL; Research Systems, Inc.) but has subsequently been integrated with OASIS montaj™.

Once the matched filter output is calculated, the user must identify individual anomalies by picking peaks above the background noise. The spatial extent of each anomaly can be estimated by using the initial fitted parameters output during the match fitting process to calculate a boundary that contains a certain percentage of the total energy.

Analytic Signal: The analytic signal (AS) is a positive quantity derived from magnetometer data. It can easily be thresholded for target detection and is commonly used by commercial practitioners. The analytic signal is the square root of the sum of the gradients in three directions:

$$AS = \sqrt{\left|\frac{\partial B}{\partial x}\right|^2 + \left|\frac{\partial B}{\partial y}\right|^2 + \left|\frac{\partial B}{\partial z}\right|^2} \quad ,$$

where the z-gradient is formed from the data in the (x,y) plane by upward continuation in the Fourier domain:

$$\frac{\partial B(k)}{\partial z} = kB(k), \quad k = 2\pi / \lambda \quad .$$

Routines to calculate the analytic signal are included with appropriately licensed versions of Oasis montaj™.

Once the analytic signal is calculated, the user must identify individual anomalies by picking peaks above the background noise. The spatial extent of each anomaly can be estimated by examining the nature of the anomaly in terms of its inflection points or change in total energy.

Manual Anomaly Selection: As a baseline measure, we manually identify individual anomalies and estimated the spatial footprint of each anomaly using an experienced analyst from NAEVA Geophysics. The analyst was asked to select all anomalies above the noise level of the given dataset. The analyst decided on the noise threshold and properly documented the rationale behind the threshold. The analyst was free to use their preferred analysis environment.

2.2 Previous Testing of the Technology

All the routines that we evaluated have been previously developed and tested commercially as part of a previous research program. We also ran shakedown tests on the four algorithms using a synthetic magnetic dataset with 60 well-characterized targets and noise characteristics as shown in Figure 1. The synthetic dataset consisted of six target sizes (20mm, 40mm, 60mm, 81mm, 105mm and 155mm) randomly placed at depths up to the 11 times the target diameter.

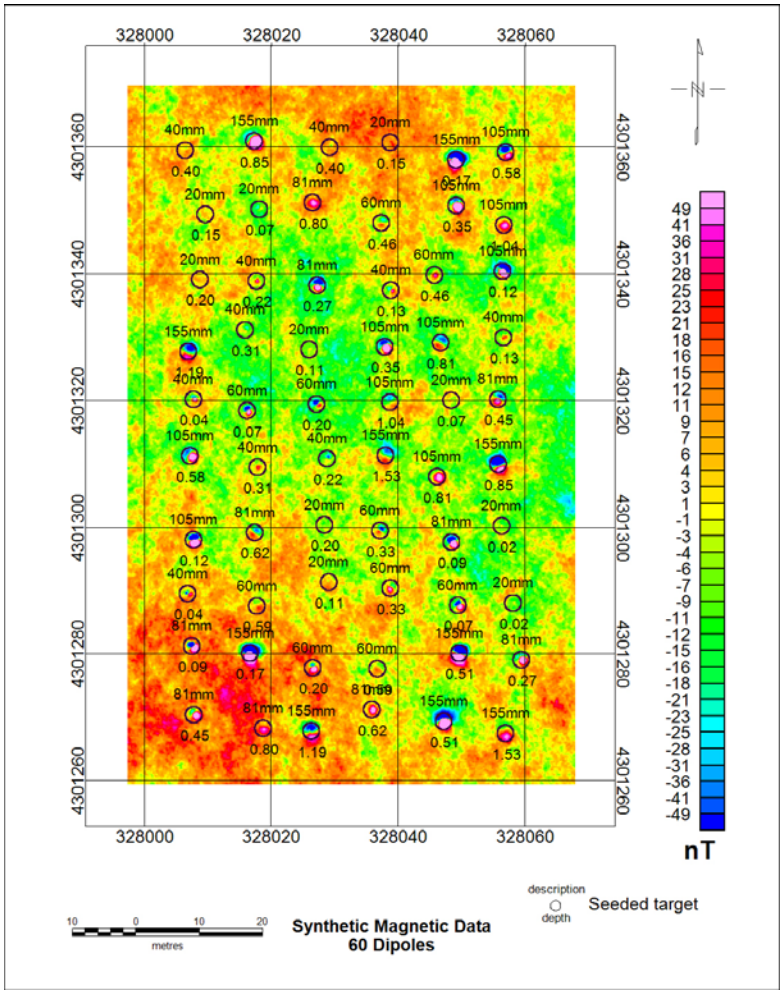

Figure 1. Synthetic magnetic data set with 60 targets.

2.2.1 Wavelet-based Algorithm

The AWD algorithm has been successfully applied at the University of British Columbia as part of the work funded by Engineer Research and Development Center (ERDC) (DAAD19-00-0-0120). The algorithm was demonstrated on three datasets with different characteristics (Billings and Herrmann, 2003). In each case, the method rapidly located the majority of dipole anomalies and produced accurate estimates of the dipole parameters.

There were two main enhancements made to the AWD algorithm under this project:

1) The algorithm was wrapped up in a segmentation routine so that grids of any size can be processed; and
2) The algorithm was implemented within the SkyNET software environment so that the original Matlab algorithm could be seamlessly accessed from with Oasis montaj™.

2.2.1.1 Segmentation Algorithm

The original Matlab implementation of the AWD algorithm was computationally efficient but required a lot of memory. Once the grid exceeded a size of about 1000 by 1000 points, the algorithm would slow down as Matlab had to use swap space to manage memory. There is no need to use the entire grid to detect individual targets with the AWD. Therefore, we developed a segmentation routine so that grids of any size could be processed with the algorithm.

The segmentation algorithm breaks the input grid up into sub-regions comprising, at most, 500 by 500 pixels. The region is then buffered by 50 pixels to avoid edge-effects. Targets are then detected in the sub-region and its buffer zone using the AWD algorithm. Any detected targets within the buffer zone are rejected as these will also be detected within the adjacent sub-region. Figure 2 shows an example of the sub-regions and the associated buffer-zones. Using this routine, we have processed grids with up to 4000 by 4000 pixels.

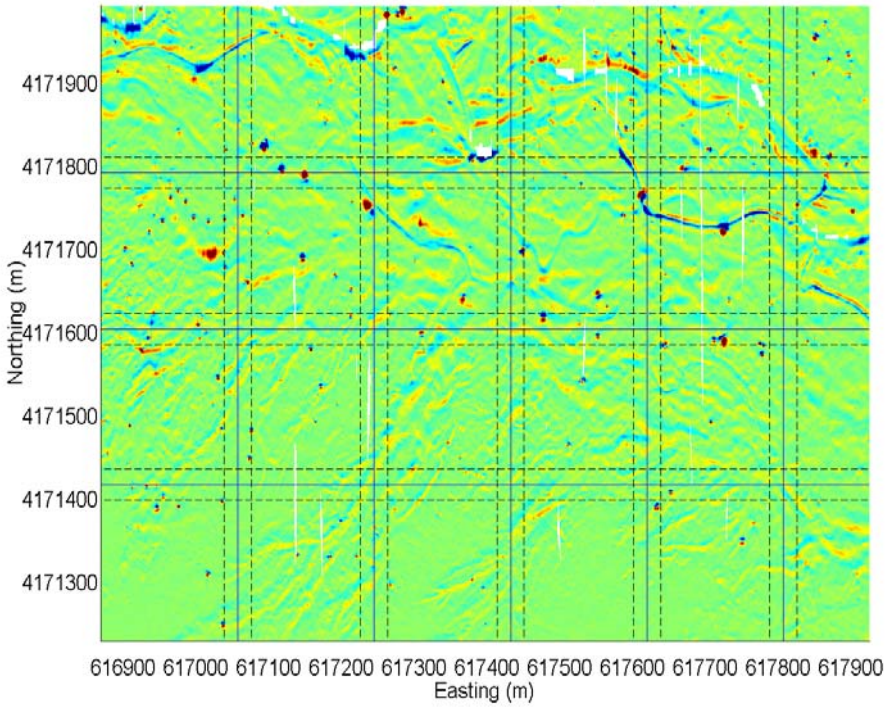

Figure 2. Segmentation algorithm applied to a large HeliMag dataset. The solid blue lines delineate the boundaries between adjacent sub-regions. The dashed lines delineate the buffer regions.

2.2.1.2 Integration with Oasis Montaj™

The AWD algorithm was written in Matlab code and is accessible from the UXOLab software environment (UBC and Sky's UXO analysis software). Rather than porting the algorithm to C++ and wrapping it within a GX (a laborious and time-consuming process) we decided to develop a mechanism to call the Matlab algorithm directly from Oasis montaj™. This was achieved by implementing the algorithm within SkyNet, Sky Research's custom designed .NET based analysis software.

SkyNet consists of several .NET dlls that can be linked to other .NET compatible applications, such as Oasis montaj™. SkyNet also uses the COM interop mechanism of .NET to expose its functionality to other applications, such as MatLab, that do not inherently support .NET. As a result, there are three different ways to run SkyNet:

1) Running SkyNet from within the Oasis montaj™ application process
2) Running SkyNet from within the MatLab application process
3) Running SkyNet by itself (from within the SkyNet application process)

For the Wavelet algorithm we used option 1 and ran everything from within the Oasis montaj™ process. Figure 3 below provides an overview of this configuration:

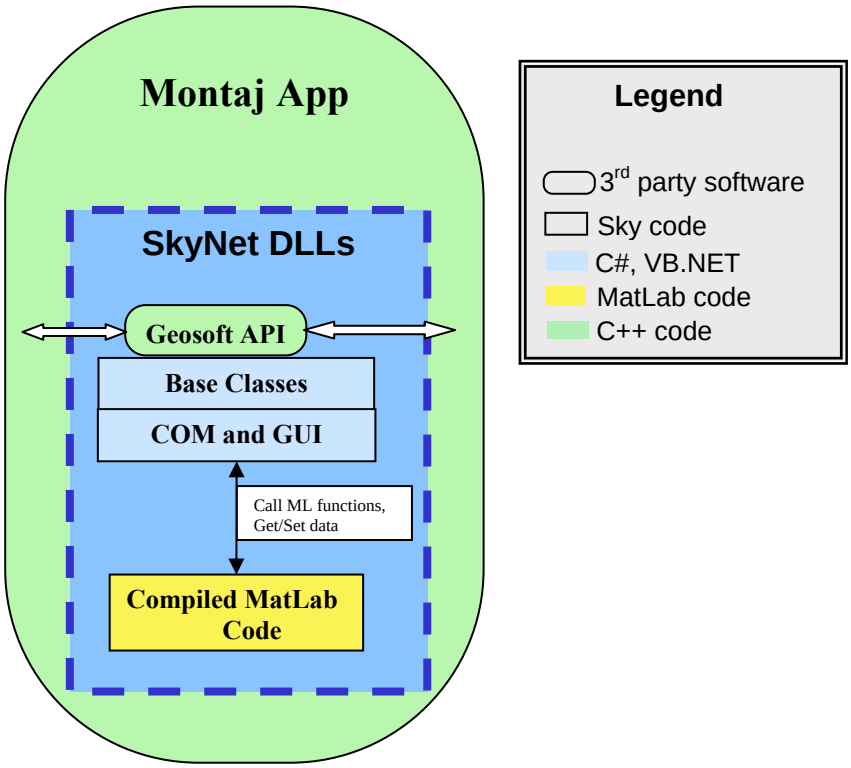

Figure 3. Schematic of the SkyNet architecture.

As shown in Figure 3, all SkyNet DLLs run within the Oasis montaj™ executable process. At startup, an Oasis montaj™ menu item calls the SkyNet COM and GUI DLL that will in turn initialize the compiled MatLab code DLL. During the initialization, a COM event callback is registered in the compiled MatLab code DLL that allows SkyNet to call MatLab functions. This also allows the MatLab function to 'Set' and 'Get' data to and from SkyNet. The Geosoft API is linked to the Base Classes DLL, allowing SkyNet to interact with the Oasis montaj™ application GUI. Once all initialization is complete, the SkyNet menu item in Oasis montaj™ can utilize any SkyNet DLL functionality (i.e. all functions found in C#, VB.NET, and MatLab compiled code). Figure 4 below shows the AWD algorithm being called directly from Oasis montaj™. The user experience is almost identical to that for any other Geosoft algorithm: the only noticeable variation is that the parameter input GUI has a slightly different appearance.

To access the algorithm, the user needs to install the Matlab run-time libraries and the SkyNET application on his/her PC. Both of these applications have been bundled into a standard installation package so that no special knowledge is required for the installation. The user then installs the SkyNet menu through a standard OMN file that is a standard menu-configuration process for any new Geosoft application. Note that the Matlab run-time library can be installed free of charge.

At present the main limitation is that SkyNet is only compatible with Geosoft Version 6.2 (the current version is 6.4). This is because SkyNet currently uses the .NET Version 1.1 whereas Geosoft 6.4 uses .NET Version 2.0. There are a number of incompatibilities between these two versions of .NET. Later this year, SkyNet will be upgraded to .NET version 2.0 and the AWD algorithm will then be accessible from Geosoft 6.4 and higher. If Geosoft then moves to .NET Version 3.0, the algorithm should still be accessible because .NET is now configured to be backwards compatible (except with version 1.1).

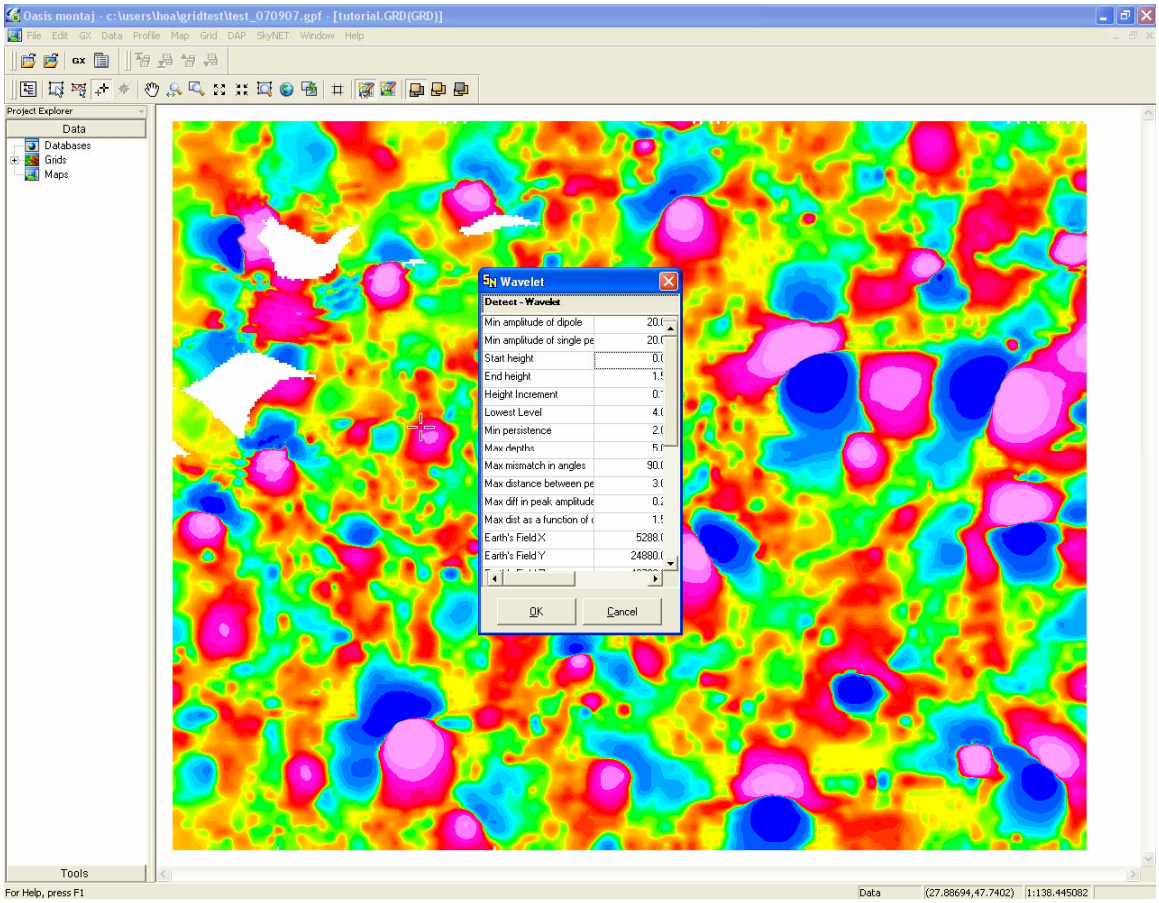

Figure 4. Screen-capture of the AWD algorithm being used directly from within Oasis montaj™.

2.2.1.3 Synthetic Magnetic Data Test

The AWD algorithm was applied to the synthetic magnetic data and found 43 of the 60 targets with 25 false positives as shown in Figure 5. By changing one of the key parameters of the wavelet, 3 additional targets were found but at the expense of 55 additional false positives.

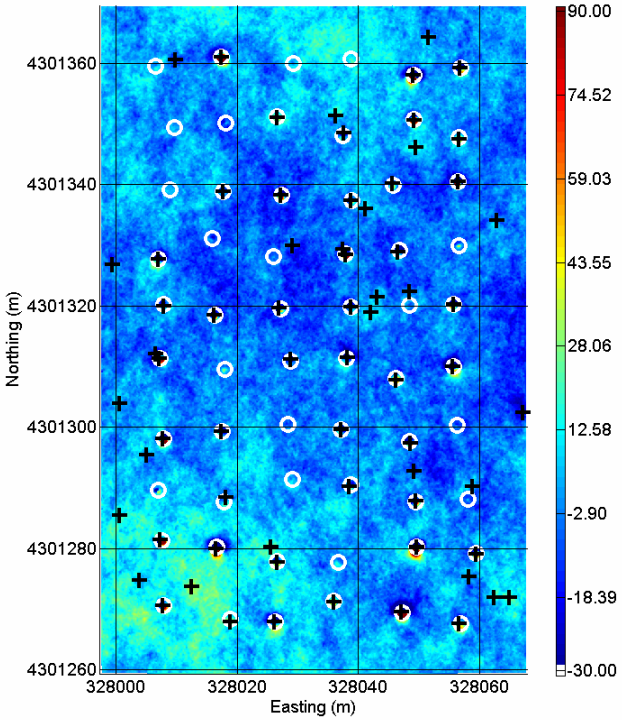

Figure 5. Results of AWD algorithm on the synthetic magnetic data. The 60 true locations are marked as white circles and the wavelet picks as black crosses.

2.2.2 Rule-based Clusters

The two rule-based clustering algorithms that were used as a basis for the clustering algorithm developed for this project were previously tested during their development as part of the work funded by SERDP (CU-1092) and NAVEODTECHDIV. The AETC Incorporated clustering algorithm was also tested on data collected at the Badlands Bombing Range (BBR) on the Pine Ridge Reservation in South Dakota and at 29 Palms in California (Barrow, 1998). The results of this test showed the automatic processor detecting about 90-100% of the objects present with the most significant detection factor being target density. In low density regions closer to 100% of the objects were found whereas in high density areas the detection rate fell to 90%. It was also estimated the automatic processor could analyze about 4 times more data than the manual processor in the same amount of time.

We reviewed both codes in detail and incorporated unique and attractive capabilities from each. We essentially used the clustering algorithm developed by AETC Incorporated and the association algorithm developed by Blackhawk. After testing the clustering method picker on a suite of synthetic test dipoles and comparing the inverted parameters to those obtained by manual

target selection, we determined the circumstances in which the automatic picker performed poorly and made the modification to the code as outlined below.

One recurring situation was the loss of a lobe due to the initial signal thresholding. Since lowering this threshold too much would result in noise being flagged as targets, an alternate method was developed. After all positive and negative dipoles have been combined, the code examines single dipoles, and searches for points of the opposite sign above a lower extraction threshold, within a certain distance from the peak, and such that the putative dipole has a declination within a certain offset of the Earth's field declination. This method successfully recovered the lost lobe in most cases, and improved the inverted target parameters. The code also tries to flag potentially overlapping targets by measuring the gradient change as one moves out from a dipole peak. These cases can be examined manually by the user. The original version was far too sensitive, however, with noise often resulting in flags where no target overlap existed. The code was modified to add an additional requirement that an already determined dipole must exist within a certain distance and angle of the gradient change location. This resulted in a significant decrease of the spurious overlap flags.

The development and testing of these additions were completed using IDL. The final version was recoded into C++ and seamlessly integrated into Oasis montaj™ through a custom GX. The GX wrapper was written in the Microsoft .NET developer environment which allows the developer to build single functions or suites of functions into a .NET DLL that is run directly from Oasis montaj™. During the integration to Oasis montaj™ an option to output an ascii file that is compatible with UX-Analyze (ESTCP funded modeling and visualization software that runs under the Oasis montaj™) was added. The ascii file contains the geographic boundary coordinates that defines the spatial footprint of the picked anomaly. The ‘polygon’ is a circle that encompasses all the points in the positive and negative clusters that are associated with the anomaly. The radius of this circle is increased by 20% to include background values around the anomaly which are a valuable input to UX-Analyze.

As part of this demonstration the clustering algorithm was applied to the synthetic magnetic data set and found 46 of the 60 targets with 11 false positives as shown in Figure 6.

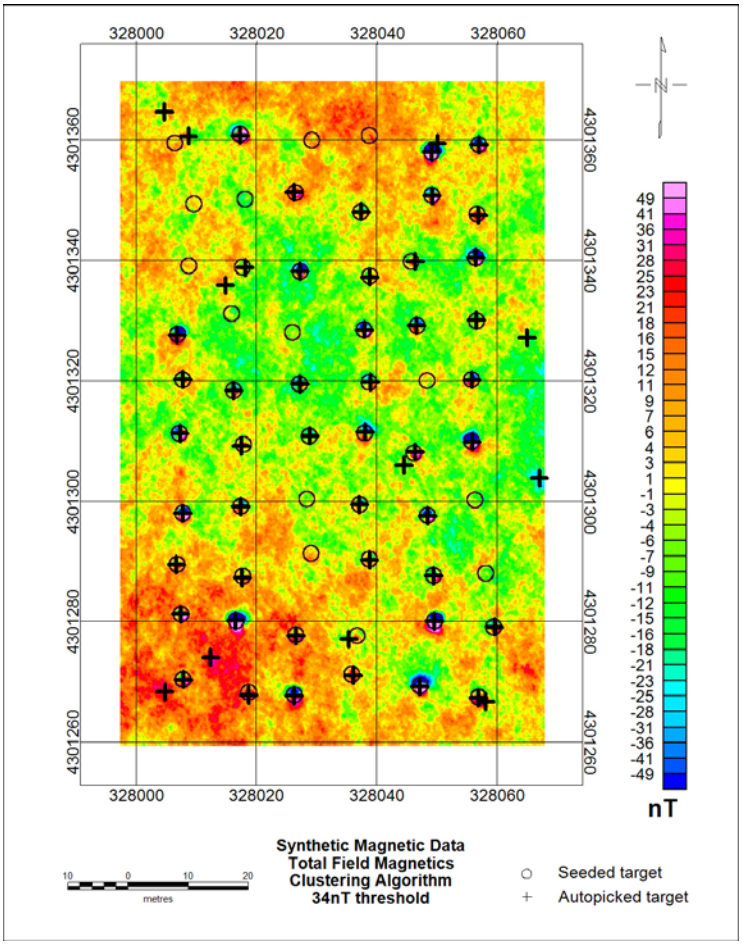

Figure 6. Results of clustering algorithm on the synthetic magnetic data. The true locations are plotted as circles and the automatic picker detections are plotted as "+".

2.2.3 Dipole based Matched Filter

Previous testing of the MF algorithm included MTADS magnetometer survey data over several sites, which include 29 Palms, Blossom Point and Buckley Field. The algorithm was also tested on the three 1-hectacre areas of the 2000 Advanced UXO Detection/Discrimination Technology Demonstration at JPG. The MF did a good job at isolating potential targets at JPG (Bell, 2001). The filter output peaked over the targets, which helped reduce the ambiguity of the exact target location. The low probability of detection (80%) was caused by data gaps and the difficulty in finding 20mm using magnetometer data with a sensor spacing of 25cm.

As part of ESTCP project 199918, the MFAP was integrated into Oasis montaj™ version 5.13 in the year 2002. Since then Oasis montaj™ has undergone a major change as is currently releasing version 6.4. The upgrade to version 6 included significant enhancements to software usability, licensing, interface and map editing functions. These upgrades created an incompatibility with the original MFAP GX. The main issues were changes to the structure of

the GX wrapper and changes to the syntax and parameters of some functions called within the GX. These incompatibilities were fixed and the GX was recompiled and tested in versions 6.3 and 6.4.

As part of this demonstration the MF algorithm was applied to the synthetic magnetic data set and found 43 of the 60 targets with 46 false positives as shown in Figure 7. Many of the false positives were the result of multiple declarations for a single target because of processing artifacts in the match filter output that are caused when the filter window contains only a portion of the dipolar signal.

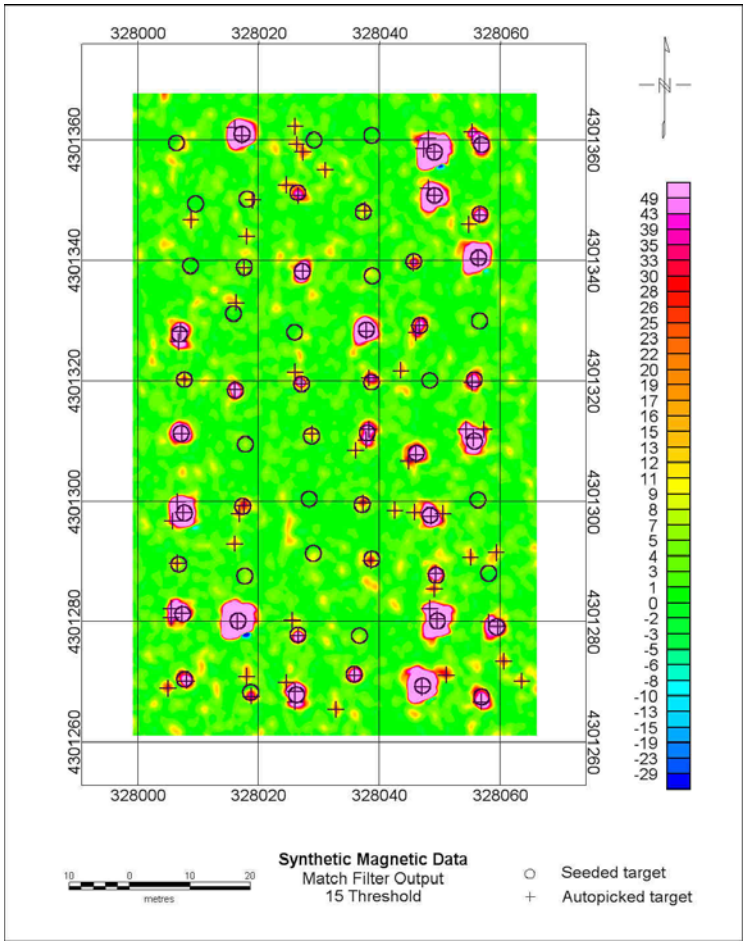

Figure 7. Color contour map of the match filter output calculated from the synthetic magnetic data. The true locations are plotted as circles and the automatic picker detections are plotted as "+".

2.2.4 Analytic Signal

The analytic signal is included with appropriately licensed versions of Oasis montaj™ and is commonly used by commercial analysts. As such, it has undergone internal testing of the algorithm at Geosoft and extensive practical testing by the user community.

The analytic signal algorithm produces an anomalous surface with peaks over potential targets but does not output a 'polygon' file containing the spatial extents of the targets. As mentioned earlier this polygon file is an essential input to UX-Analyze. For this reason, a GX was developed to estimate the spatial extents and output the boundary coordinates to a UX-Analyze compatible file. For each anomaly location, the 'footprint' algorithm uses the analytic signal grid and starts at the nearest grid cell to a given target location. The algorithm searches along each of the eight directions and stops if one of the following three conditions is met: 1) one of the surrounding grid cells away from the peak is larger in amplitude, 2) the value is less than the user defined background value, and 3) the distance from the initial location exceeds the user defined limit. Upon completion of the search, there are eight stopping locations surrounding the anomaly. At this point the user has the option to output these points to a file or to output a circle to the file. The radius of the circle is the median of the distances from the anomaly location to each of the eight stopping locations. Areas with many close or overlapping anomalies favor the former option while areas with isolated anomalies will the benefit from the calculated circle as shown in Figure 8.

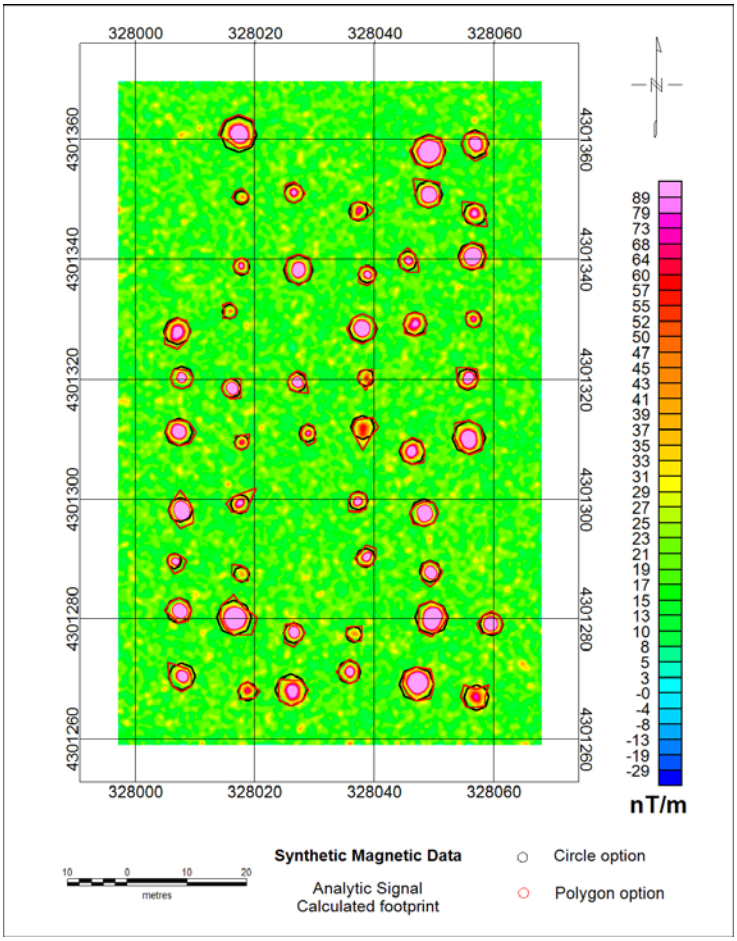

Figure 8. Color contour map of the analytic signal grid calculated from the synthetic magnetic data. The calculated footprint of selected anomalies using the polygon (red) and circle (black) options are shown.

The analytic signal algorithm was applied to the synthetic magnetic data to create an analytic signal grid. The grid was filtered with two passes of a 9 point hanning filter and anomalies were picked using the Blakely method (Blakely, 1986). The Blakely method compares the value of each grid cell with values of the eight (8) nearest grid cells in four directions (along the row, column, and both diagonals). If the grid value is greater than the input threshold and all the nearest grid cells are lower, it is selected as a peak. Using a threshold of 45nT/m, 49 of the 60 targets were found with no false positives as shown in Figure 9.

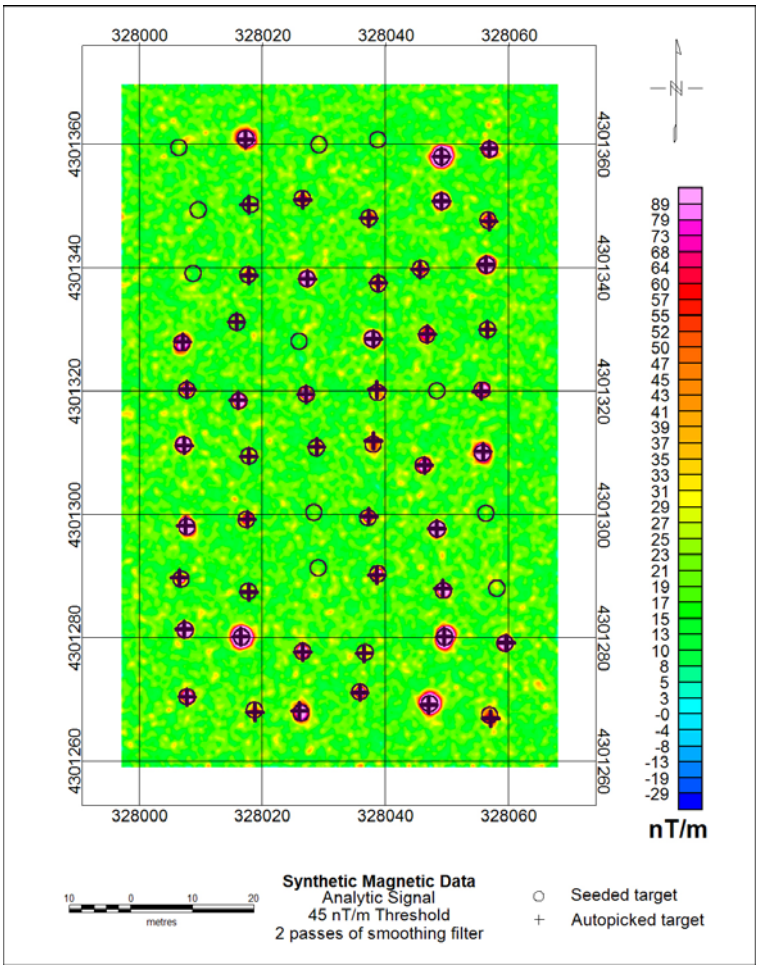

Figure 9. Color contour map of the analytic signal grid calculated from the synthetic magnetic data. The true locations are plotted as circles and the automatic picker detections are plotted as "+".

2.3 Factors Affecting Cost and Performance

Implementation of the automatic picking methods used in this Demonstration should considerably reduce the time and thus cost required to pick anomalies when compared to the manual method. It is anticipated this will be the case in areas with low anomaly density but as the anomaly density increases to the point that overlapping anomalies are prevalent, the performance of the automatic pickers may be degraded. Also, the quality of the data would have an impact on the performance of the automatic methods. If the data is sufficiently noisy, the automatic methods will likely either pick too many targets if the threshold is set to capture smaller anomalies or miss the small anomalies if the threshold is set above the background noise level. Whereas the analyst using the manual method may be able to screen out the anomalies caused by noisy data by using his experience and the "look" of the anomaly.

2.4 Advantages and Limitations of the Technology

This demonstration used already collected survey data to test four automatic target pickers and transitioned the algorithms to the user community through Oasis montaj™. The main advantage of using automatic methods to pick anomalies is the time it can save. On large remediation projects with thousands of anomalies, the manual method is very slow. Another aspect of the manual method is its subjective nature. Different data analysts may have different criteria on what is and is not an anomaly. It may be based on signal level and signal shape which is directly affected by the way the data is displayed. The target density of the data may also affect the analyst's decision. In areas of low density, the analyst may be prone to pick smaller and weaker anomalies for the sake of picking something. Conversely, in high-density areas the analyst may set his threshold higher. Based on these two difficulties, automatic target pickers are desirable because they would only be limited by the speed of the computer and can be set to select targets using fixed criteria.

Previous testing of the automatic pickers has shown limitations to the technology. The clustering and analytic signal algorithms may have trouble with low signal-to-noise signatures and high background noise. In these areas, a low threshold must be chosen to pick the weaker anomalies but by lowering the threshold, the automatic pickers will pick many anomalies that are caused by noise in the data.

The matched filter algorithm cannot filter a point if there are any missing data in the filter box. Thus, the edges of a survey site cannot be filtered as well as any interior regions that are missing data. Therefore, a small data gap of 0.5x5m becomes an unfilterable region of 3.5x8m if a 3m filter box is used. For this reason the match filter algorithm cannot be used on the WAA vehicular transect data because the width of the transect is only 1.75m.

The analytic signal and AWD algorithms map and interpolate the magnetic data to a regular x-y grid and apply their respective filters to the grid. For normal surveys, this would not be an issue but applying them to transect data may require some optimization. Because transects can cover large areas in a single sortie the resultant grid can get very large given that the grid produced is based on the minimum and maximum XY values. If the transect lines are relatively straight along one geographic heading, the data can be rotated prior to creating the grid such that the lines are oriented along either the grid rows or columns.

The analytic signal and matched filter algorithms output an anomalous surface and not the locations of the anomalies. Therefore, a second program must be run to pick the peaks in the surfaces. Thus, the success of these methods is partially dependent on the peak picking program.

The clustering and AWD algorithms have several parameters that need to be set. The option to change many of the parameters allows the user the flexibility to tune the algorithms to the individual data characteristics. However, this flexibility adds to the complexity and setup time to ensure the proper parameters are picked to achieve optimum performance of the algorithms.

3. Demonstration Design

3.1 Performance Objectives

Table 1 and Table 2 outline the performance objectives for the production and WAA surveys, respectively. The values of the quantitative performance objectives for the production surveys were chosen to measure how practical the methods are for use in the "real" world. The picks by the different methods were compared to the ground truth for the production surveys by calculating the Probability of detection (Pd) defined as (# of detections picked by an automatic picker that are coincident to a ground truth object / # of ground truthed objects). The Background alarm rate (rBAR) defined as (# of detections picked by automatic picker not caused by ground truthed object / arbitrary number (in order to conceal the absolute number of truth items)) was calculated only for the APG data set. This was because none of the other data sets contained complete ground truth so the additional picks may or may not have been caused by a valid object. Because the calculation used an arbitrary number the actual performance metric is meaningless but useful information is gained by comparing the number among the different target picking methods. The manual method was used as the baseline to judge the efficiency of the different methods. Our goal is for the processing time (time required to run automatic picker / time required to manually pick the anomalies) to be less than 0.25. This would allow plenty of time to manually alter the automatic picks to achieve the best possible performance and still complete the analysis in less time than the using only the manual method.

We compared the fitted parameters using results from the automatic methods and the manual method to ground truth information for 80 targets at APG. The XY location and a boundary file that estimates the anomaly's spatial extent were used as inputs to advanced physics based inversion routines that output target features such as XY location, depth and size. The detection location accuracy is defined as the average horizontal distance between the picked location that is output directly from the target picking algorithms and the ground truth location. The characterization location accuracy is the average horizontal distance between the XY position output from the inversion routines and the ground truth location. Therefore, assuming good data quality the characterization location should be more accurate than the detection location. The characterization size accuracy is defined as (the absolute difference between the fitted target diameter and the ground truth diameter)/(ground truth diameter). The location, depth and size metrics were set to values that would enable the dig teams to easily find the target.

Table 1. Performance Objectives for production surveys

Type of Performance Objective	Primary Performance Criteria	Expected Performance (metric)	Actual Performance
Qualitative	Ease of use	General Observations	Some training required to set proper parameters for data processor experienced in Oasis montaj™
	Robustness	General Observations	Analysis flow not seriously interrupted by bugs
Quantitative	Probability of Detection (ground truth)	>0.9	0.15-0.99
	Background Alarm Rate (APG only)	NA	0.105-0.615
	Setup Time	<4hours	0.1 – 5.45 hours
	Processing Time	<0.25	.02-.25
	Detection Location Accuracy	90% <0.5m	63-95%
	Characterization Size Accuracy (APG only)	90% <0.3	39-44%
	Characterization Location Accuracy (APG only)	90% <0.3m	90-93%
	Characterization Depth Accuracy (APG only)	90 % <0.3m	94-97%

The WAA surveys have the similar performance criteria as the production surveys but because of differing objectives the expected performance will be different. The general objective of the WAA surveys is to delineate munitions response sites, support regulatory disposition of non munitions response sites and provide reliable data to support risk analysis and remedial cost estimation. The probability of detection metric is lower because of the different objectives. To achieve these goals airborne magnetometer data and vehicle based magnetic transect data were collected. These data sets have much lower data densities which results in the location metrics being higher than for production surveys. Also, ground truth data was not available for the WAA data sets so the Pd and Pfa were calculated using the manual picks as the baseline.

Table 2. Performance Objectives for WAA surveys

Type of Performance Objective	Primary Performance Criteria	Expected Performance (metric)	Actual Performance
Qualitative	Ease of use	General Observations	Some training required to set proper parameters for data processor experienced in Oasis montaj™
	Robustness	General Observations	Analysis flow not seriously interrupted by bugs
Quantitative	Probability of Detection (manual declarations)	>0.8	0.49-0.76
	Probability of False Alarm (manual declarations)	<0.25	0.02-0.90
	Setup Time	<4hours	0.15-5.08 hours
	Processing Time	<0.25	0.04-0.26
	Detection Location Accuracy	90% <1.5m	92-100%

3.2 Selecting Test Sites

This demonstration was performed in the Cary, NC office of SAIC (formerly AETC) on data that was previously collected on government ranges for other purposes. There are thus no regulatory, health or safety issues affecting this demonstration.

The COE was asked to provide examples of data sets that are representative of that acquired by their contractors and that support our requirements. Our criteria for the demonstration data sets were the following:

target type, size and density. A range of data density and target sizes, and a variety of target types were needed to explore the capabilities and performance of the four automatic pickers.

signal and noise levels and signal to noise ratio (SNR). Picking anomalies can be relatively easy if the SNR is extremely high, but can be very difficult if the SNR is extremely low (since identifying the positive and negative lobe of individual anomalies can be impossible). Thus, we desired a range of SNR from marginal to excellent in order to derive conclusions that can be extrapolated for future use. This same reasoning applied to the requirements for noise characteristics and data density as well.

geologic noise levels. Data sets should represent a range of geologic noise from low to high. This is critical to being able to say that the results of this demonstration are applicable for COE contractors in general.

platform. The target pickers were demonstrated on data collected from different platforms, including vehicular, man portable and airborne (e.g., helicopter-towed data from the NRL system)

data quality. Data sets were obtained that are of both Standard Contractor and Research quality in terms of sensor noise, lag, etc.

site location. The data sets should not all be from the same site.

number of targets. Each data set should contain at least 100, but ideally no more than 500, anomalies.

available ground truth. Because this proposed work was primarily concerned with the detection of all anomalies above the sensor noise floor whether they are UXO or not and not the discrimination of the anomalies, ground truth information was desirable for all data sets but not absolutely necessary. When available, we focused our analysis on comparing the anomaly picks to the ground truth information. If this information was not available, we used the manual picks as the baseline for comparison to the automatic picks. Accurate ground truth information (location, burial depth, size, and description) was needed for 50-100 targets in order to compare the location accuracy and the extracted spatial footprint of the anomaly for the different picking algorithms.

In addition to the data sets provided by the COE, the program office requested that we also include helicopter data and ground based transect data from the ESTCP WAA Pilot Program. We also ran the target pickers on a few research grade data sets that met our requirements. The following briefly describes each of the data sets.

Three of the data sets were acquired using the vehicle towed MTADS by NRL and AETC Incorporated. The MTADS hardware consists of a low magnetic signature vehicle that is used to tow an array of eight magnetic sensors that are spaced .25 meters apart. The sensor positions were determined using real-time kinematic (RTK) GPS receivers. The three data sets were collected at; 1) Open field grid of the Aberdeen Proving Ground Standardized test site in June 2004, 2) Target S1 on the Pueblo of Isleta near Albuquerque, NM in February 2003, and 3) Area near Bombing Target 4 (BT-4) at Pueblo Precision Bombing Range in Colorado in September 2005.

Another data set was collected by Sky Research and AETC Incorporated using the airborne MTADS system. The system hardware includes an array of seven magnetometers spaced 1.5 meters apart in a 9 meter boom mounted on a Bell 206L Helicopter. The sensor positions were

determined using RTK GPS technology. The data collected was in the same vicinity as the above-mentioned vehicle towed MTADS data near BT-4 at Pueblo Precision Bombing Range.

USACE contractors acquired the remaining three data sets. American Technologies Incorporated acquired data on a removal action over a 300-acre area at JPG. The data were collected using the handheld Geometric G-858G vertical gradiometer system in fiducial positioning mode. Two magnetometers were vertically separated by 2 feet and data were collected using a lane spacing of 2.5 feet. NAEVA Geophysics collected magnetic data over a Geophysical Proveout (GPO). (The USACE has requested that the site specifics be confidential.) The data were collected using a single handheld magnetometer with a line spacing of 2 feet and positioned using RTK GPS. The last data set was collected by Parsons over the Seaside area at the Former Fort Ord. The data were collected using a handheld array of four magnetometers spread cross line at 2-foot intervals and positioned using RTK GPS.

Six of these seven data sets had at least 100 anomalies and a few exceeded the 500 anomaly limit which increased our analysis time but were beneficial to the demonstration (in the case of very large data sets, we selected only a portion to analyze). The one data set (USACE GPO data) with fewer than 100 anomalies was chosen because we had a limited number of datasets (three) that were representative of data acquired by USACE contractors.

An action item for Project MM-1455 following the 6 February IPR made the following request:

> ***The Program Office is interested in a comparison between this method and the auto pickers that are being evaluated in the AETC ESTCP project "Target Picking Methods for Magnetic Data, MM-0502." ….select one or more common datasets.***

After discussions with Jim McDonald, it was decided that the vehicular data set from Isleta and the vehicular data set from APG were the two best candidates for the comparison. Additional information can be found in a White Paper submitted by Jim McDonald to the Program Office addressing the action item above for project MM-1455. Following discussions with Anne Andrews, it was decided that the Isleta data set would be used for the comparison conducted under project MM-1455.

Figure 10 to Figure 16 shows the data as color contour maps with ground truth locations overlaid with circles or crosses for each of the data sets. Table 3 below summarizes how well the data sets fit our demonstration criteria.

Table 3. Criteria and Data sets

data set/ criteria	NRL *MTADS* APG June 2004	USACE JPG	USACE GPO data	WAA Pueblo BT4 ground transects	WAA Pueblo BT4 airborne	Isleta vehicle	Seaside
target sizes	20mm 40mm 57mm 60mm 81mm 2.75in 105mm 155mm bdu28 blu26 M42 MK118	OE scrap 4.5in head, mortar burster	MKIIgrenade MKII17#bomb MKI 25#bomb range clutter	M38 MK15 GP Bomb	M38 MK15 GP Bomb	60mm 81mm 2.75in 105mm BDU33 MK76 M38 GP Bomb	37mm, 60mm, 3.5in M29, Grenade fuze, Non OE scrap
target density	low-high	low-high	low-med	low-med	low-med	low-med	low-high
platform	vehicle	handheld	handheld	vehicle	airborne	vehicle	handheld
data quality	high [research]	low [standard]	med [standard]	high [research]	high [research]	high [research]	med [standard]
SNR	low-high	low-high	low-high	low-high	low-high	low-high	low-high
geologic noise	low-med	low	low-high	low-med	med-high	low-med	low-med
number of ground truthed anomalies	All but not released to public	253	33	2	0	150	481
Survey objective	production	production	production	WAA	WAA	production	production
Picking methods	AWD, AS, Matched filter, Clustering, Manual	AWD, AS, Matched filter, Clustering, Manual	AWD, AS, Matched filter, Clustering, Manual	AWD, AS, Clustering, Manual	AWD, AS, Matched filter, Clustering, Manual	AWD, AS, Matched filter, Clustering, Manual	AWD, AS, Matched filter, Clustering, Manual

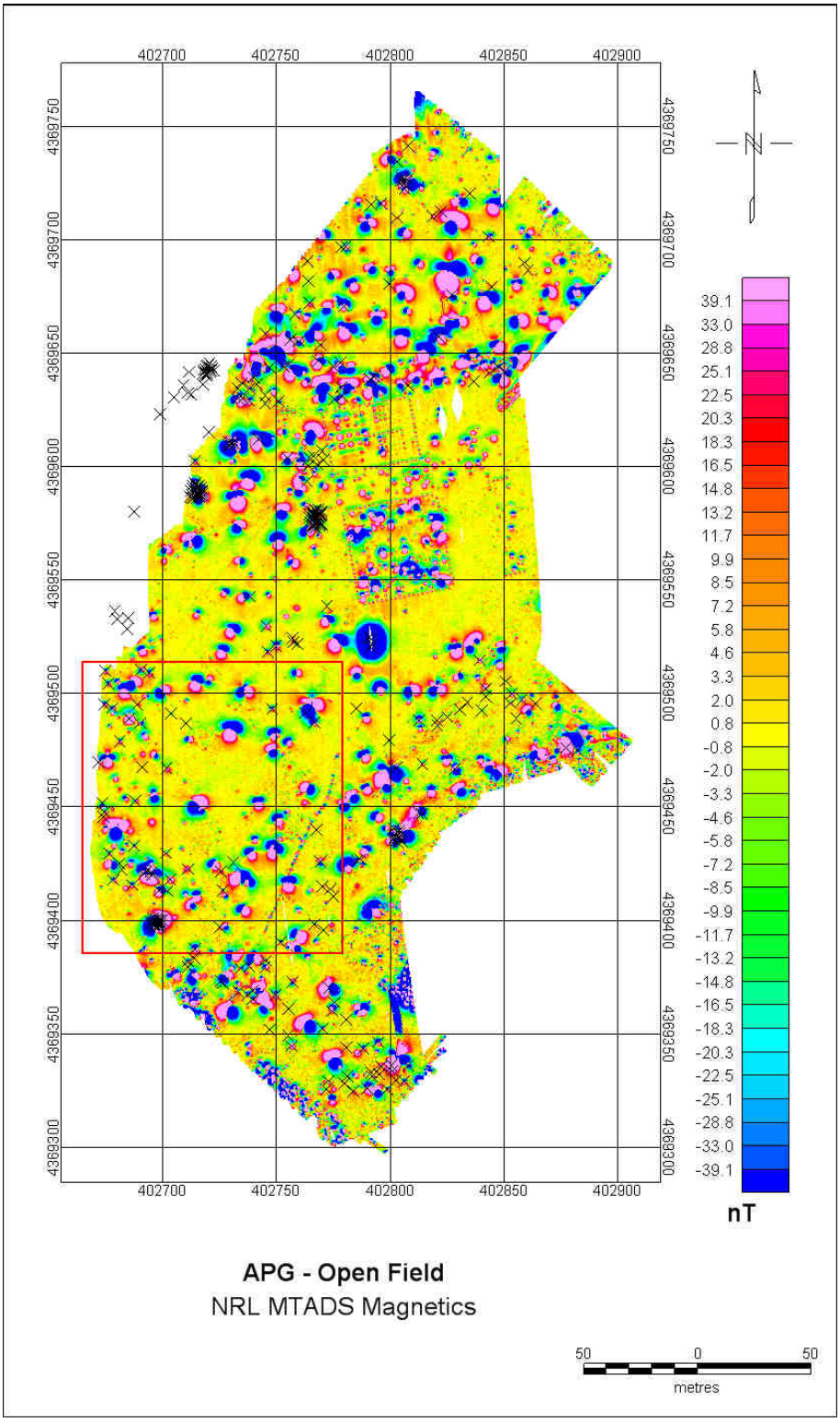

Figure 10. NRL MTADS magnetic data collected at APG Open field. The red box outlines the area evaluated by the target pickers. The crosses show publicly released ground truth.

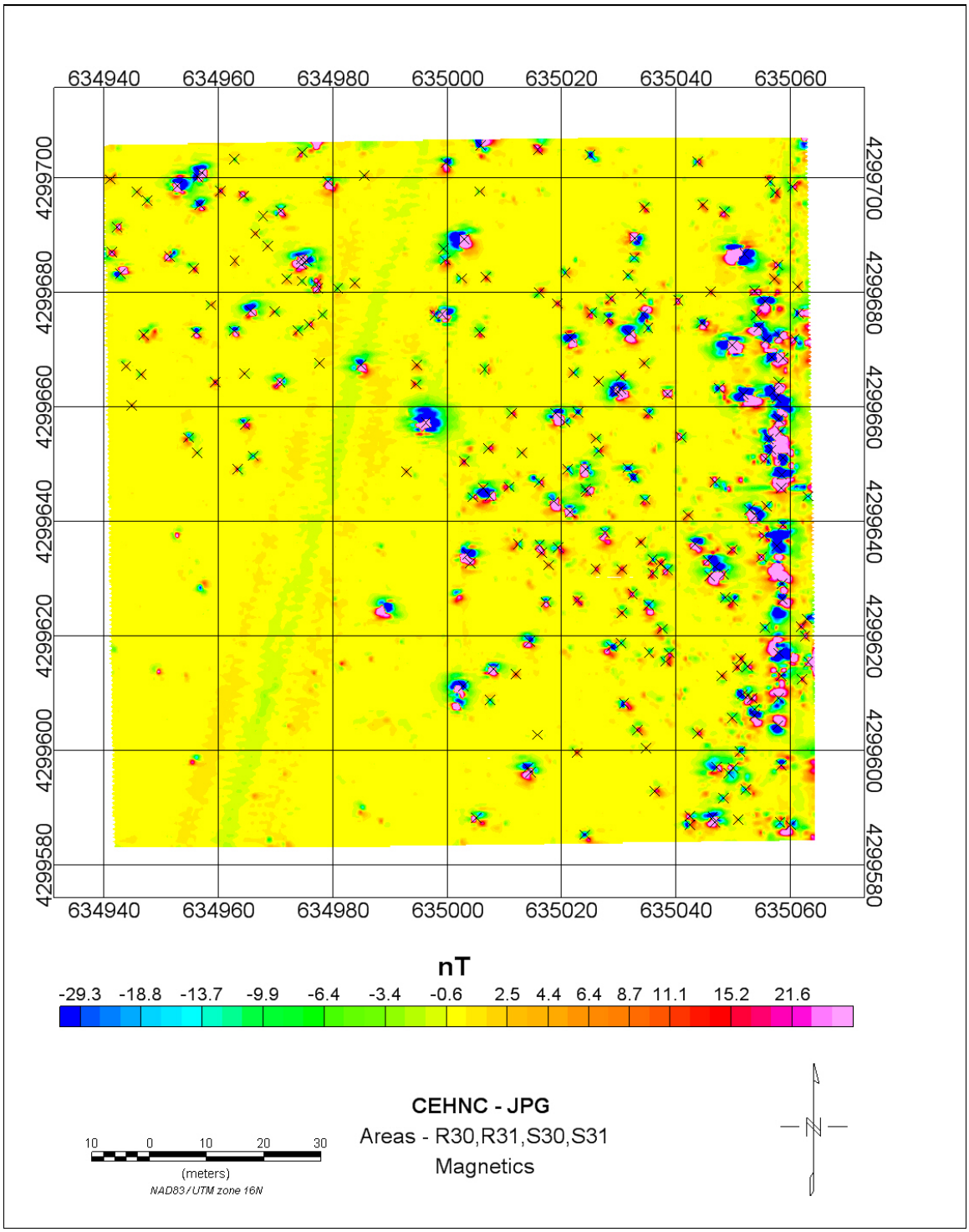

Figure 11. USACE magnetic data collected at Jefferson Proving Ground. The crosses show known ground truth.

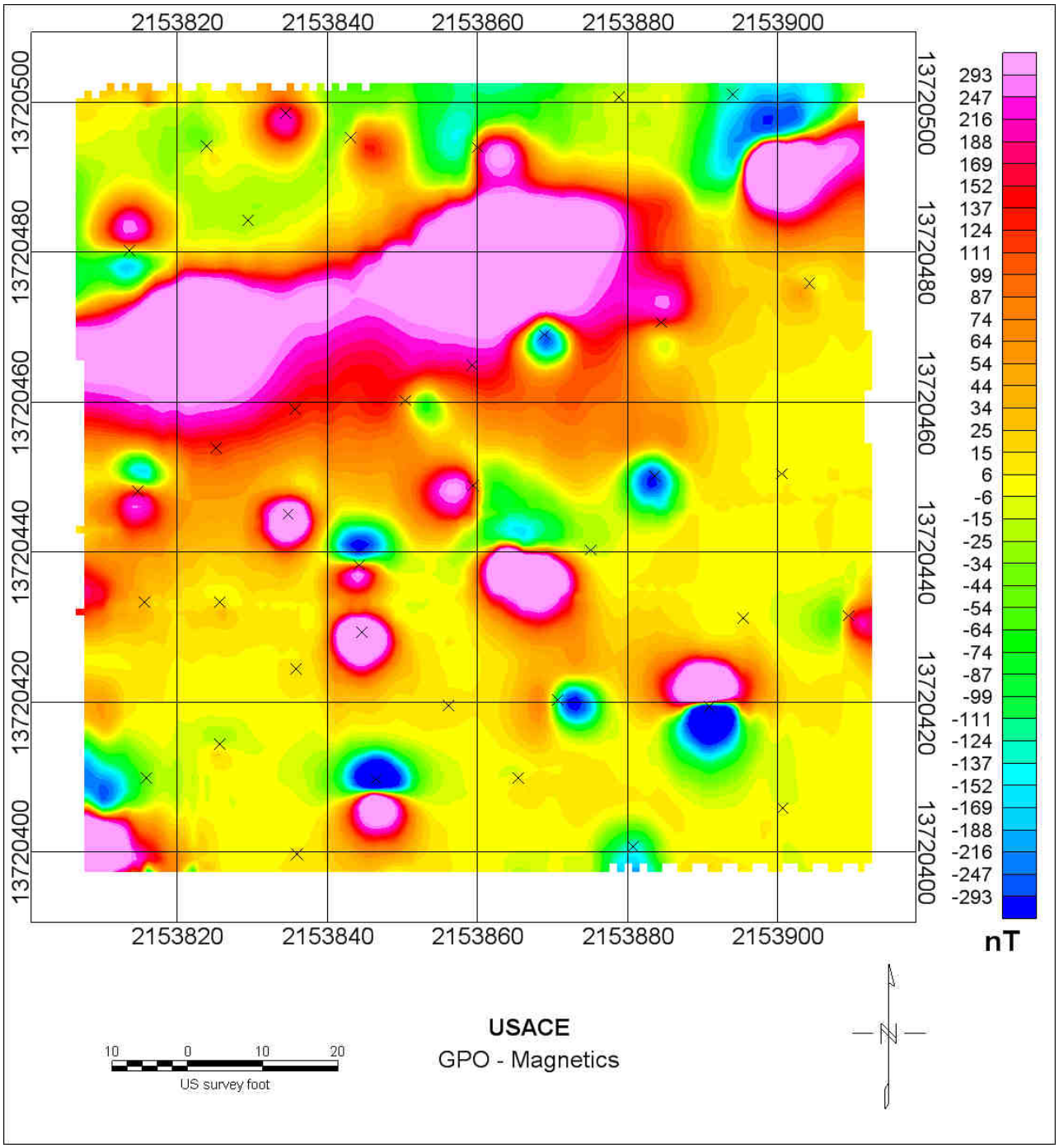

Figure 12. USACE-supplied magnetic data over GPO. The crosses show known ground truth.

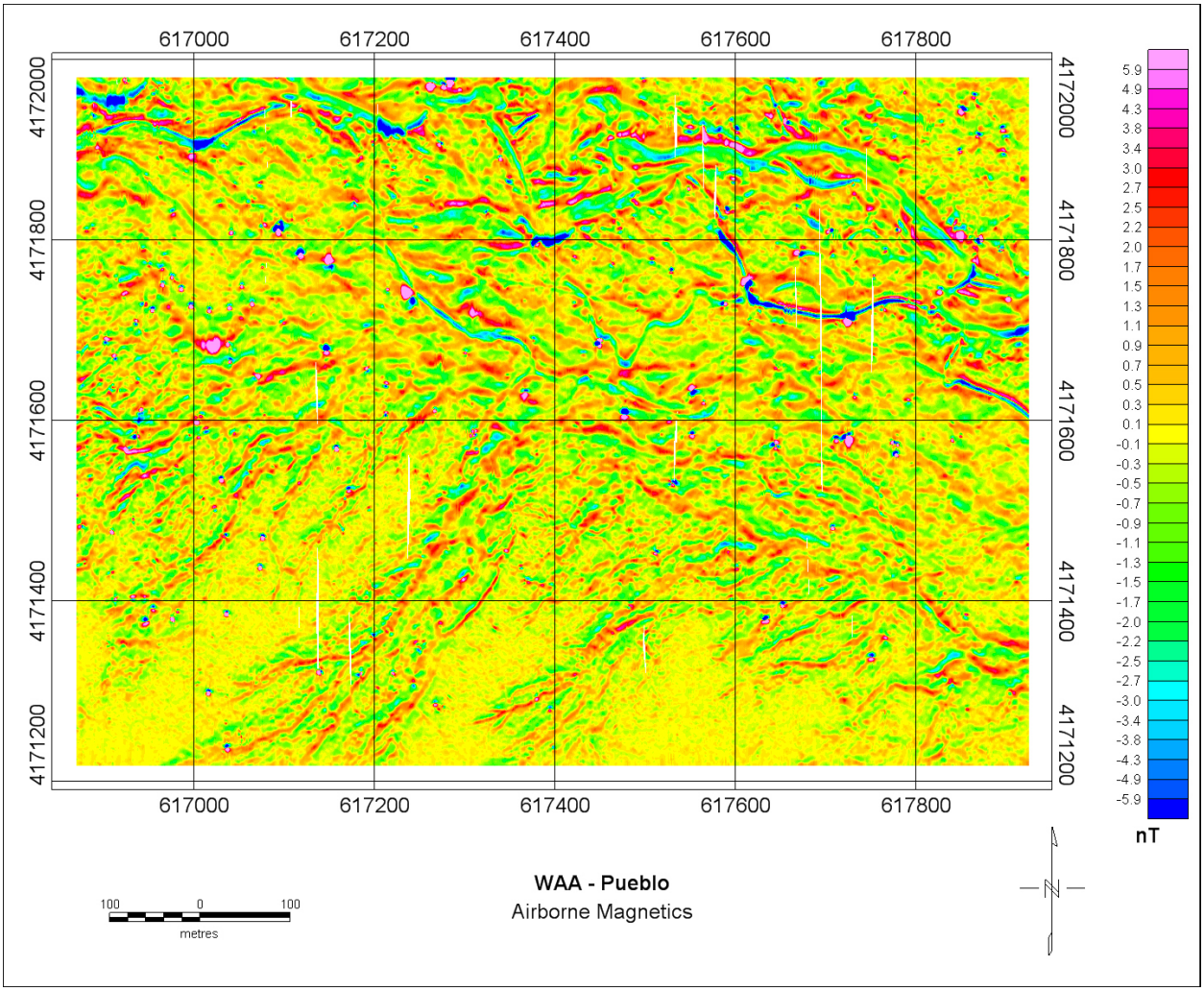

Figure 13. Airborne magnetic data from near BT4 at the Pueblo Precision Bombing Range in Colorado.

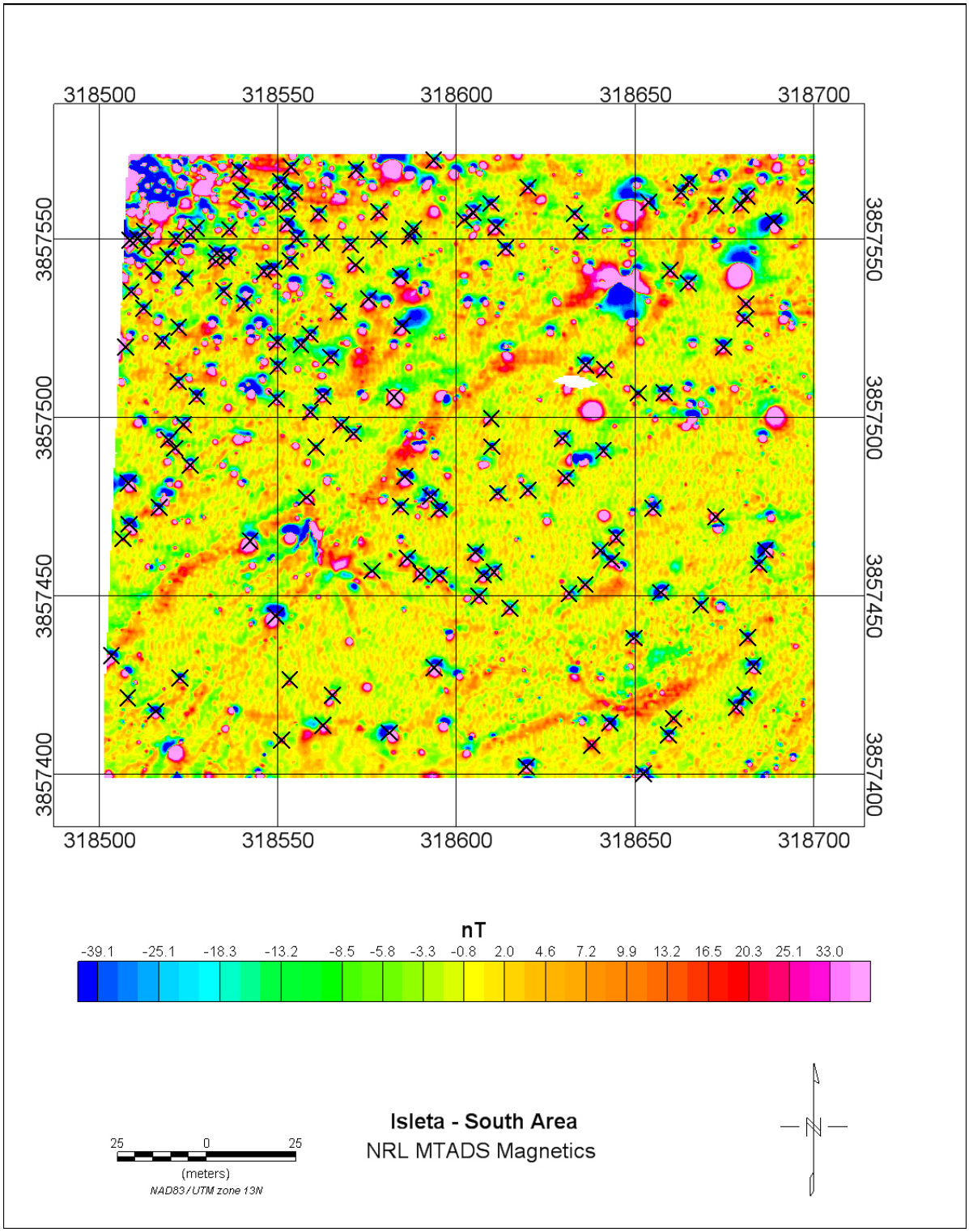

Figure 14. Vehicular magnetic data from Isleta South. The crosses show known ground truth.

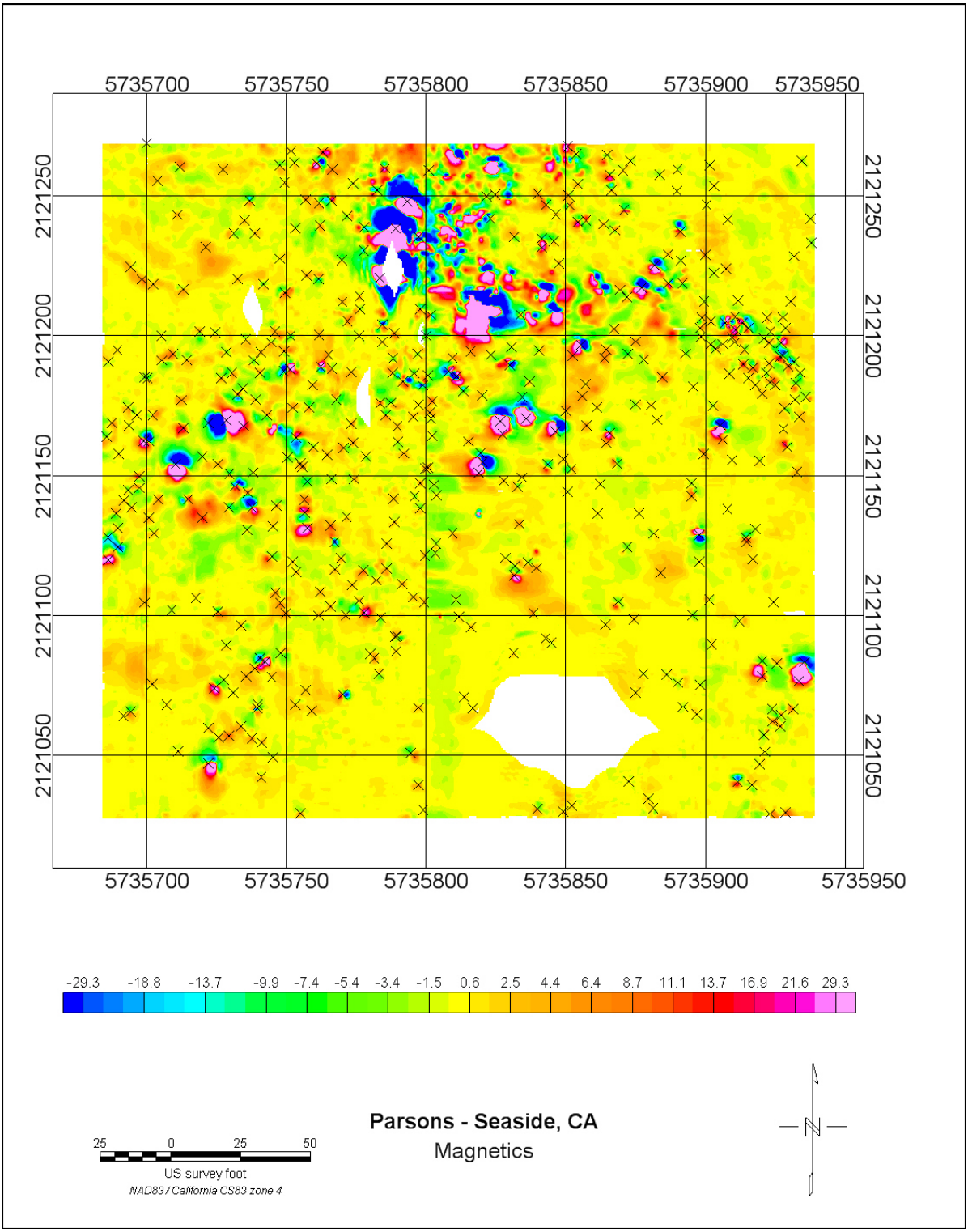

Figure 15. Magnetic data from Seaside. The crosses show known ground truth.

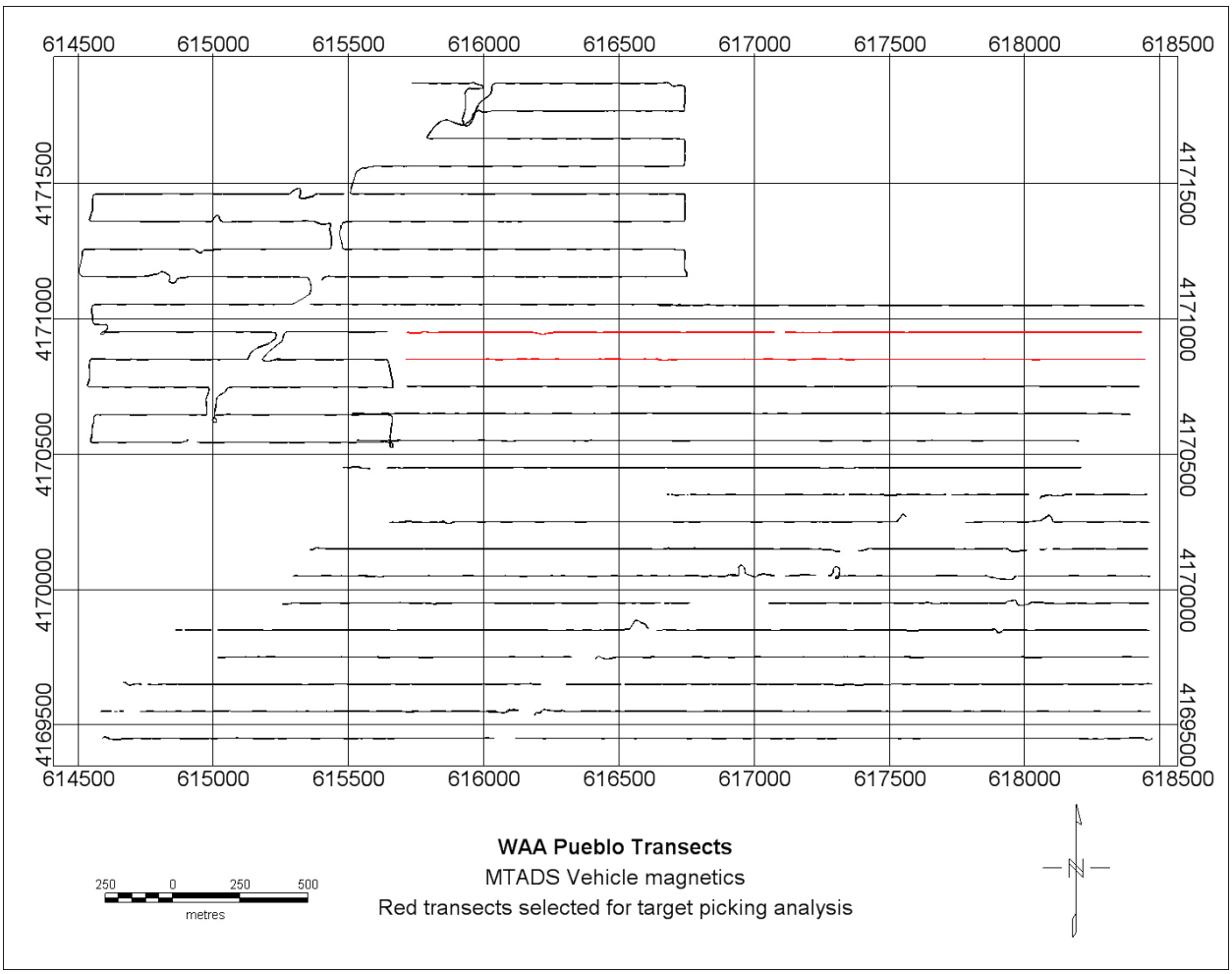

Figure 16. This map shows the location of the vehicle based magnetic transect data near BT4 at the Pueblo Precision Bombing Range in Colorado. The red lines show the transects included in this demonstration.

3.3 Test Site History/Characteristics

The area of the Aberdeen Test Site is adjacent to the Trench Warfare facility at the APG. The APG Standardized Test Site is located within a secured range area of the Aberdeen Proving Grounds. The Aberdeen Area of APG is located approximately 30 miles northeast of Baltimore at the northern end of the Chesapeake Bay. The Standardized Test Site encompasses 17 acres of upland and lowland flats, woods and wetlands. The Test Site is divided into areas including calibration lanes, blind grid test grid, open field, mogul, and wooded areas. Additional details regarding the layout of the APG Standardized Test Site can be found at http://aec.army.mil/usaec/technology/uxo03c01.html.

The former Pueblo Precision Bombing and Pattern Gunnery Range #2 consists of a total of 67,769 acres and is located approximately 20 miles south of La Junta, Colorado, in Otero County. The closest community is La Junta, a rural town with a population of about 7,637. The MRA was used by local populations for cattle grazing until the War Department assumed control of the lands to construct the Pueblo Precision Bombing and Pattern Gunnery Range #2 (1942 to 1946).

The Pueblo of Isleta is located in north-central New Mexico, approximately 10 miles south of Albuquerque. The reservation is bordered on the north by the Sandia Military Reservation, which includes Kirtland Air Force Base, the Manzano Mountains on the east, and the Rio Puerco and Laguna Pueblo Reservation on the west. The area that contains target S1 comprises an area of approximately 7000 acres that were leased from the Tribe in the 1950's for use as a target bombing range for aircraft from Kirtland. The site consists of open, semi-arid terrain. The area is relatively flat, open grassland with elevation increasing from 5100 feet above sea level on the west, to 5400 feet above sea level on the east. Documentation in Bureau of Indian Affairs files indicate that this area was used as a practice bombing range from 1956 to 1961 to determine the performance of fast aircraft during bombing runs. In the 1960's, Kirtland collected and piled visible ordnance debris for removal. Up to 2 tons of practice bombs and ordnance waste per acre were removed but no explosive ordnance was found.

JPG, a 55,265 acre facility established in December 1940, fired its first round 5 months later, and operated until 1995. JPG's primary mission was to perform production and post-production tests of conventional ammunition components and other ordnance items and conduct tests of propellant ammunition/weapons systems and components for the U.S. Army. JPG is located in southeastern Indiana, approximately 8 miles north of the Indiana-Kentucky border and about 5 miles north of Madison, Indiana. The installation occupies parts of Jefferson, Jennings and Ripley Counties, and is about 17.2 miles in length and ranges from 4 to 6 miles in width. Lands surrounding JPG are predominantly farmland and woodlands, with some small towns and rural residential land use nearby.

The former Fort Ord is located 80 miles south of San Francisco and occupies approximately 28,000 acres adjacent to Monterey Bay and the cities of Marina, Seaside, Sand City, Del Rey

Oaks, and Monterey. Fort Ord became a training installation in 1917 and was used to train Army infantry, cavalry, and field artillery divisions for WWI and II, Korea, Vietnam, and Desert Storm. The topography of the Seaside area at the former Fort Ord is flat to gently rolling terrain. The vegetation is comprised of maritime chaparral and oak woodlands.

3.4 Present Operations

APG is currently home to a diverse array of weapons development and testing programs. The APG Standardized Test Sites have been – and continue to be - utilized to benchmark a significant number of technologies and contractors.

The former Pueblo Precision Bombing and Pattern Gunnery Range #2 are primarily Federal lands that are managed by the U.S. Forest Service as the Comanche National Grasslands, with portions leased to private owners or owned by the State of Colorado. There is some private ownership of parcels in the middle of the study area. All privately owned lands within the study area are used for cattle grazing. The general recreational use of the site is very broad and encompasses hiking, camping, and use by all-terrain vehicles. The entire site is also used for cattle grazing, which may require well drilling and pipe laying to supply water to the cattle, as well as fences.

The Isleta Pueblo is currently home to the Tigua tribe. The area of interest is primarily used for raising cattle, horses and sheep by Isleta ranchers.

In 1989, JPG was identified for base closure under the BRAC program. The base was closed in 1995 and the property disposal process, which included UXO removal actions, began the following year. The U.S. Fish and Wildlife Service entered into Memorandums of Agreement with the Army and established the Big Oaks National Wildlife Refuge to help ensure a balance use of the land and maintenance of the natural resources. The Jefferson Range air to ground training area is also currently used by the Indiana Air National Guard.

In 1991, Fort Ord was included on the BRAC list and closed in 1994. Since the BRAC listing and closure of Fort Ord, cleanup operations have been performed to address explosive hazards and to prepare Fort Ord property to be transferred to federal, state, and local agencies and the surrounding Monterey County communities.

3.5 Pre-Demonstration Testing and Analysis

This Demonstration used target picking algorithms that have been prototyped and undergone limited testing during previous research programs. Three of the algorithms (AWD, Matched filter and clustering) have been seamlessly integrated into Oasis montaj™.

Prior to the demonstration, we verified that the Oasis version produced the same results as the prototype code. The AWD and Matched filter actually called the same DLL's as the prototype. Only the clustering algorithm needed significant recoding in order to run in the Oasis montaj™ environment.

3.6 Testing and Evaluation Plan

3.6.1 Demonstration Set-up and Start-up

Not applicable to this demonstration.

3.6.2 Period of Operation

The schedule for the major items in the Demonstration is given in tabular form in Table 3-3.

Table 4. Target Picking Demonstration Schedule

Date	Action
November 2006	Receive approval for Demonstration Plan.
December 1-15, 2006	Phase 1 testing using a 60 dipole synthetic data set
December 15,2006 – January 15, 2007	Applied analytic signal and matched filter algorithms to all demonstration data sets.
January 15 – February 1, 2007	Applied clustering algorithm to 3 of 7 demonstration data sets
January 15 – February 15, 2007	Applied AWD algorithm to all demonstration data sets
May 2007	Presented preliminary results at IPR
July 2007	Received new TAA with Geosoft and fixed memory related bug in clustering algorithm
July 15 – August 1, 2007	Applied clustering algorithm to final 4 demonstration data sets
March 2008	Submitted ESTCP Draft Final Report

3.6.3 Area Characterized or Remediated

The demonstration was broken up into two phases. The first phase used the 60 dipole synthetic data set described in section 2.2 to explore the parameter space and optimize the algorithms for the four automatic target pickers. The result of phase one was a set of starting parameters that was used in phase two. The second phase applied the target pickers to the seven magnetic data sets described in section 3.2 using the parameters output from phase one. Because each data set has its own unique data characteristics the starting parameters were adjusted iteratively to

achieve the best performance. The knowledge gained from phase one was used to guide these adjustments.

3.6.4 Residuals Handling

Not applicable to this demonstration.

3.6.5 Operational Parameters

Each of the target pickers that were evaluated during this demonstration has parameters that need to be tuned to achieve optimum performance. The starting parameters were calculated during phase one of the demonstration. Even though the different target pickers have different parameters the process of adjusting the starting parameters to achieve the best performance was the same. The process involved running the algorithm on the data sets (for large data sets a small portion of the data was used) and changing the parameters based on a visual review of the results. Several iterations were run until the optimal parameters were chosen. The visual review involved looking at the types of anomalies that were visible in the data and changing the parameters to select the desired anomalies. We also looked at all the automatic picks and determined if they were valid or in the noise levels of the data set and adjusted the threshold accordingly.

Figure 17 and Figure 18 show the parameter dialog boxes for the AWD and clustering algorithms, respectively. The match dipole algorithm iterates over six depths so the only parameter to set is the size of the filter box. Once the match filter output and derived model parameters are calculated they may be combined using Boolean logic to minimize the processing artifacts in the match filter output that are caused when the filter window contains only a portion of the dipolar signal. The only parameters to set for the analytic signal are the number and type of filters to apply to the analytic signal grid prior to running the peak picking algorithm.

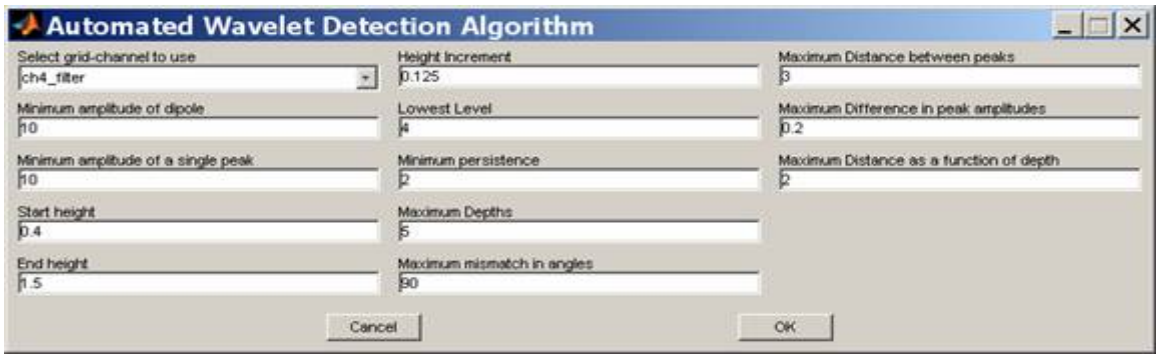

Figure 17. Parameter dialog box for AWD algorithm.

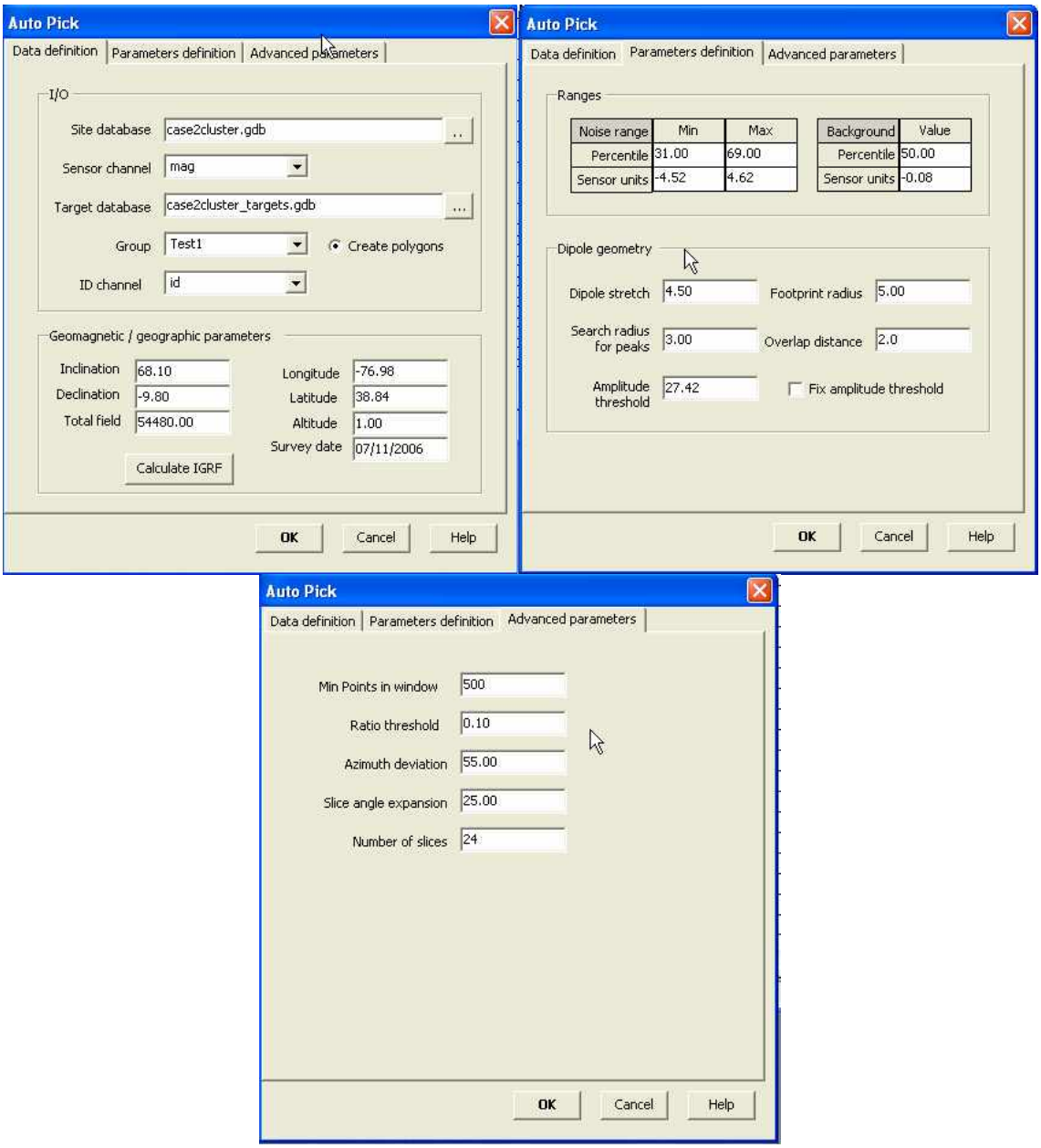

Figure 18. Parameter dialog boxes for clustering algorithm.

3.6.6 Demobilization

Not applicable to this demonstration.

3.7 Selection of Analytical/Testing Methods

Not applicable to this demonstration.

3.8 Selection of Analytical/Testing Laboratory

Not applicable to this demonstration.

4. Performance Assessment

4.1 Performance Criteria

Table 5. Performance Criteria for this Demonstration

Performance Criterion	Description	Primary or Secondary
Ease of Use	Describe the processing flow and the anticipated skill level required. The goal of the program is that data processors experienced with data analysis and Oasis montaj™ could utilize the software by reading a manual but without hands-on training.	Primary
Robustness	No major bugs that artificially limit the analysts' ability to conduct analysis.	Primary
Probability of Detection (Pd) ground truth	(# of detections picked by automatic picker that are coincident to ground truth target)/(# of ground truth targets)	Primary
Probability of Detection (Pd) manual	(# of detections picked by automatic picker that are coincident to a manual pick)/(# of detections picked manually by expert)	Primary
Background Alarm Rate (rBAR)	(# of detections picked by automatic picker but not matching ground truth object)/ (arbitrary number)	Primary
Probability of False Alarm (Pfa) manual	(# of detections picked by automatic picker but not picked by expert)/ (# of detections picked manually by expert)	Primary
Setup Time	Time required to setup optimum parameters	Secondary
Processing Time	(Time required to run automatic picker)/(time for commercial expert to pick anomalies)	Primary
Detection Location Accuracy	The average horizontal distance between picked and ground truth location	Primary
Characterization Size Accuracy	(The absolute difference between the fitted target diameter and the ground truth diameter)/(ground truth diameter)	Secondary
Characterization Location Accuracy	The average horizontal distance between the fitted XY position and ground truth location.	Secondary
Characterization Depth Accuracy	The average difference between the fitted depth and ground truth depth.	Secondary

For the baseline manual picking demonstration, the objective for both the production and WAA surveys was to identify all anomalies that warrant further investigation and analysis. In the analysis for Standardized Test Site demonstrations, this is referred to as the Response Stage. The person performing this target selection was an experienced analyst. The analyst was asked to decide on the threshold of the given data set, document the rationale behind the choice, and then

select all anomalies above this threshold. The threshold was based on the overall noise levels of the data set and was different for each data set. It was set at a point just above the background noise to maximize the number of detections while minimizing false alarms. The analyst estimated the location of each anomaly, using his preferred analysis environment. The analyst did not have a method to estimate the spatial footprint of each anomaly, so SAIC made these estimates using the analyst's dig sheet and data.

All the production survey data sets compared the declarations made by the different methods to the available ground truth to calculate the Pd. All the WAA survey data sets compared the declarations made by the automatic pickers to the picks made by the commercial expert to calculate the Pd and Pfa because ground truth did not exist. The maximum Pd is 1 but the maximum Pfa could be greater than 1 because it is based on the number of manual picks. A high Pfa means the automatic picker selected a lot of anomalies that were not picked by the manual method. In general a high Pfa is bad because it most likely means that the automatic pickers started picking noise in the data. To verify this we analyzed the false alarms to see if they were due to picking noise in the data or caused by valid targets that the manual method missed.

The ground truth for APG is well documented. For this reason the rBAR and location accuracy were also calculated for the APG data set. Because only a select number of targets have been released to the public the scoring for the APG data set will be done by the program office.

This demonstration resulted in 32 sets of scores. A set of scores for each target picking method (5) run on each of the production survey data sets gave 25 scores. The WAA airborne data was compared to the manual picks and produced 4 sets of scores. Finally, the WAA transect data consisted of only 3 sets of scores because the matched filter algorithm was not be applied and the other automatic methods were compared to the manual picks.

4.2 Performance Confirmation Methods

The 'Ease of Use' criterion reports the analysts' experience regarding the time and experience required for a user to learn to use each automatic target picker and set up optimum parameters as well as the level of user interaction required. It will be derived from notes taken by the analysts.

The 'Robustness' criterion reports the analysts' experience relating to bugs and program deficiencies that hinder efficient data analysis. The Robustness report will be derived from notes taken by the analysts.

The Probability of detection, background alarm rate, and location and depth-accuracy criterions will be calculated from the results of our analysis and the provided ground truth information.

Analysis time will be logged manually. To provide meaningful baseline metrics, we will separately record time spent A) selecting the optimum parameters for each target picker, and B) computational time to execute the target picker.

A successful demonstration would be defined as having some or all methods meeting the primary performance criteria previously outlined in Table 1, Table 2 and Table 5 for some or all of the data sets. Areas with high target density where ambiguous results impeded our analysis were removed from the ground truth comparison. We conducted a failure analysis on the data sets that did not meet the performance criteria. The failure analysis determined if data quality was the determining factor in not reaching the performance criteria or if the problem resided in the target picking algorithm or other factors. If the failures were due to data quality the demonstration was still deemed successful and these limitations were noted in the final report. It is not fair to penalize the target picking algorithms for poor data quality.

4.3 Data Analysis, Interpretation, and Evaluation

4.3.1 Phase 1 – Synthetic Magnetic data

The first phase of the demonstration used the 60 dipole synthetic data set described in section 2.2 to explore the parameter space and optimize the algorithms for the four target pickers. We varied their different parameters to evaluate and document their effect and to determine if certain "rules of thumb" could be developed. For example, changing certain parameters may allow deeper or larger targets to be selected. This information was then used to guide us when applying the target pickers to the data sets in the demonstration. In addition to this knowledge, phase one was also used to select a set of starting parameters for each automatic picker that was used in phase two. The performance of the different automatic target pickers is summarized in Figure 19. As we can see none of the automatic target pickers detected all the targets. The analytic signal and the wavelet produced the best results followed by the clustering algorithm and finally the matched filter. All 60 targets cannot be recovered by any of the target pickers without including thousands of false alarms because the amplitudes of the missed targets are of an amplitude comparable to that of the background noise. The SNR for the 11 targets that were consistently missed by all the target pickers ranged from -1.7 to 9.2. The SNR is defined as 20xlog(peak signal/noise) where the noise is the standard deviation of the synthetic noise within a 3 meter circle surrounding target location. In general the smaller 20mm and 40mm targets were missed.

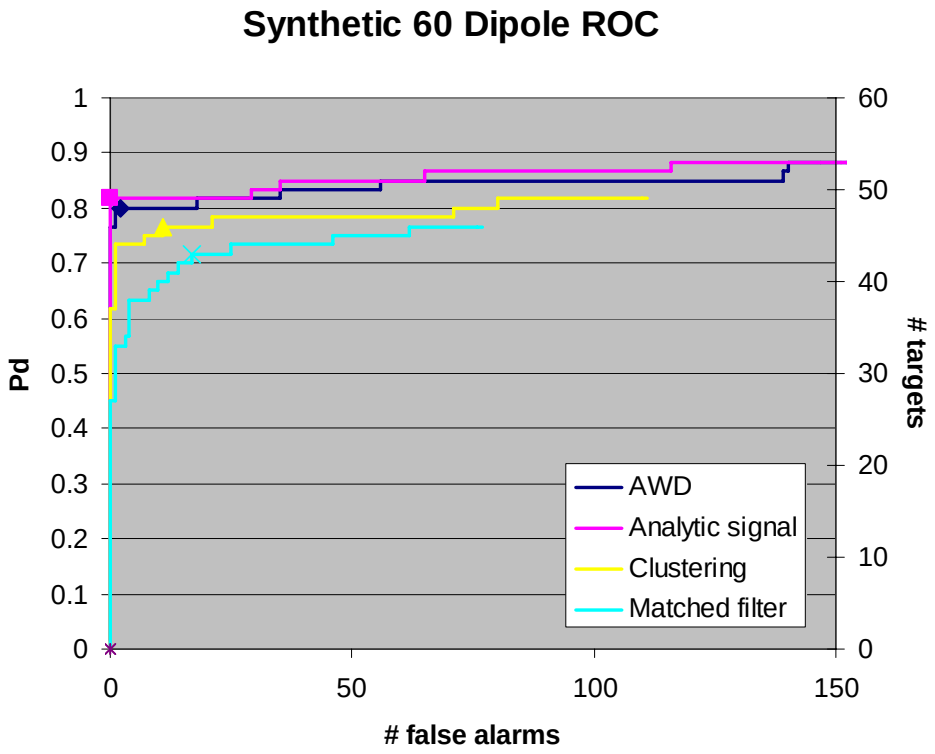

Figure 19. Receiver Operating Characteristic (ROC) curve of the different target pickers for the synthetic 60 dipole data. The symbols along each line represent the analyst's threshold value.

4.3.1.1 Automated Wavelet Detection algorithm

Target picking with the AWD algorithm is a two stage process: the first step is the detection of anomalies above a defined threshold; the second is the Upward Continuation (UpC) of these anomalies to determine their persistence and convergence to an original dipole. Performance of AWD is controlled by a set of parameters that the user can adjust to the characteristics of a data set. During our testing on the synthetic data we have found the following generalizations for the different parameters.

The two parameters that have the largest effect on the number of detected targets are the "minimum amplitude of dipole" and the "minimum amplitude of a single peak". These parameters define the amplitude threshold for an anomaly to be considered as a potential target. The values for these amplitudes should be set by the user to a value above the estimated noise in the dataset.

The AWD algorithm searches for the negative peak associated to a positive in a circle of radius defined by the parameter "maximum distance between peaks", which can be increased when

AWD obviously fails to associate anomalies for the same target. For a dipole or “monopole” (actually a vertical or near-vertical dipole) anomaly to be identified as a target, the peaks of the anomaly must persist at several levels through UpC. Furthermore, the origin of these peaks must converge to dipoles within a given depth and distance range and the peaks must move together within a given angular tolerance.

The parameter "start height" defines the first level at which UpC should be started. We have found that it is best to keep that parameter to 0 if the noise level in the data is not too high in order to maximize the probability of detection; otherwise the parameter can be increased to a survey pixel size (e.g., 0.125 m) to filter out small short wavelength noise.

The parameter "end height" generally requires no change unless one is particularly interested in large deep targets, whose signal would persist at high UpC levels, or to increase the potential of detection.

The "height increment" for the levels of UpC should be set to a pixel size, or modified to increase/decrease the chance of an anomaly to be kept as a target. This parameter works in combination with the "minimum persistence", which defines the number of levels through which an anomaly must persist to be identified as a target. The latter can be increased when data are contaminated with short wavelength noise, e.g., as for the synthetic data set.

The "lowest level" can also be increased/ decreased to include/exclude potentially shallow targets with small amplitude.

Selection of deep targets is set by the "maximum depths" parameter.

Positive and negative peaks are associated if they have the same estimated source. In practice, noise, interference and limited resolution of the data can limit convergence. The algorithm requires instead that sources converge within a given depth (parameter "maximum difference in peak amplitude", set to 0.25, can be lowered to 0.2) and distance range (parameter "maximum distance away as a function of depth", set to 1.5, can be increased to 2). Peaks must also move toward one another across scales within a given angular sector (parameter "maximum mismatch in angles", set to 90 degrees, up to 120 degrees). These parameters can be altered when changing the "maximum distance between peaks" is ineffective at helping AWD associate anomalies for the same target.

Using the above knowledge 45 of the 60 targets can be picked without any false alarms, which is an improvement over the results from the shakedown described in section 2.2.1. Additional targets can be detected at the cost of including false alarms: 48 targets are found with 2 errors (Figure 20), 49 for 18. Among the key parameters, the minimum amplitude of the dipoles and single poles are the most important ones. For this synthetic dataset the threshold has to be set quite high at a minimum of 30nT to limit picking of noise artifacts. Up to 48 targets can be picked in that manner, depending on the value of the other parameters. Parameters for the best results are presented in Table 6(for pixel size of 0.125 m).

Additional targets were picked up by lowering the amplitude thresholds. For instance, 49 targets were obtained with minampdipole = 25 nT and minampsingle = 20 nT, with all other parameters being the same. False alarms can be weaned out by setting a high value to the minimum persistence, e.g., 7 when the default value is 2.

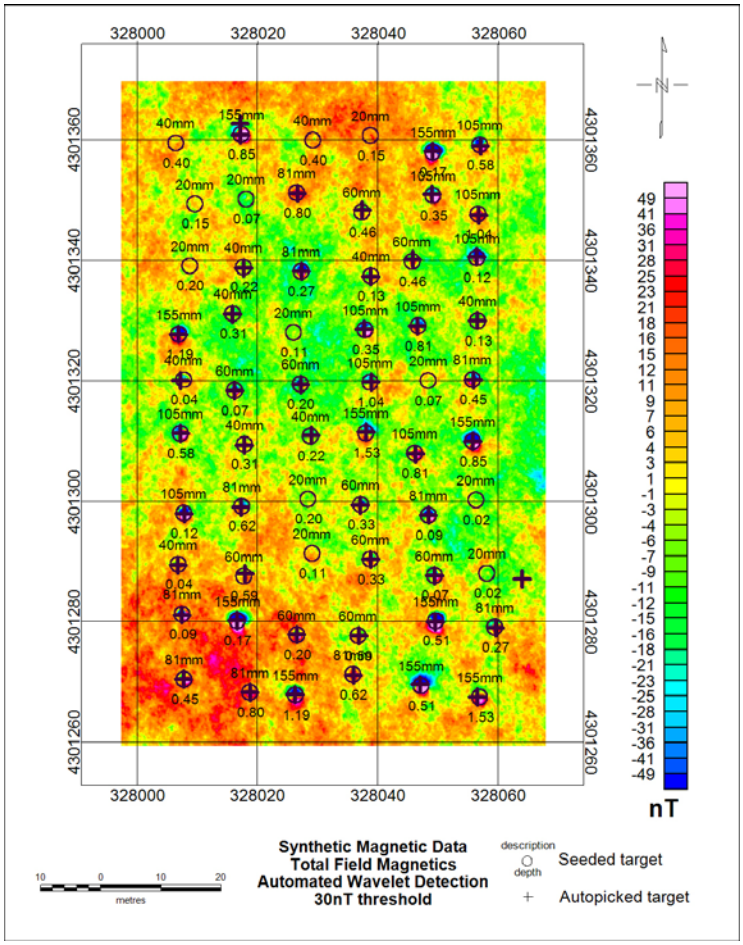

Figure 20. Results of AWD algorithm on the synthetic magnetic data. The true locations are plotted as circles and the automatic picker detections are plotted as "+"

4.3.1.2 Clustering algorithm

The clustering parameters can be divided into three main groups: target detection, data extraction and target overlap detection. The main parameters that affect target detection are the amplitude threshold, search radius, and dipole stretch. During our testing the first two behaved as expected. Either increasing the amplitude threshold or increasing the search radius decreases both the number of true targets found and the number of spurious targets. The latter tend to fall off faster at low values. We found that a good amplitude threshold was approximately 3 times the noise range of the data. We estimated the noise range by subtracting the amplitude at the 69th

percentile from the amplitude at the 31st percentile of the cumulative distribution function (CDF). These values are automatically calculated and displayed in the input parameters dialog box for the user to either accept or override. The values can be overridden by either altering the percentiles used or by inputting the actual amplitude threshold to be used. The search radius should be set to at least as large as the cross track spacing of the survey data; otherwise, the algorithm may be calling something a peak by only looking up and down track. Ideally, the search radius should also be less than the separation between adjacent dipoles because only the largest dipole within the search radius is flagged as a target. Unfortunately, these two criteria may be exclusive. If so, the user must choose which one to apply. The dipole stretch should be large enough to cover the widest observed lobe separation. If the dipole stretch is set too small the positive and negative lobes of certain large targets may be not get associated and will be counted as separate targets. On the other hand, a dipole stretch that is too large may increase the number of possible lobes of opposite sign that is associated with each peak. This in turn will increase the possibility of associating the wrong two lobes. Also with too large a dipole stretch, single lobes will often find an erroneous secondary lobe that is too far away in the secondary association. This results in errors for the final calculated location for those dipoles.

The parameters that mainly affect data extraction are the footprint (maximum radius), the noise range, and the number of slices. The footprint should be large enough to cover the largest visible dipole. The noise range as describe above is a good starting point. It is used both as a stopping criterion in moving out from the peaks, and in the second association. The data within a circle around each peak is divided into slices. The algorithm sorts all the data within each slice by distance to the peak. For each slice the algorithm looks down the sorted data for a gradient crossover to define the stopping criterion for the cluster. During our extensive testing we found that using 24 slices gives good results and should not need to be changed.

The parameters that control the overlap detection are ratio threshold, slice angle expansion and overlap distance. These parameters only determine if the overlap flag is set and do not affect the number of targets detected or their association. For this reason they are not as important and the default settings are normally satisfactory.

The clustering algorithm found 46 of the 60 targets with 11 false positives using a 34nT amplitude threshold as shown in Figure 21. Among the parameters, the amplitude threshold and search radius were the most important for this data set. One target (2nd row from bottom and 4th column) had a pick that was just outside the 1 meter tolerance. The positive peak of this dipole was correctly selected but was associated with the wrong negative peak causing the final location error.

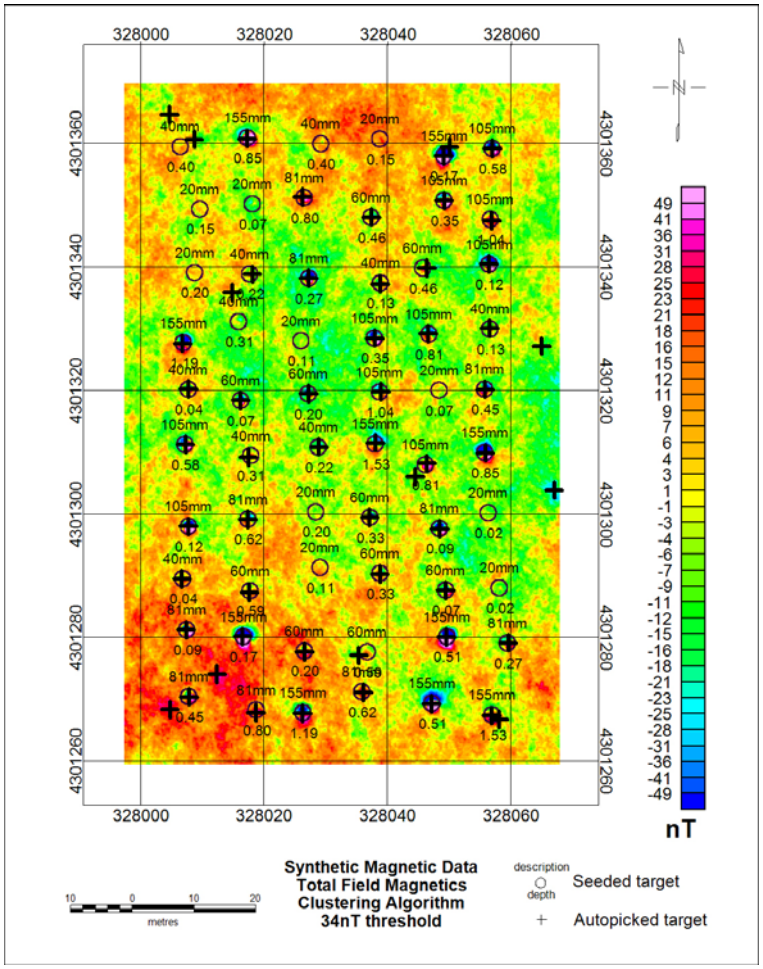

Figure 21. Results of clustering algorithm on the synthetic magnetic data. The true locations are plotted as circles and the automatic picker detections are plotted as "+".

4.3.1.3 Analytic signal

The analytic signal method only has two parameters to change: 1) the number of filters to apply to the analytic signal grid and 2) the amplitude threshold for the peak picking algorithm. To test these parameters, the Geosoft peak detection routine was run using the analytic signal grid with 0 to 5 passes of a 3x3 Hanning filter applied. The amplitude threshold for the peak picking routine was set to value sufficiently small to pick at least 1000 targets. The actual value of the amplitude threshold was different with each grid because the grid amplitudes decreased with each successive pass of the Hanning filter. The picks were sorted from largest to smallest based on the analytic signal amplitude and the results are shown in Figure 22. It is clearly seen that at least one pass of the filter is needed to get decent results. In this case, two passes of the filter shows a definite improvement over one pass. There does not appear to be much advantage in applying three or more filter passes.

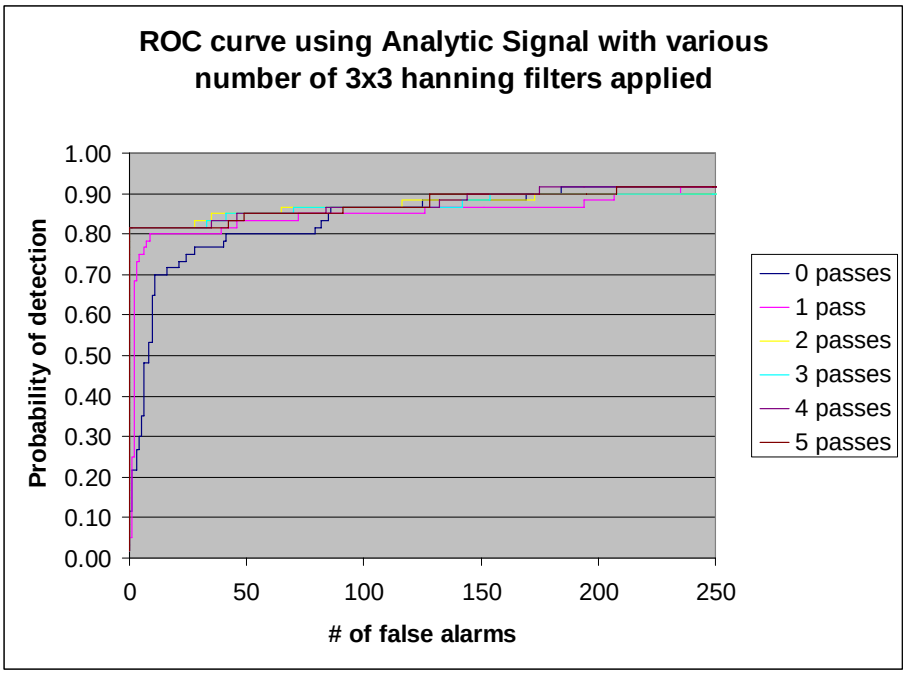

Figure 22..ROC curve of the analytic signal algorithm applied to the 60 dipole synthetic data set using different number of 3x3 Hanning filters.

As stated in Section 2.2.4, the analytic signal algorithm found 49 of the 60 targets with no false positives using a 45nT/m amplitude threshold. Two passes of a 3x3 Hanning filter were applied to the analytic signal grid. The targets missed consisted of nine 20mm at various depths and two 40mm that were buried at 0.4 meters.

4.3.1.4 Matched Filter Algorithm

The matched filter algorithm has only one main parameter (filter box size) to set but because it runs on the gridded magnetic data care must be taken when generating the input grid. We found that a good starting grid cell for the matched filter input grid is 1/4 of the mean track spacing. Increasing the grid cell size will decrease the processing time because the grid will contain fewer grid cells. But if the cell size is set too large, smaller anomalies begin to disappear from the grid. Data gaps in the input grid create problems for the matched filter algorithm because they are enlarged by one-half the size of the filter box window during the matched filtering process. As a result, anomalies near the margin of data gaps will be missed if the data gaps are not interpolated during the gridding process. By allowing data gaps to be interpolated during the gridding process, the problems associated with data gaps are minimized. Oasis montaj™ allows the user to define the distance over which grid values are interpolated. The built in Oasis montaj™ interpolation routines are based on published schemes (Briggs, 1974 and Swain, 1976).

A filter box is created around each point in the magnetic grid and the data within the filter box is convolved using a dipole based model. The output of the matched filter algorithm is maximized

at locations that show a good approximation to the dipole model. The filter box size should be set large enough to cover the largest dipole but not too large because the run time scales as the filter box size squared. So using a slightly smaller filter box that does not degrade the results will greatly decrease the run time. Adjusting the filter box in conjunction with the input grid cell size described above will improve the overall run time of the algorithm.

The matched filter output data, shown in section 2.2.3, clearly indicated the presence of some of the 60 dipoles but processing artifacts are also apparent. These artifacts are evidenced by the numerous false alarms and the multiple picks surrounding some of the larger anomalies. These additional picks occurred even though the output grid was filtered several times to smooth out the errors. The artifacts occurred when the filter window contained only a portion of the dipolar signal (typically a single positive or negative lobe) that is associated with the causative source. When this happened, the filter incorrectly created the missing lobe, which produced erroneous output values. The matched filter algorithm stored the output filter results and all derived model parameters in a database for each grid cell. These model parameters were used to refine the filter output. The matched filter output was divided by the Chi square model error ('Chisq') to produce the ratio ('MFoutput/Chisq') shown in Figure 23. When the filter window coincides with the center of a dipolar signal, the error term is dramatically reduced. In other words, the derived model closely matches the input (measured or synthetic) data when it is directly on top of the center of the dipole. As observed in the figure, the anomalies now possess a very high signal-to-noise ratio and the processing artifacts are reduced.

The MFoutput/Chisq grid was input to Geosoft's peak detection routine. As with the analytic signal, the input grid needs to be filtered two or three times with a 3x3 Hanning filter to produce the best results. A very small threshold was used and the results were sorted from largest to smallest ratio amplitude. The results were analyzed to locate the threshold value that maximized the targets detected while minimizing the false alarms. Using a threshold value of 2.1 the matched filter method detected 43 targets with 17 false alarms. Compared to the results of using only the matched filter output presented in section 2.2.3, the ratio found the same number of targets with 29 fewer false alarms.

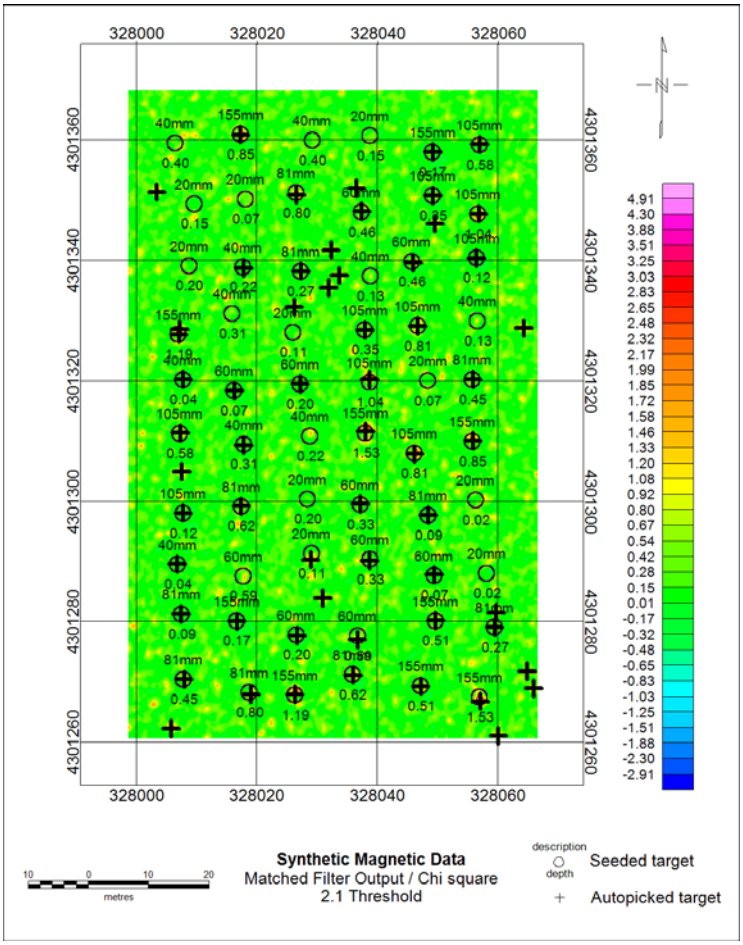

Figure 23. Results of matched filter algorithm on the synthetic magnetic data. The color coded map shows the ratio (Matched filter output/Chi square). The true locations are plotted as circles and the automatic picker detections are plotted as "+"

4.3.2 Phase 2 – Live Site data

The second phase applied the target pickers to the seven magnetic data sets using the default parameters output from phase one. Because each data set had its own unique data characteristics the starting parameters needed to be adjusted to achieve the best performance. The knowledge gained from phase one was used to guide these adjustments. Even though the different target pickers had different parameters the process of adjusting the starting parameters to achieve the best performance was essentially the same. The process involved running the algorithm on the data sets (for large data sets a small portion of the data was used for time efficiency) and changing the parameters based on a visual review of the results. This was an iterative process of intelligently changing parameters and visually looking at the results. The visual review examined the different types of anomalies that were selected and those that were not selected and altering the parameters accordingly. One of the limitations noted in past studies of the automatic

pickers is their inability to pick targets at or below the local geologic signal without picking numerous false targets. For this reason we also looked at all the automatic picks and determined if they are visually valid or in the noise levels of the data set and adjusted the threshold accordingly. By testing different thresholds, we were able to determine the point at which we maximized the number of targets picked while minimized the number of apparent false alarms. Table 6 to Table 9 summarizes the final parameters used on each data set for each of the automatic target picking methods.

We calculated the Pd by comparing the declarations made by the different picking methods to the available ground truth data. We eliminated high density areas where ambiguous results impeded our analysis. The WAA data sets did not have sufficient ground truth over the areas analyzed. For this reason we compared the automatic picks to the picks made by the commercial expert. For the APG data we also calculated the rBAR because it was the only data set that had complete ground truth. The three USACE data sets had ground truth but only for anomalies that were declared by the contractor. There were anomalies observed in the magnetic data that were not excavated so we could not ascertain whether they were caused by noise or a metallic object. Also, the locations for the ground truth (except for the proveout) were locations that were selected by the analyst and not the actual location of the found item.

As part of our analysis we plotted the ground truth sorted by decreasing analytic signal amplitude versus the number of targets detected by each picking method. This will ideally give a straight line along the diagonal if all the ground truth were detected. By sorting according to signal strength we are able to visually see if there are trends in the types of targets missed for the different data sets. It also allowed us to visualize the picking thresholds for the different methods. We also created maps (shown in the next section) for each data set and each method and overlaid the automatic target declarations, ground truth found and ground truth not detected as well as the manual declarations.

Since *characterization* is a vital part of any UXO cleanup operation, the ability of an automatic target picker to define, for each identified anomaly, an appropriate and effective spatial footprint to be given to a fitting (or characterization) routine is an important metric to measure and compare among the methods. We used the spatial footprint produced by each method as input to a target fitting routine for 80 anomalies that were picked by all the methods over the APG data set. The effect that the selection has on the fitted model parameters was compared and included in the demonstration.

Table 6. Best Parameter Set for AWD Algorithm for All Surveys.

Dataset/ Parameter	*Default*	*GPO*	*Pueblo Airb.*	*Isleta*	*Seaside*	*APG*	*JPG*	*Pueblo Trans.*
minampdip	**10**	10	5	10	6	8	6	7
minampsing	**10**	10	7	10	6	8	6	7
startheight	**0**	0	0	0.1	0	0	0	0
endheight	**1.5**	2	4	1.6	1.5	1.5	1.5	1.5
incheight	**0.125**	0.125	0.2	0.125	0.125	0.125	0.125	0.125
lowestlev	**4**	3	10	4	3	2	2	3
minpersist	**2**	2	4	3	2	2	2	2
maxdepth	**5**	5	10	5	5	8	7	8
maxangle	**90**	120	90	90	90	90	130	90
maxdist	**3**	5	8	3	5	5	5	5
maxampdiff	**0.25**	0.2	0.25	0.2	0.2	0.25	0.25	0.25
maxdistdep	**1.5**	2.5	1.5	2	2	1.5	1.5	1.5

Table 7. Best Parameter Set for Clustering Algorithm for All Surveys.

Dataset/ Parameter	*Default*	*GPO*	*Pueblo Airb.*	*Isleta*	*Seaside*	*APG*	*JPG*	*Pueblo Trans.*
Amplitude threshold (nT)	**3 x noise**	175	4	30	9	15	7	10
Dipole stretch (m)	**3**	2	7.5	3	2	1	2	1.75
Search radius (m)	**3**	1	8	1.25	1.5	3	1.25	1.5
Footprint radius (m)	**5**	5	10	5	5	5	5	5
Overlap distance (m)	**2**	2	7	2	2	2	2	2
Ratio threshold	**.1**	.1	.1	.1	.1	.1	.1	.1
Azimuth deviation (°)	**55**	179	179	179	179	179	179	179
Slice angle expansion(°)	**25**	25	25	25	25	25	25	25
Number of slices	**24**	24	24	24	24	24	24	24

Table 8. Best Parameter Set for Matched Filter Algorithm for All Surveys.

Dataset/ Parameter	*Default*	*GPO*	*Pueblo Airb.*	*Isleta*	*Seaside*	*APG*	*JPG*
Input grid cell (m)	**¼ line spacing**	.15	.9	.2	.15	.2	.2
Filter box size (m)	**3**	6	12	5.5	3.75	5	4
Peak picker grid cell (m)	**¼ input grid cell**	.075	.45	.05	.0375	.1	.05
Number filter passes	**3**	4	3	3	3	3	4
Peak Threshold	**1**	.3	.9	.55	1.25	.35	.7
Line spacing (m)	**NA**	.6	1.75	.25	.6	.25	.75

Table 9. Best Parameter Set for Analytic Signal Method for All Surveys.

Dataset/ Parameter	*Default*	*GPO*	*Pueblo Airb.*	*Isleta*	*Seaside*	*APG*	*JPG*	*Pueblo Trans.*
Amplitude threshold (nT/m)	**NA**	83.9	3	50	5	42	5	25
Number filter passes	**2**	2	2	2	2	2	4	2

4.3.2.1 USACE GPO

The performance of the different target picking methods is summarized in Table 10 and Figure 24. Color coded maps showing the different target picking declarations and ground truth overlain on their respective data are presented in Figure 25 to Figure 29. The red symbols on the figures represent items that were not detected by the respective method. The Pd's for the different methods were lower than expected with only the manual method approaching our goal of 0.90. The lower Pd's can be attributed to the following factors. First, there were a limited number of seeded items so each missing item significantly affected the Pd. The seeded items consisted of 18 ordnance items (17lb and 25lb bombs) and 10 clutter items. Two of the clutter items were masked by a large anomaly that bisected the area and were not seen by any of the methods. So in order to meet our goal all the remaining items needed to be detected. Second, the area had a high magnetic background which forced higher thresholds for each of the methods. This resulted in missing some of the weaker clutter items. It should be noted that both the manual method and the analytic signal method detected all the emplaced ordnance and the clustering and AWD methods only missed two ordnance items. The vast majority of the missed items that led to the lower Pd's were range clutter.

The matched filter method was severely hampered by the requirement of the filter box to have complete data coverage. This effectively reduced the size of the area that could be analyzed

which in turn eliminated 10 of the seeded items. Of the remaining 18 items, two ordnance items were missed. They were both partially masked by a large anomaly, although one of the items could have been detected with a lower threshold. Even though these anomalies were visually seen in the magnetic data, the nearby larger anomalies created a large Chisq, which resulted in a small value for the ratio (MFoutput/Chisq) and thus the missed detection.

Table 10. USACE GPO - Detection and location accuracy

Parameter / Method	*Total # picks*	*# matching ground truth*	*Pd*	*# <.25m*	*# .25m - .5m*	*# .5 - 1.0m*	*% within .5m*
Ground Truth	28						
Manual	36	25	0.89	8	14	3	88
Clustering	27	16	0.57	5	5	6	63
Wavelet	39	21	0.75	9	8	4	81
Matched filter	14	10	0.36	2	5	3	70
Analytic signal	50	22	0.79	5	16	1	95

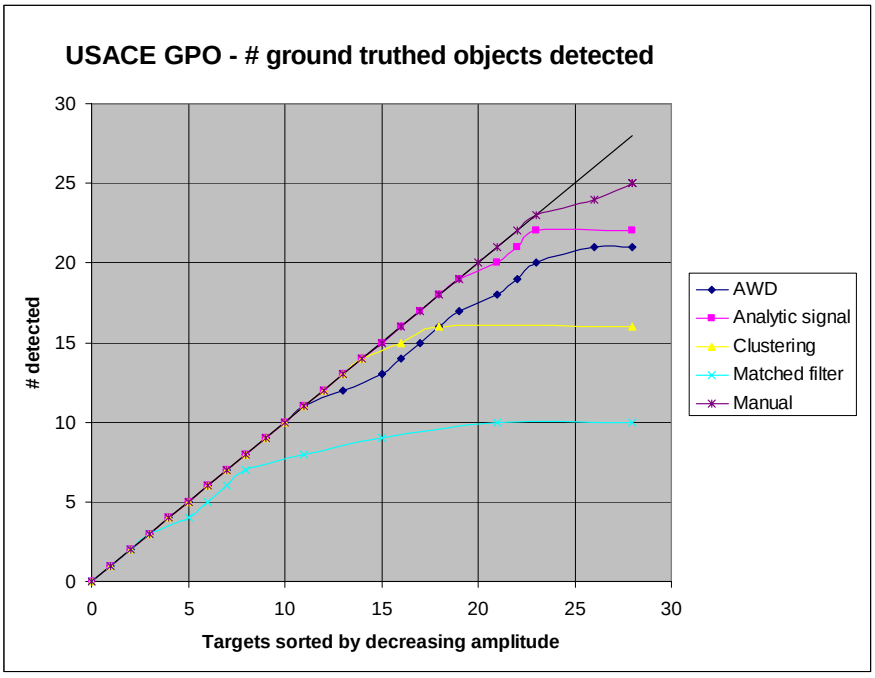

Figure 24. Graph showing the number of ground truth objects detected by each method as a function of signal amplitude; USACE GPO.

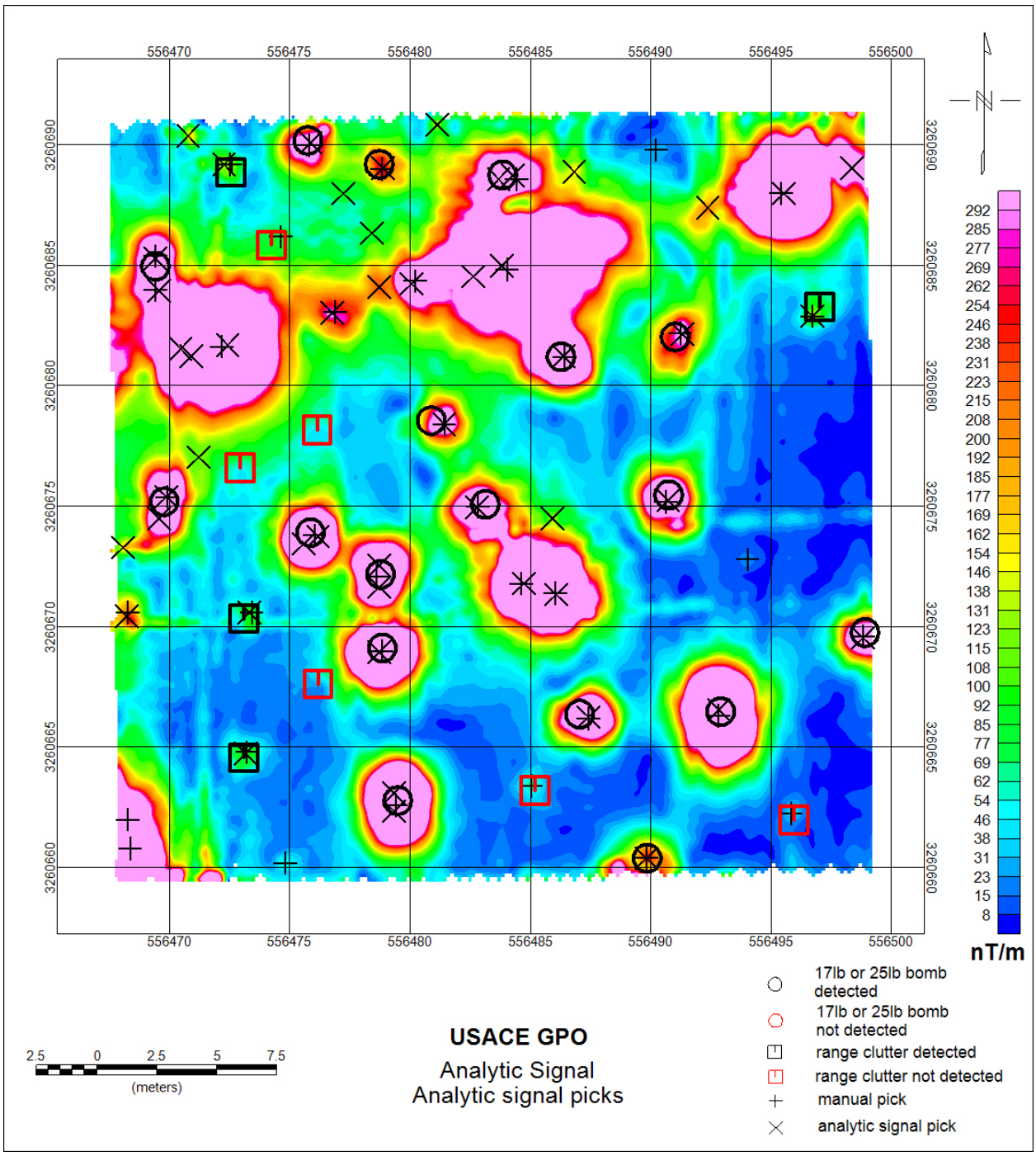

Figure 25. Color-coded map showing the analytic signal data overlain by the ground truth, manual picks and anomalies identified by the analytic signal method; USACE GPO.

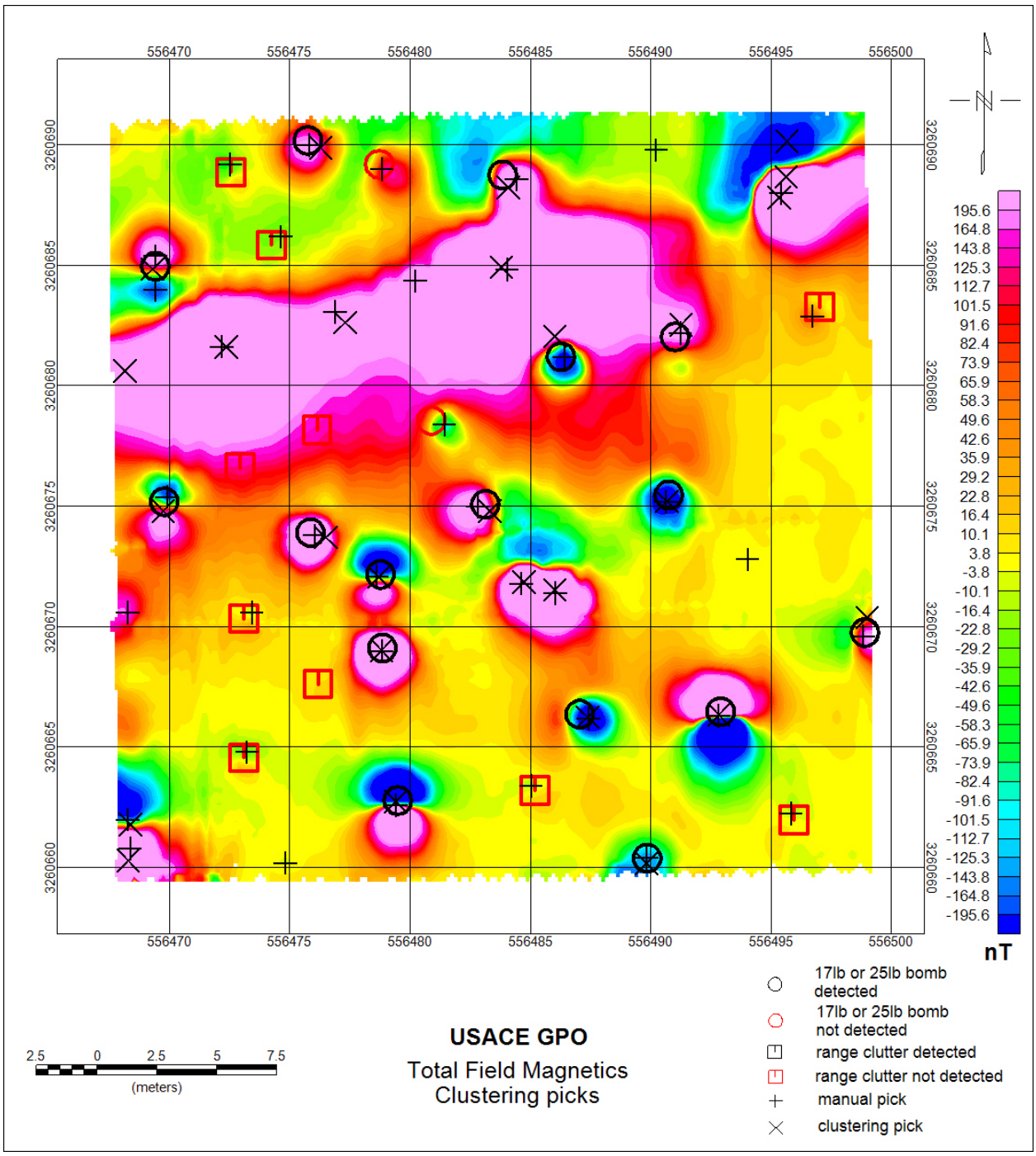

Figure 26. Color-coded map showing the total field magnetic data overlain by the ground truth, manual picks and anomalies identified by the clustering method; USACE GPO.

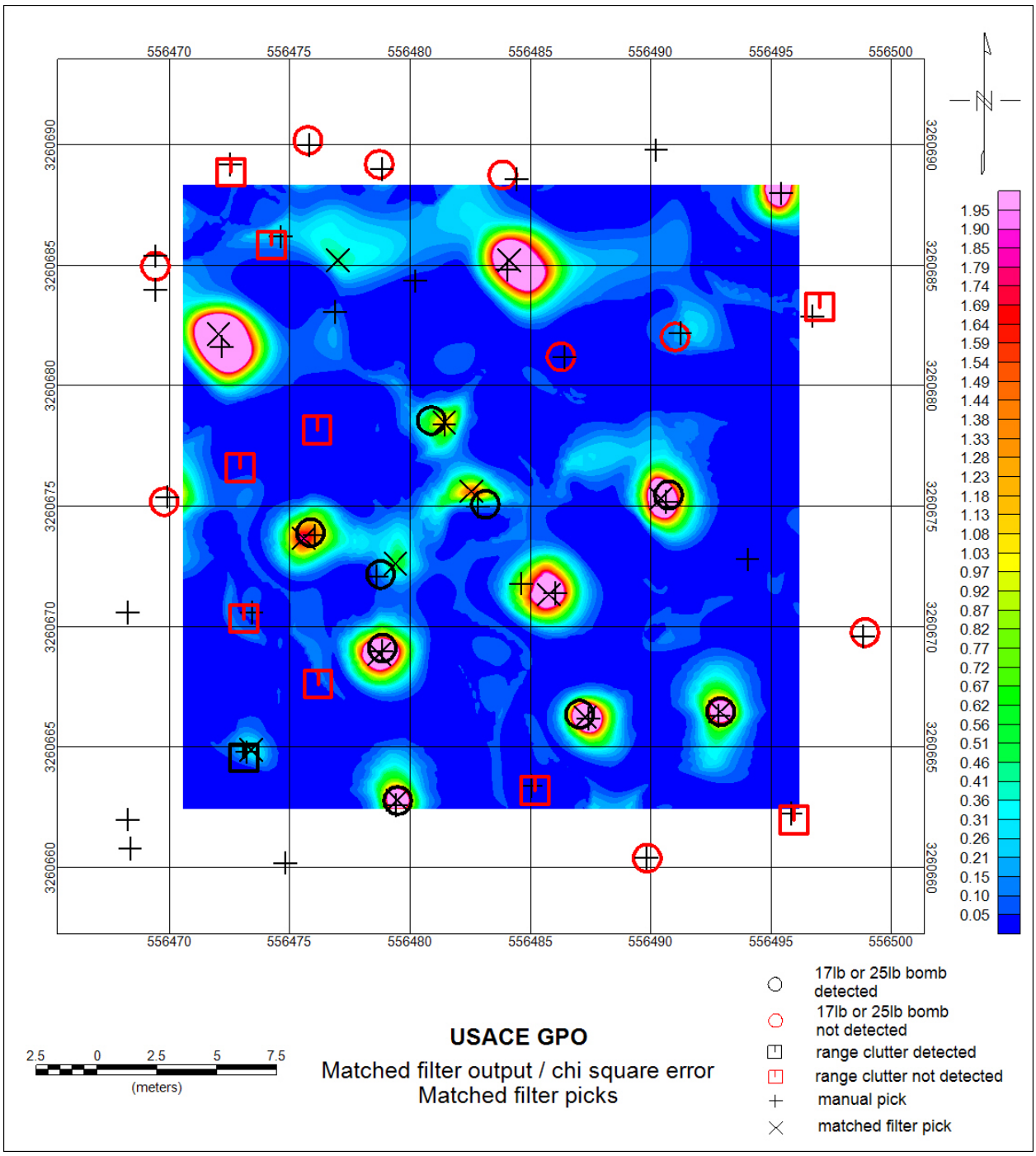

Figure 27. Color-coded map showing the (Matched filter output / Chi square) data overlain by the ground truth, manual picks and anomalies identified by the matched filter method; USACE GPO.

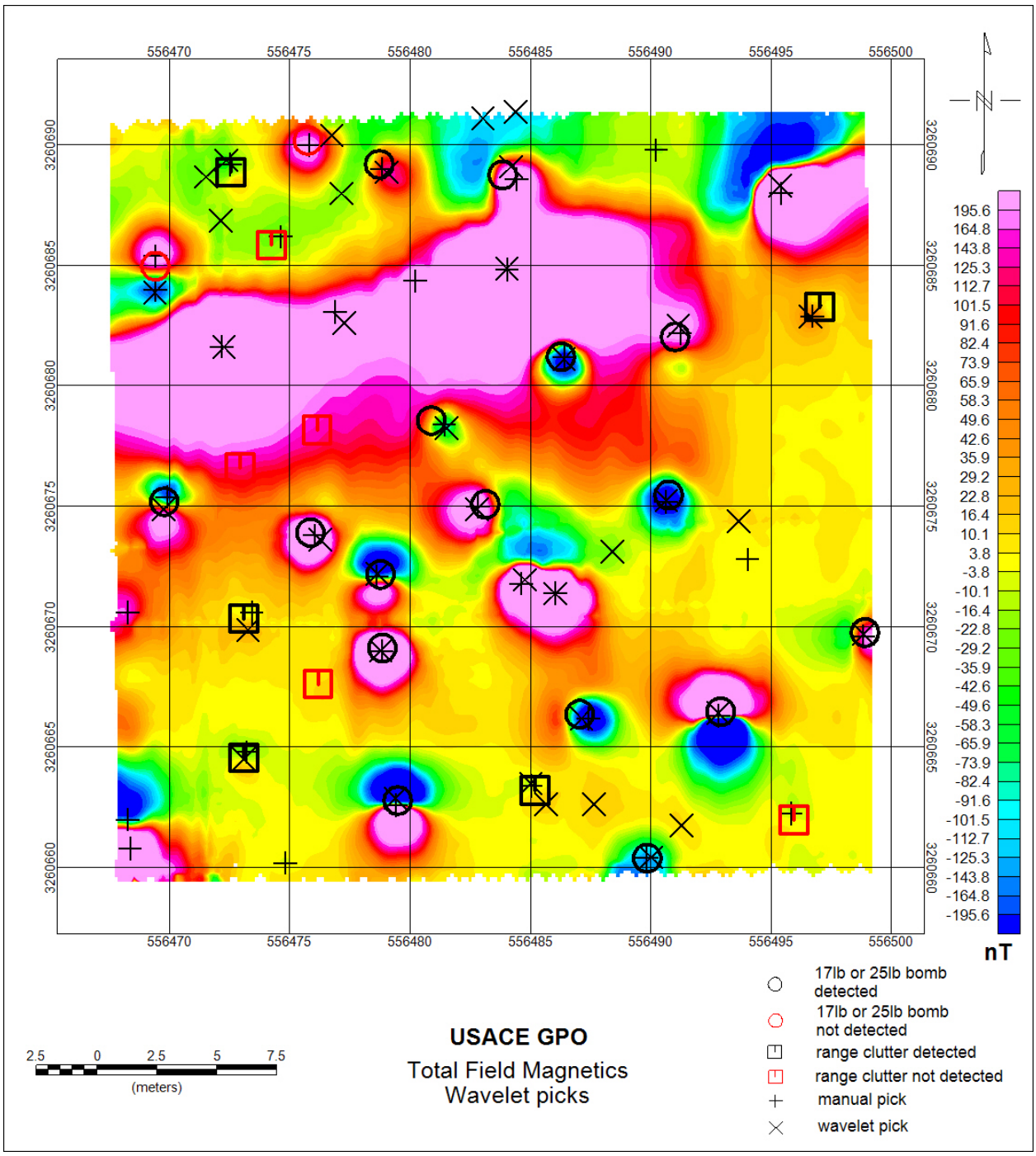

Figure 28. Color-coded map showing the total field magnetic data overlain by the ground truth, manual picks and anomalies identified by the AWD method; USACE GPO.

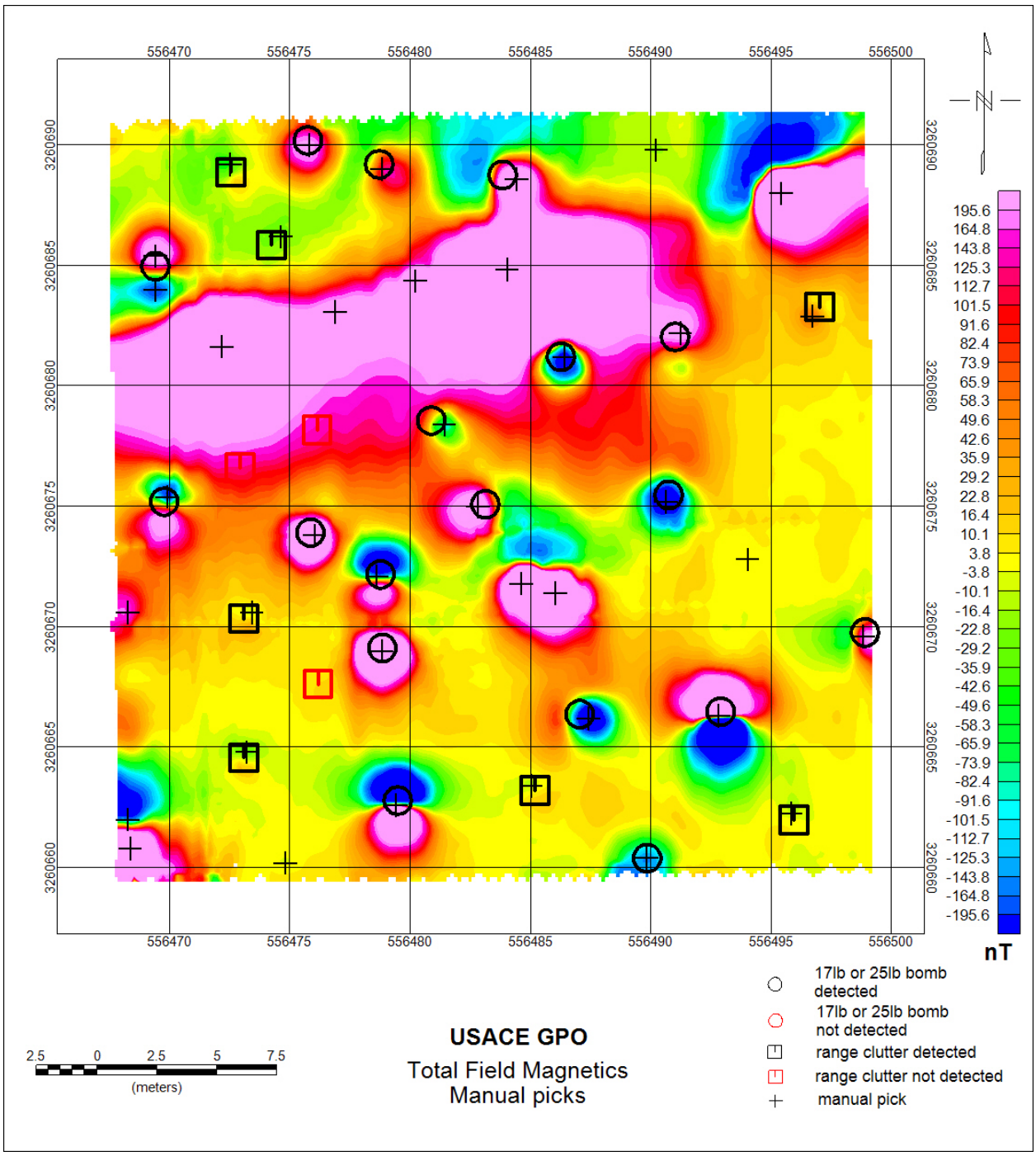

Figure 29. Color-coded map showing the total field magnetic data overlain by the ground truth and anomalies identified manually; USACE GPO.

4.3.2.2 Pueblo of Isleta, NM

The performance of the different target picking methods is summarized in Table 11 and Figure 30. Color coded maps showing the different target picking declarations and ground truth overlain on their respective data are presented in Figure 31 to Figure 35. The manual, analytic signal, clustering and AWD methods all achieved Pd's greater than .98. The few ground truth targets that were missed by these methods had a pick just outside the one meter tolerance that was used to define a detection. Most of the missed targets were common to different methods which suggest the location error may stem from errors in the ground truth location or position errors in the input sensor data and not problems with the target picking algorithms.

The matched filter method was again hampered by the requirement of the filter box to have complete data coverage. Also, the matched filter had the fewest number of total picks for this area which points to a more conservative threshold chosen by the analyst. Additional ground truth could be detected if a lower picking threshold were used. This is evident by looking at the responses of the missed targets (red circles in Figure 33).

Table 11. Isleta - Detection and location accuracy

Parameter / Method	***Total # picks***	***# matching ground truth***	***Pd***	***# <.25m***	***# .25m - .5m***	***# .5 - 1.0m***	***% within .5m***
Ground Truth	145						
Manual	1466	142	0.98	47	67	28	80
Clustering	758	142	0.98	49	70	23	84
Wavelet	1454	143	0.99	51	72	20	86
Matched filter	472	131	0.90	51	62	18	86
Analytic signal	1278	142	0.98	38	78	26	82

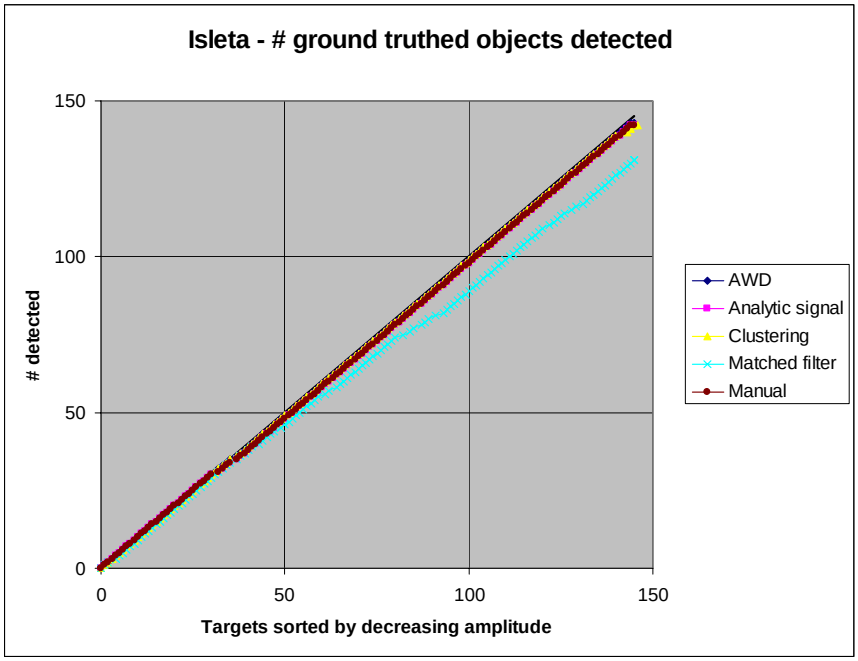

Figure 30. Graph showing the number of ground truth objects detected by each method as a function of signal amplitude; Isleta.

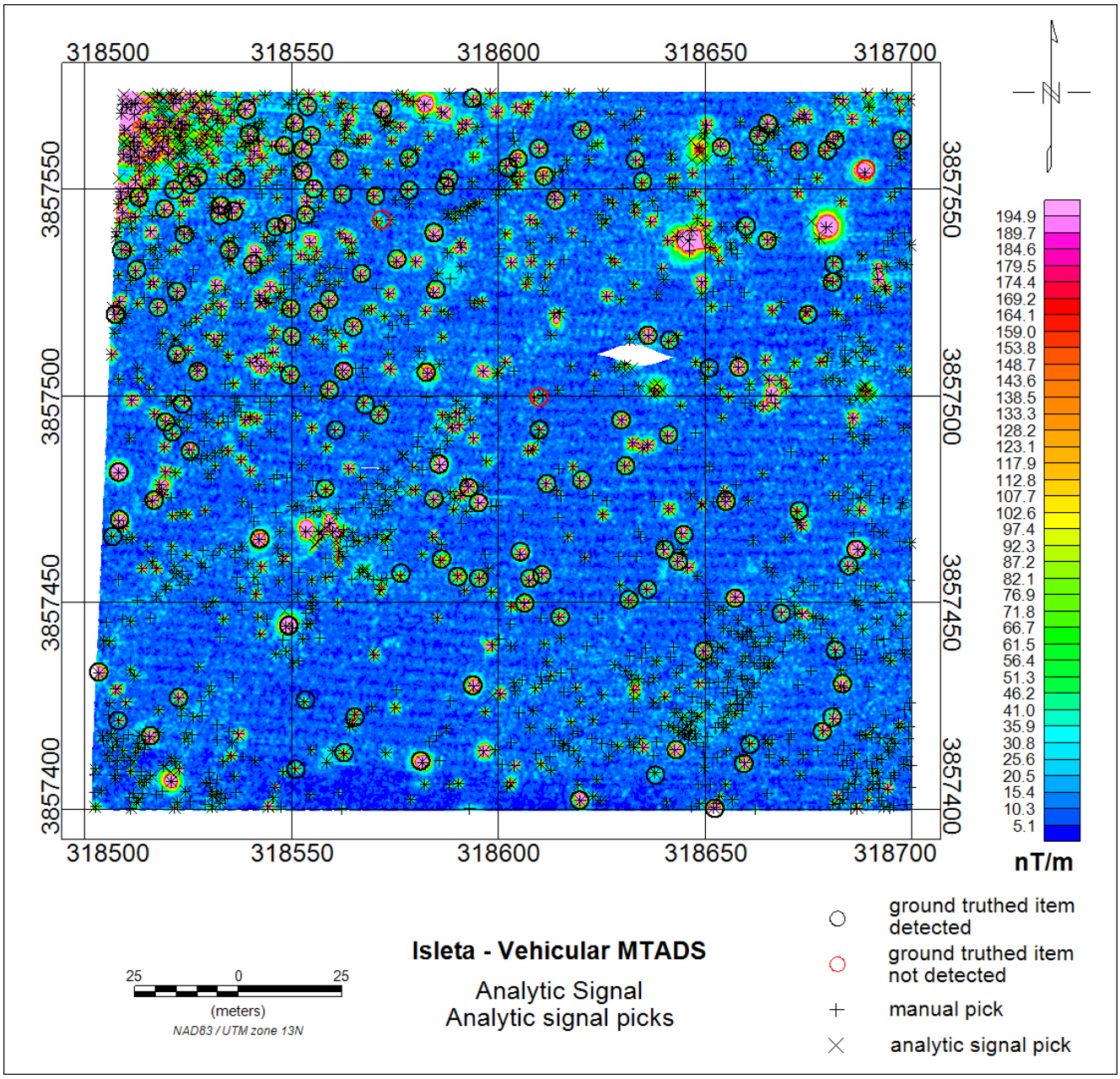

Figure 31. Color-coded map showing the analytic signal data overlain by the ground truth, manual picks and anomalies identified by the analytic signal method; Isleta.

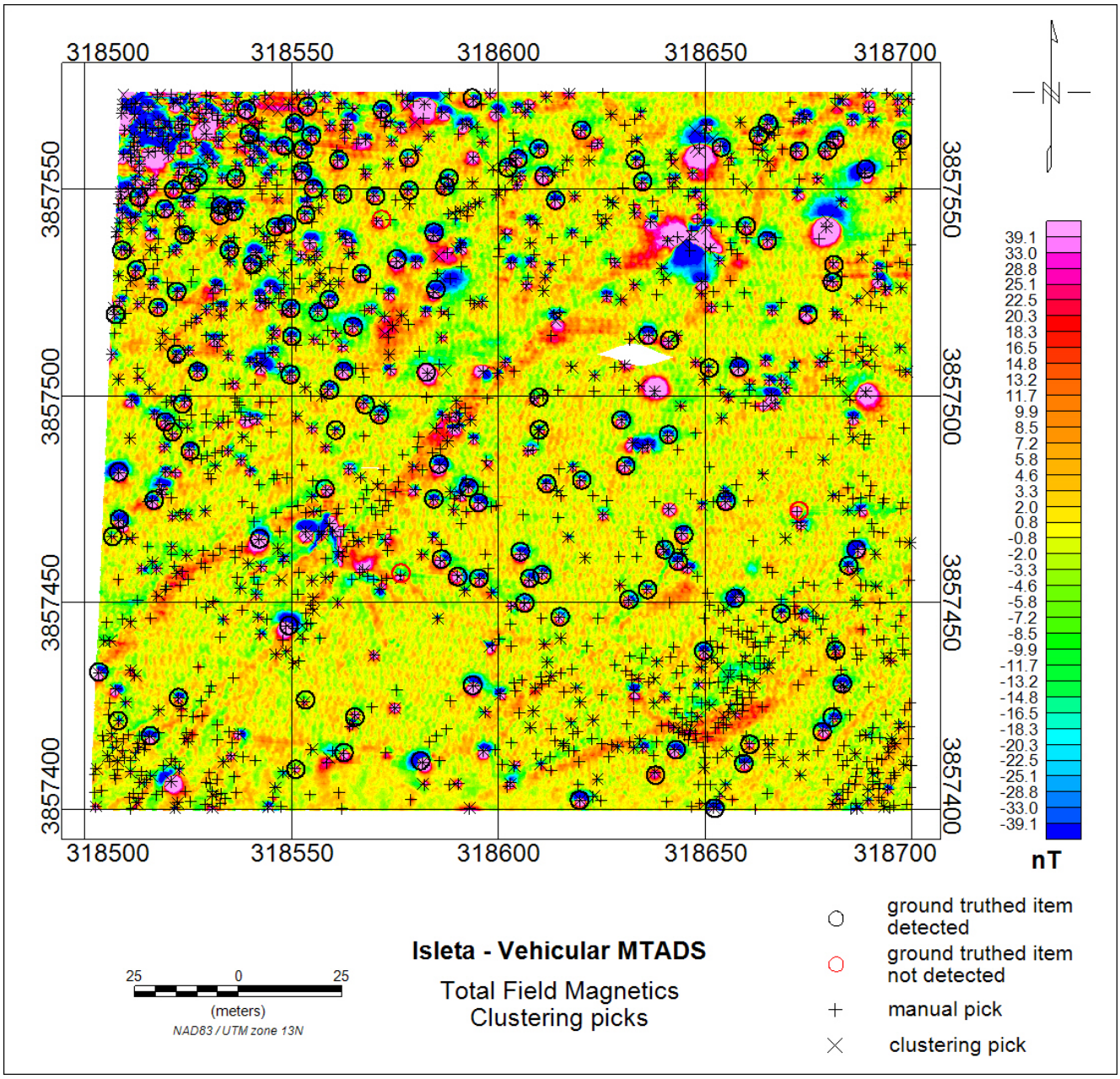

Figure 32. Color-coded map showing the total field magnetic data overlain by the ground truth, manual picks and anomalies identified by the clustering method; Isleta.

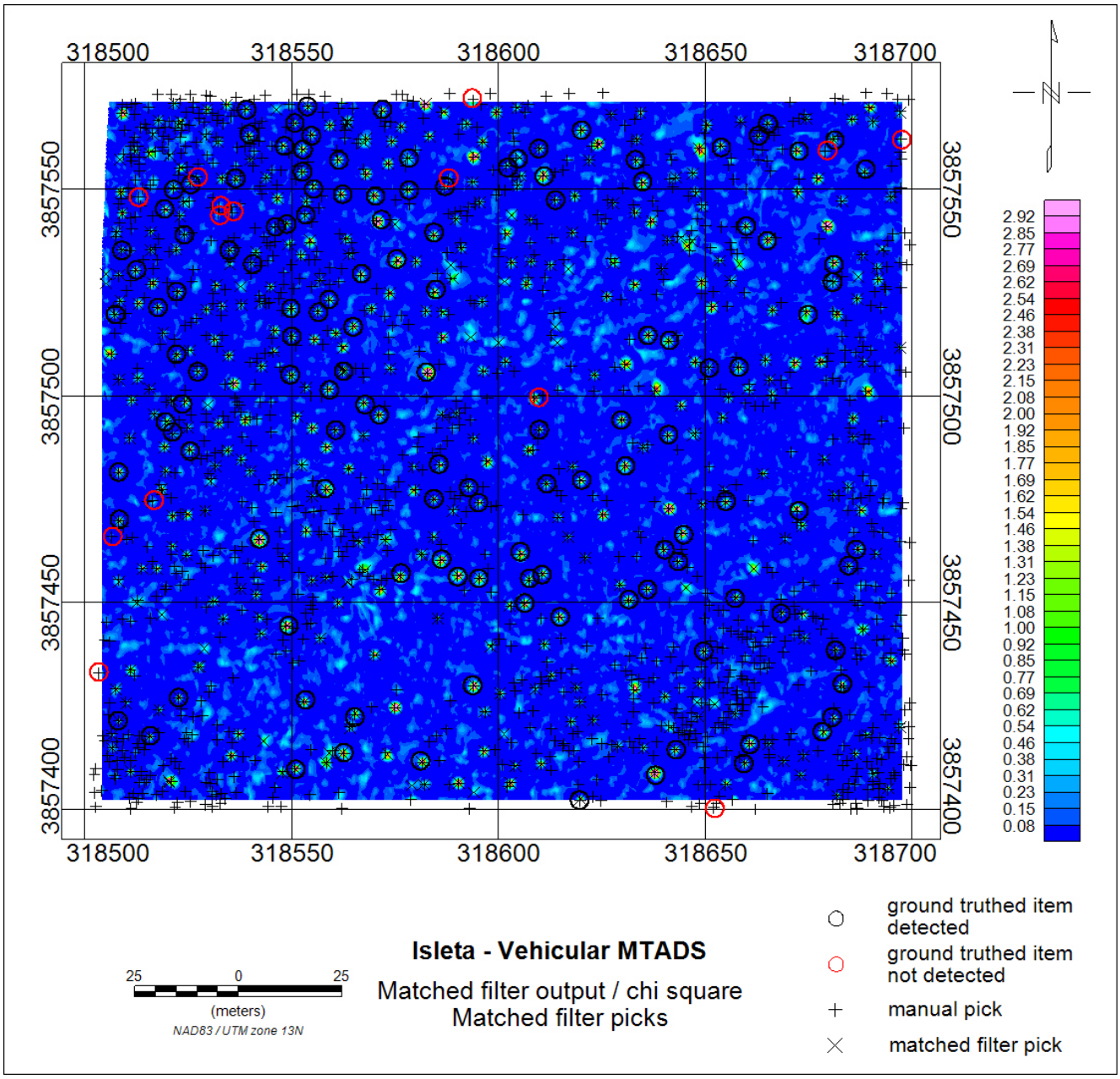

Figure 33. Color-coded map showing the (Matched filter output / Chi square) data overlain by the ground truth, manual picks and anomalies identified by the matched filter method; Isleta.

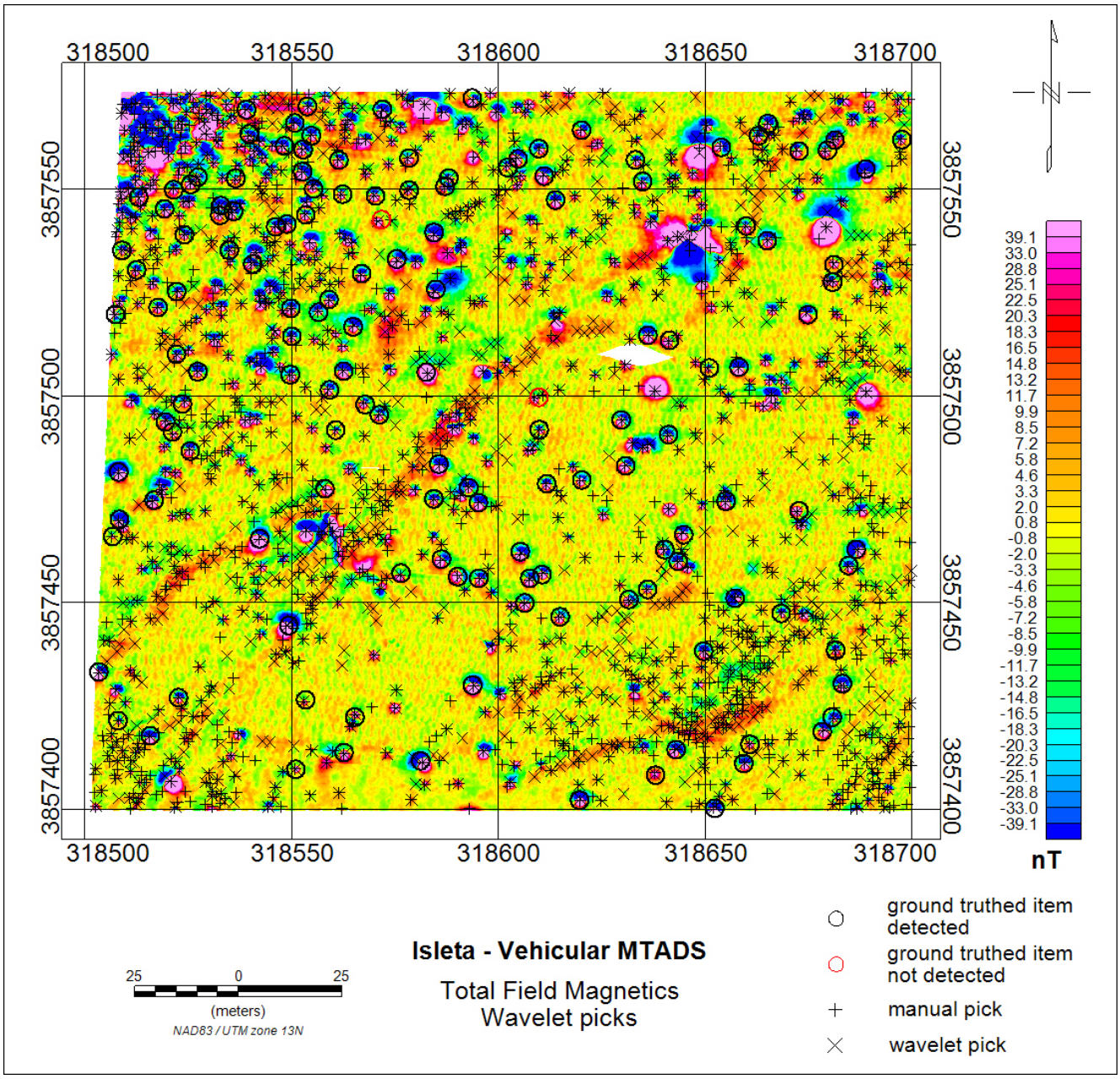

Figure 34. Color-coded map showing the total field magnetic data overlain by the ground truth, manual picks and anomalies identified by the AWD method; Isleta.

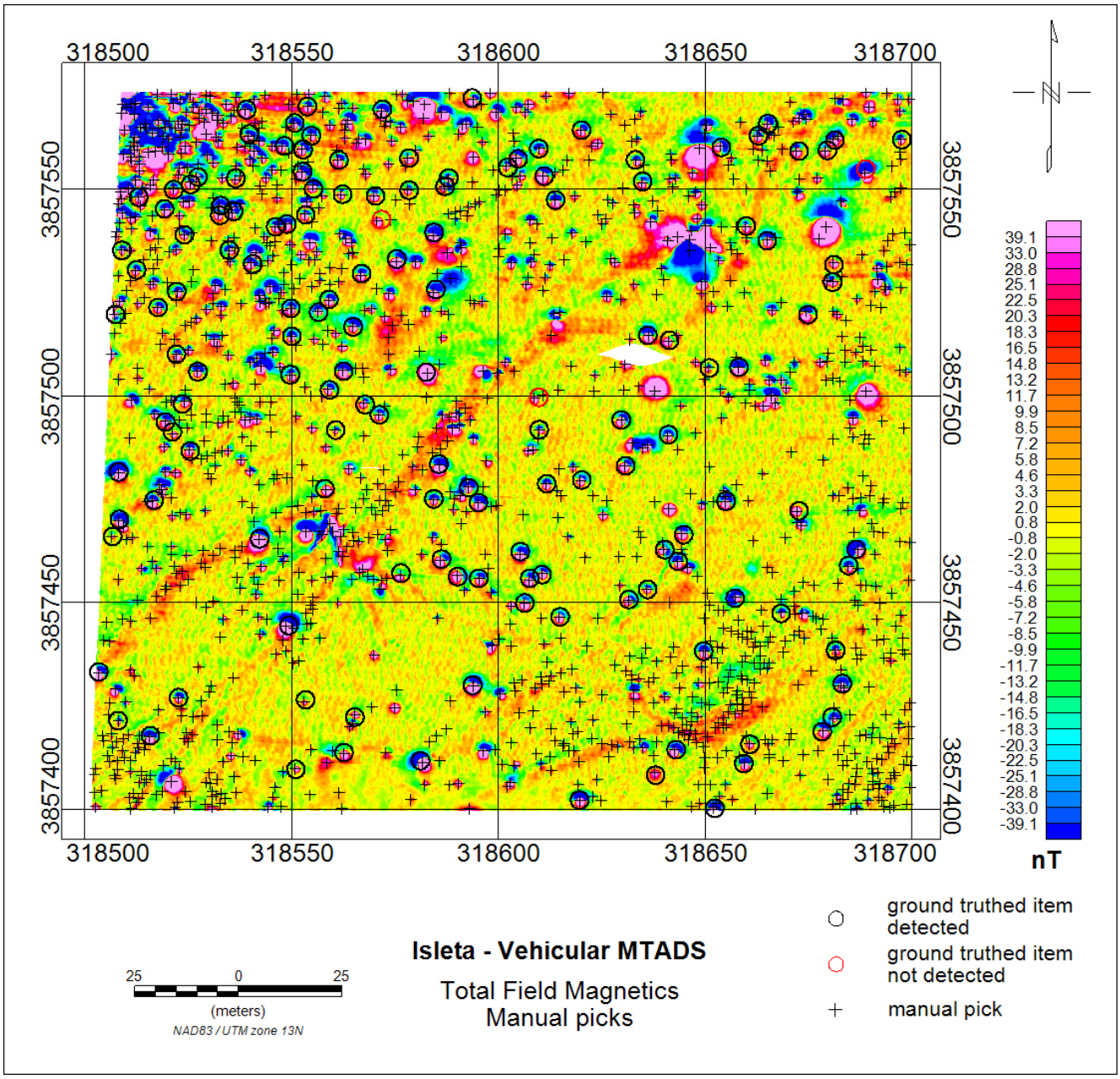

Figure 35. Color-coded map showing the total field magnetic data overlain by the ground truth and anomalies identified manually; Isleta.

4.3.2.3 Seaside, CA

The performance of the different target picking methods is summarized in Table 12 and Figure 36. Color coded maps showing the different target picking declarations and ground truth overlain on their respective data are presented in Figure 37 to Figure 41. This dataset shows some large-amplitude anomalies and cluttered areas as well as many low amplitude anomalies. The overall background noise of the data is of the same order of magnitude as the weak anomalies which caused problems in setting the detection threshold. In order to pick many of the weaker anomalies a low threshold was needed but the low threshold in turn would pick many false alarms caused by noise in the data. The thresholds and parameters for the manual, analytic signal, clustering and matched filter methods were set to reduce the number of false alarms. On the other hand, the AWD method used parameters that were more aggressive which produced a higher Pd but with the drawback of obtaining multiple alarms for the same target. Many of the AWD false alarms were in the cluttered area located in the north central part of the map.

Table 13 outlines the weights of the objects missed by each of the methods. For comparison purposes, a 20mm projectile has a weight of approximately 0.25 pounds. Therefore, over 90% of the missed targets for each of the methods were smaller than a 20mm. This implies the thresholds of the automatic target pickers were set at reasonable values to detect small ordnance but not so low as to detect very small pieces of clutter. Most of the heavy items (>1lb) that were missed were accompanied by multiple nearby anomalies that were picked. When we looked at these situations we noticed that, according to the ground truth, the objects surrounding the missed targets were very often smaller than the detected ones. An example is shown in Figure 40. At the center of the map there is a large circle that encompasses three ground truthed objects. According to the ground truth, the only object detected by the target pickers was the one in the middle (black circle) and weighed 0.1lbs. The objects above and below (red symbols) were not detected and weighed 4.0lbs and 0.1lbs, respectively. The more likely scenario has the 4.0lb object located in the middle and responsible for the high amplitude anomaly seen in the data. The two 0.1lb objects were likely masked by the larger anomaly and thus not picked by the automatic target picking methods.

The combination of large and weak anomalies and cluttered areas was especially difficult for the matched filter algorithm and attributed to the very low Pd. The 3.75m filter box needed to detect the large anomalies caused problems detecting the closely spaced weak anomalies. The filter box routinely contained several dipoles which resulted in a low (MFoutput/Chisq) value and thus a missed target.

Table 12. Seaside - Detection and location accuracy

Parameter / Method	***Total # picks***	***# matching ground truth***	***Pd***	***# <.25m***	***# .25m - .5m***	***# .5 - 1.0m***	***% within .5m***
Ground Truth	412						
Manual	205	134	0.33	60	53	21	84

Parameter / Method	*Total # picks*	*# matching ground truth*	*Pd*	*# <.25m*	*# .25m - .5m*	*# .5 - 1.0m*	*% within .5m*
Clustering	160	102	0.25	24	46	32	69
Wavelet	616	246	0.60	114	100	32	87
Matched filter	123	62	0.15	24	29	9	85
Analytic signal	346	220	0.53	73	109	38	83

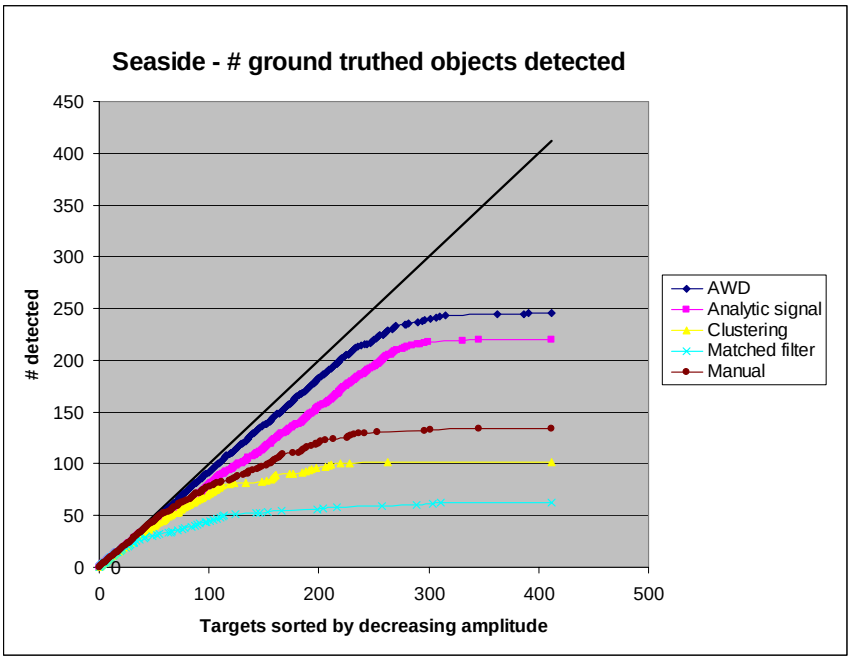

Figure 36. Graph showing the number of ground truth objects detected by each method as a function of signal amplitude; Seaside.

Table 13. Seaside - Weight of targets missed

Parameter / Method	*# <0.1lbs*	*#0 .1lbs -0 .25lbs*	*# >0.25lbs*	*% <0 .25lbs*
Manual	217	44	17	94
Clustering	235	52	23	93
Wavelet	134	22	7	96
Matched filter	260	58	32	91
Analytic signal	154	24	13	93

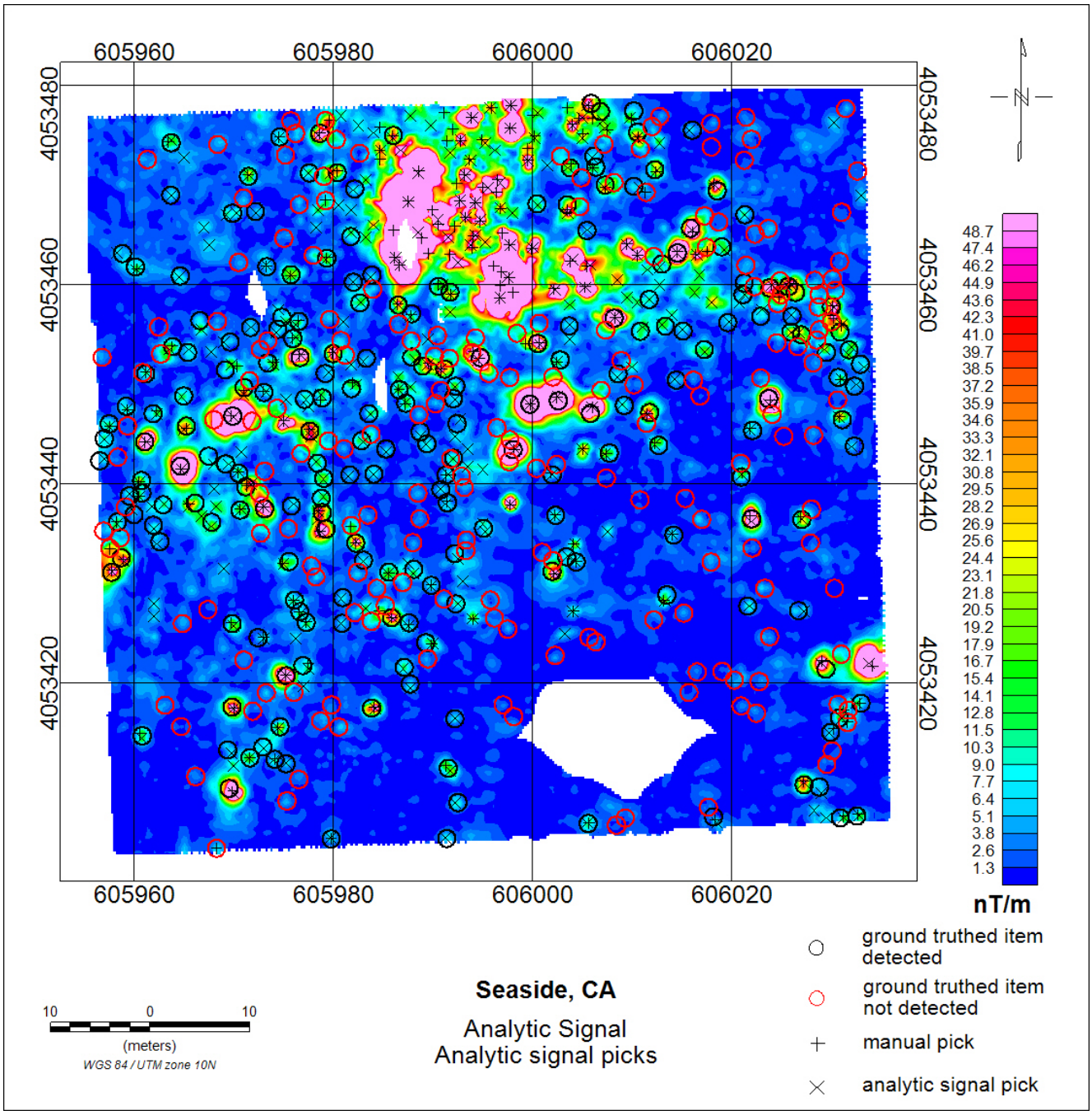

Figure 37. Color-coded map showing the analytic signal data overlain by the ground truth, manual picks and anomalies identified by the analytic signal method; Seaside.

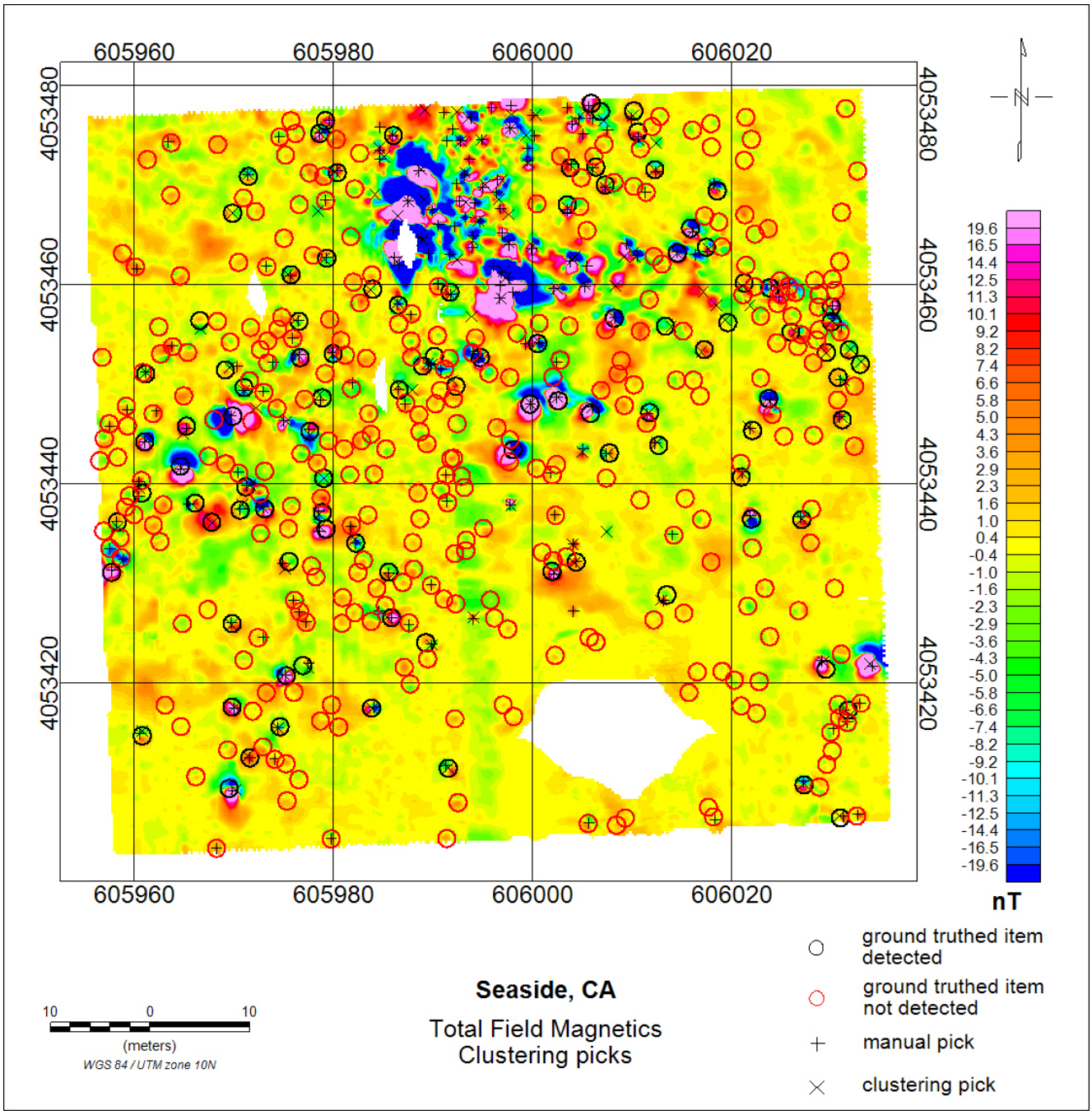

Figure 38. Color-coded map showing the total field magnetic data overlain by the ground truth, manual picks and anomalies identified by the clustering method; Seaside.

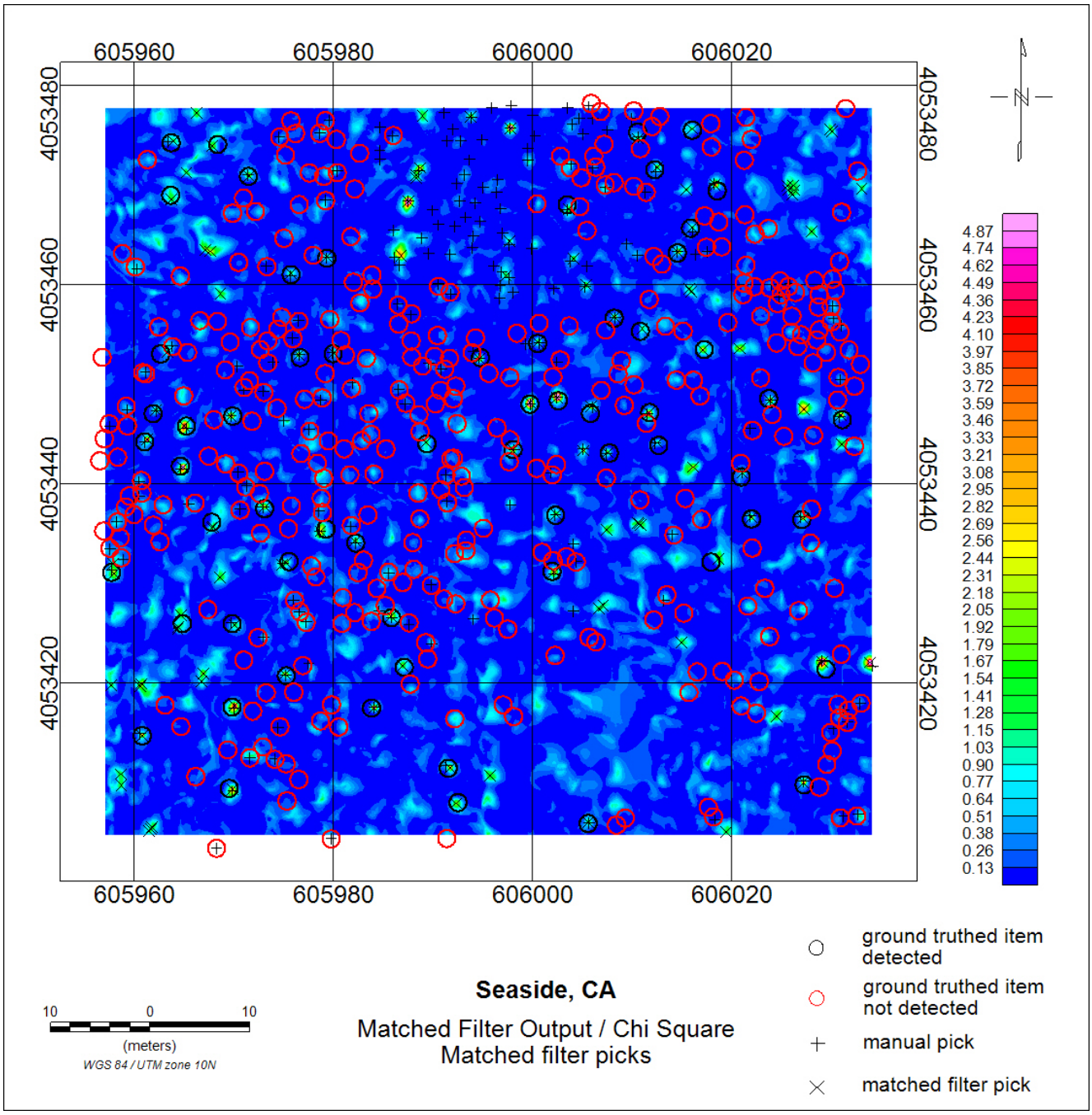

Figure 39. Color-coded map showing the (Matched filter output / Chi square) data overlain by the ground truth, manual picks and anomalies identified by the matched filter method; Seaside.

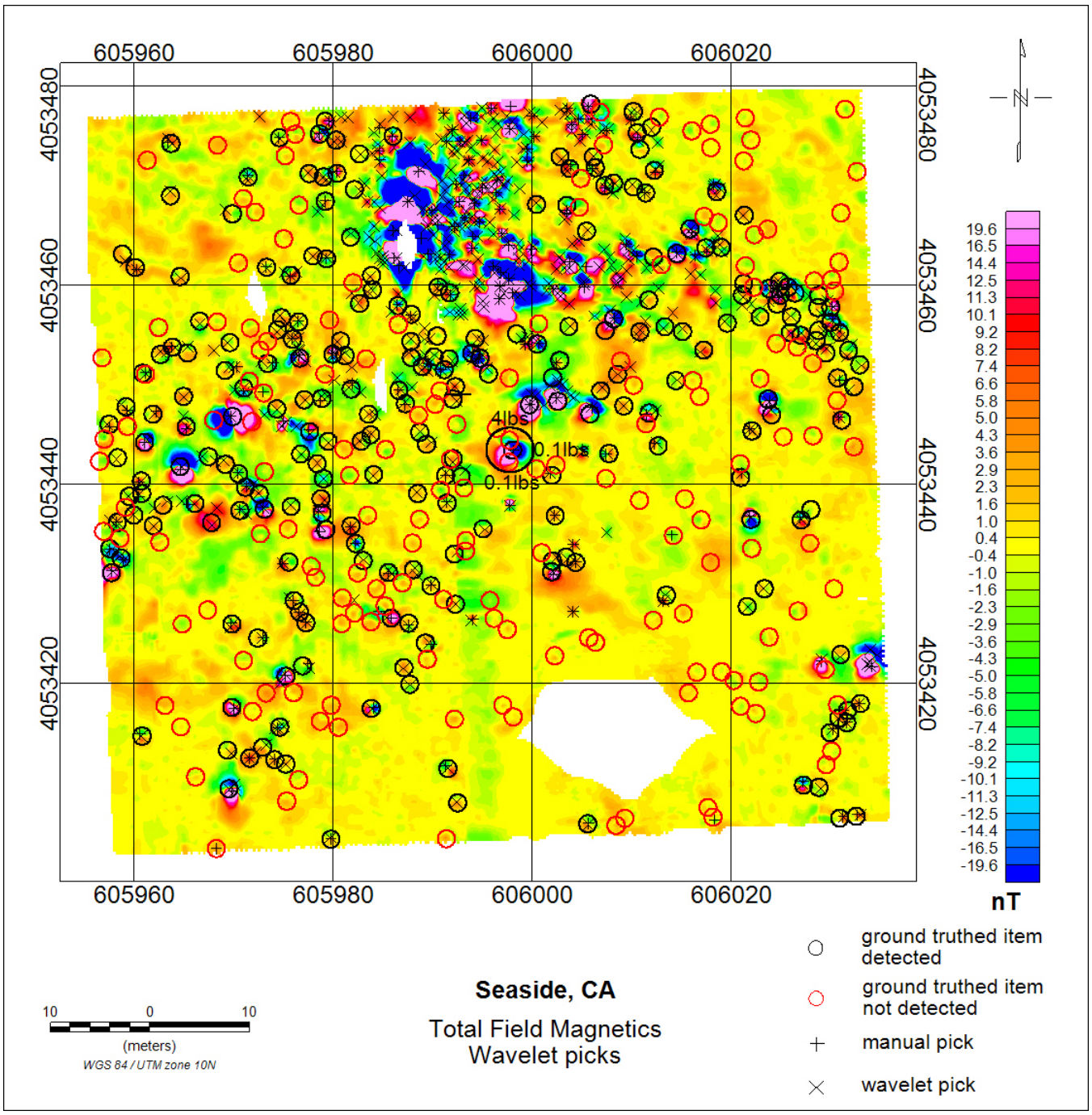

Figure 40. Color-coded map showing the total field magnetic data overlain by the ground truth, manual picks and anomalies identified by the AWD method; Seaside. The larger circle in the center of the figure is an example of an object with questionable ground truth.

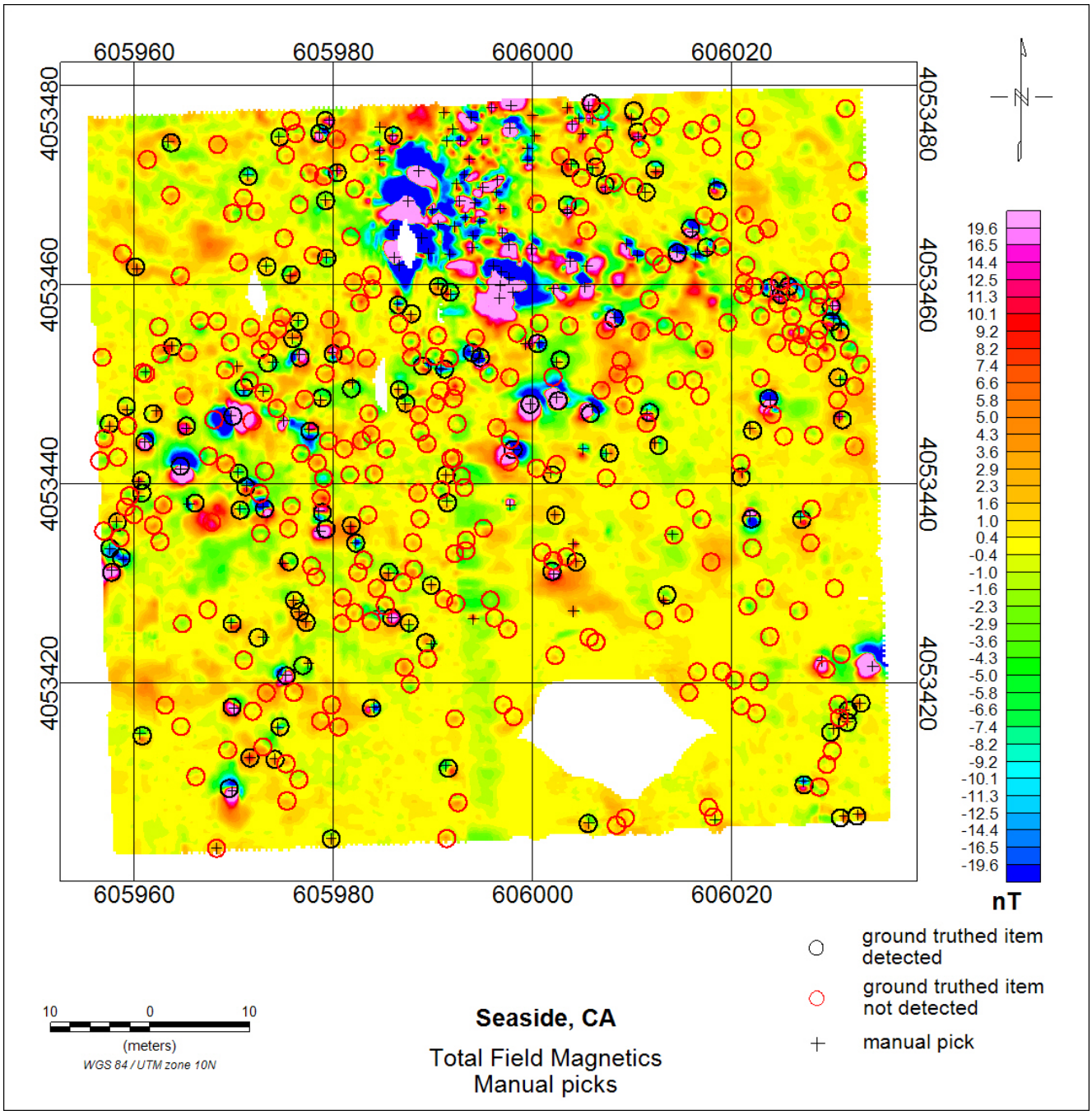

Figure 41. Color-coded map showing the total field magnetic data overlain by the ground truth and anomalies identified manually; Seaside.

4.3.2.4 Jefferson Proving Ground, IN

The performance of the different target picking methods is summarized in Table 14 and Figure 42. Color coded maps showing the different target picking declarations and ground truth overlain on their respective data are presented in Figure 43 to Figure 47. The manual, analytic signal, clustering and AWD methods all performed similarly and achieved Pd's greater than .92. Similar targets were missed by the different methods with two common themes. First, the majority of the missed objects were masked by the responses of nearby objects. On several occasions two or more objects were located within a few meters of each other. The AWD method appeared to do a better job than the other methods with these overlapping situations. Second, a few objects had weak responses that were at or just below the detection thresholds used. The data contained a low amplitude feature in the north-south direction that cut across the western portion of the area. The threshold for the automatic detectors needed to be set at a level just above the response of this feature to minimize the number of false alarms caused by the feature. This resulted in a slightly higher than desired threshold which produced a few missed objects.

These data were characterized by positioning problems as seen by the herringbone nature of the anomalies shown in Figure 48. The data problems caused multiple AWD declarations over several of the objects. These data position problems in conjunction with the closely spaced anomalies caused problems for the matched filter method. In contrast to the AWD, the match filter resulted in fewer detection because the data had a poorer match to the dipole model. This resulted in a smaller MF output as well as a larger Chisq so the (MFoutput/Chisq) ratio used was significantly reduced.

Table 14. JPG - Detection and location accuracy

Parameter / Method	***Total # picks***	***# matching ground truth***	***Pd***	***# <.25m***	***# .25m - .5m***	***# .5 - 1.0m***	***% within .5m***
Ground Truth	190						
Manual	532	180	0.95	67	84	29	84
Clustering	359	174	0.92	80	70	24	86
Wavelet	491	180	0.95	85	76	19	89
Matched filter	309	137	0.72	73	46	18	87
Analytic signal	393	174	0.92	61	82	31	82

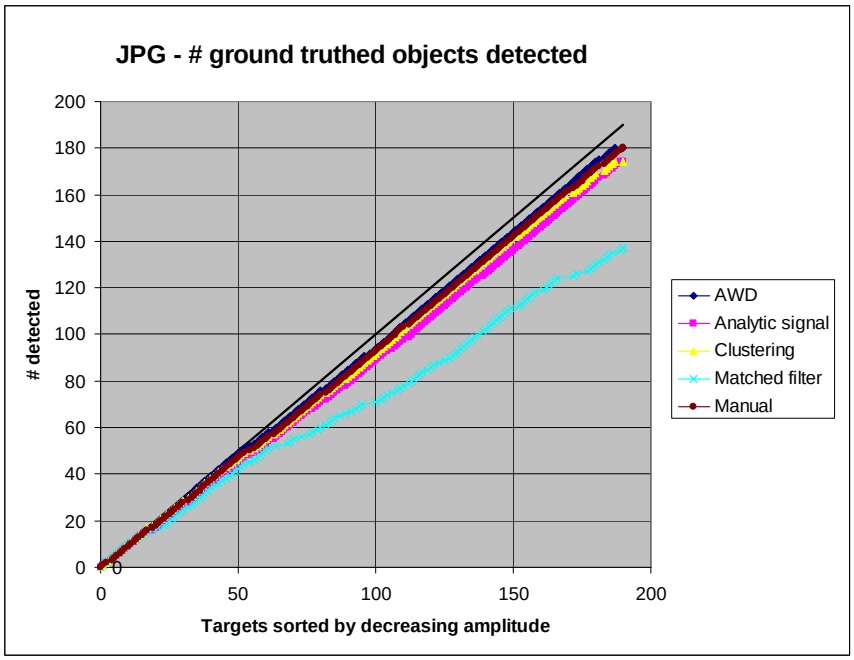

Figure 42. Graph showing the number of ground truth objects detected by each method as a function of signal amplitude; JPG.

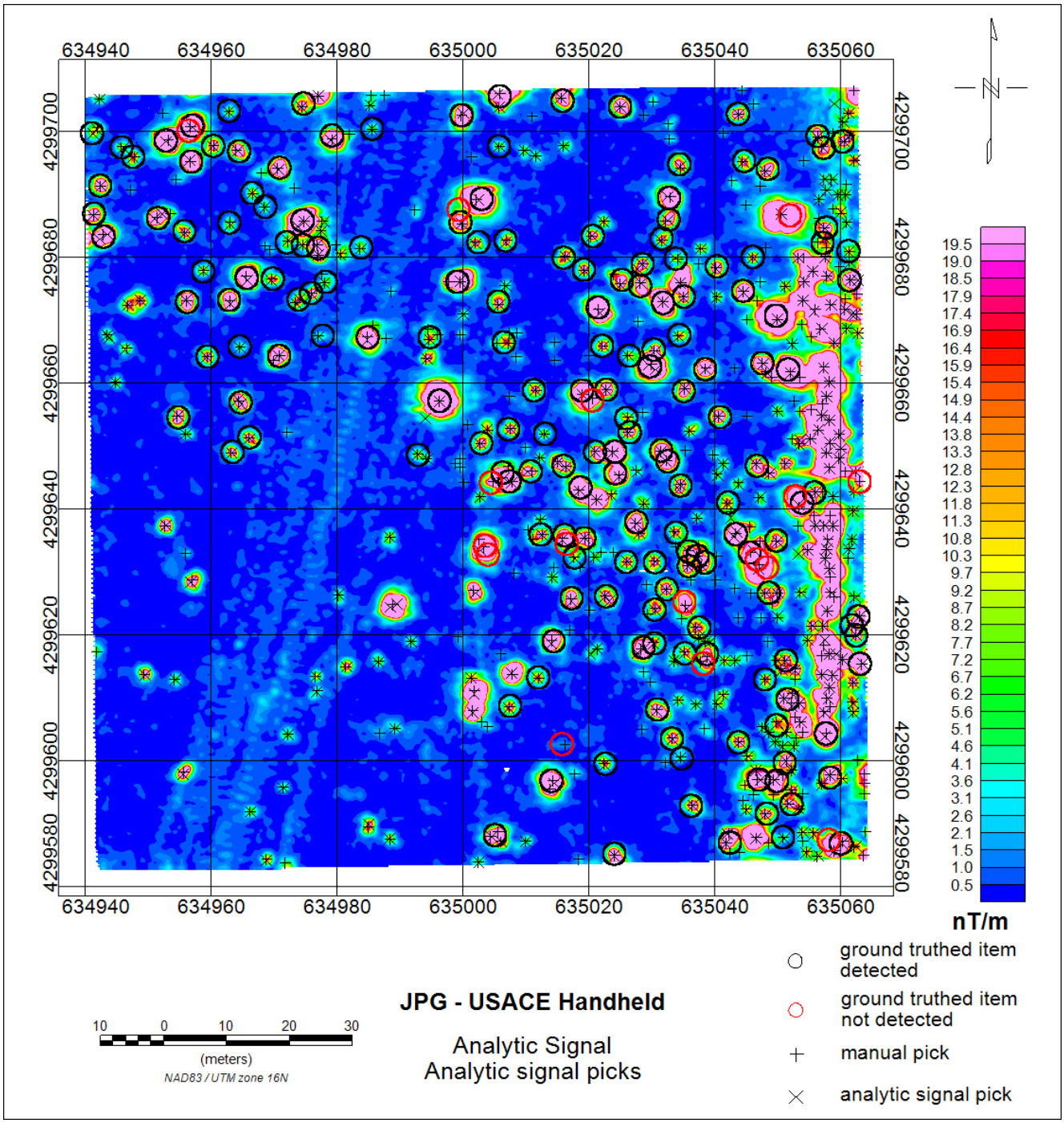

Figure 43. Color-coded map showing the analytic signal data overlain by the ground truth, manual picks and anomalies identified by the analytic signal method; JPG.

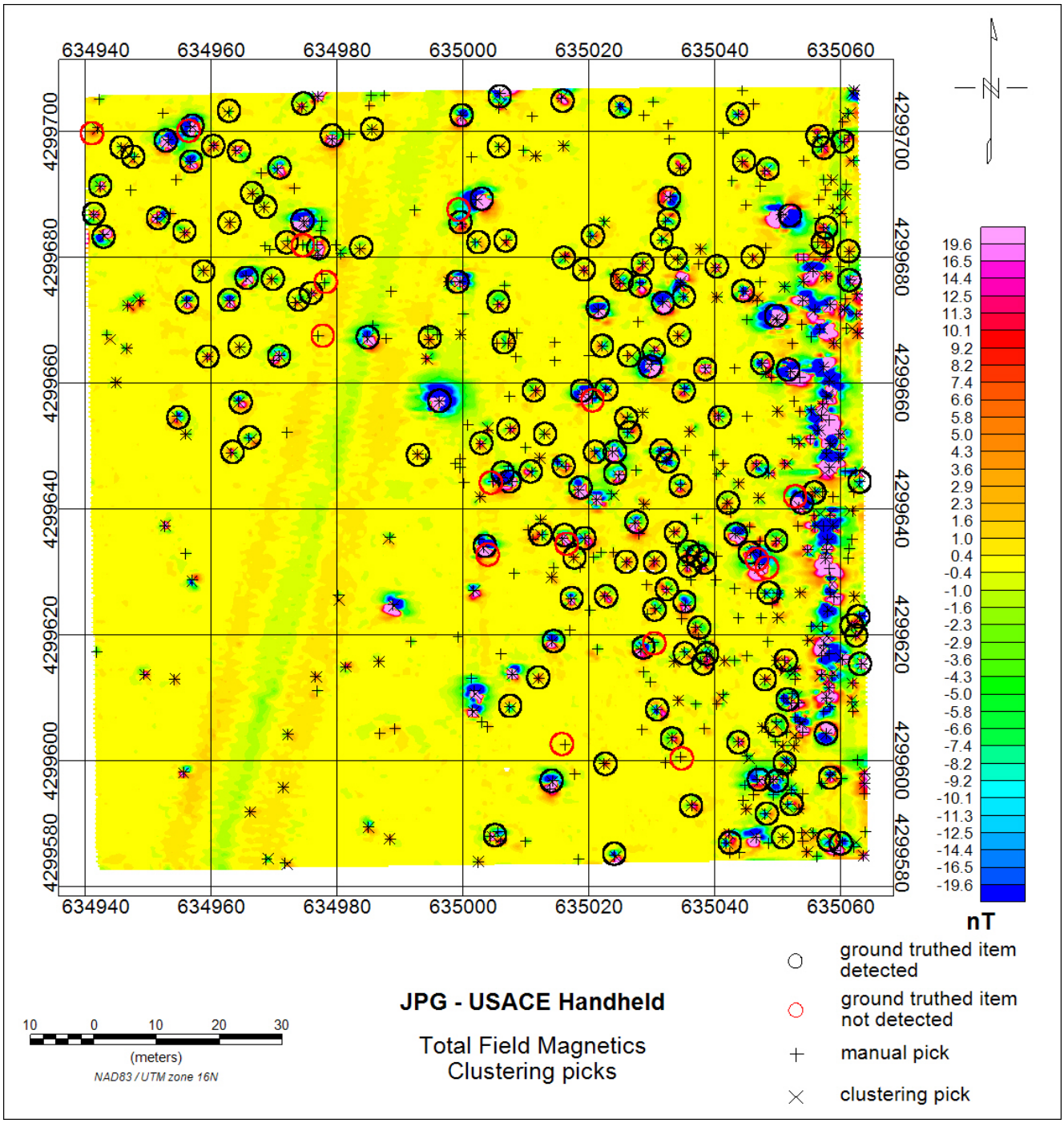

Figure 44. Color-coded map showing the total field magnetic data overlain by the ground truth, manual picks and anomalies identified by the clustering method; JPG.

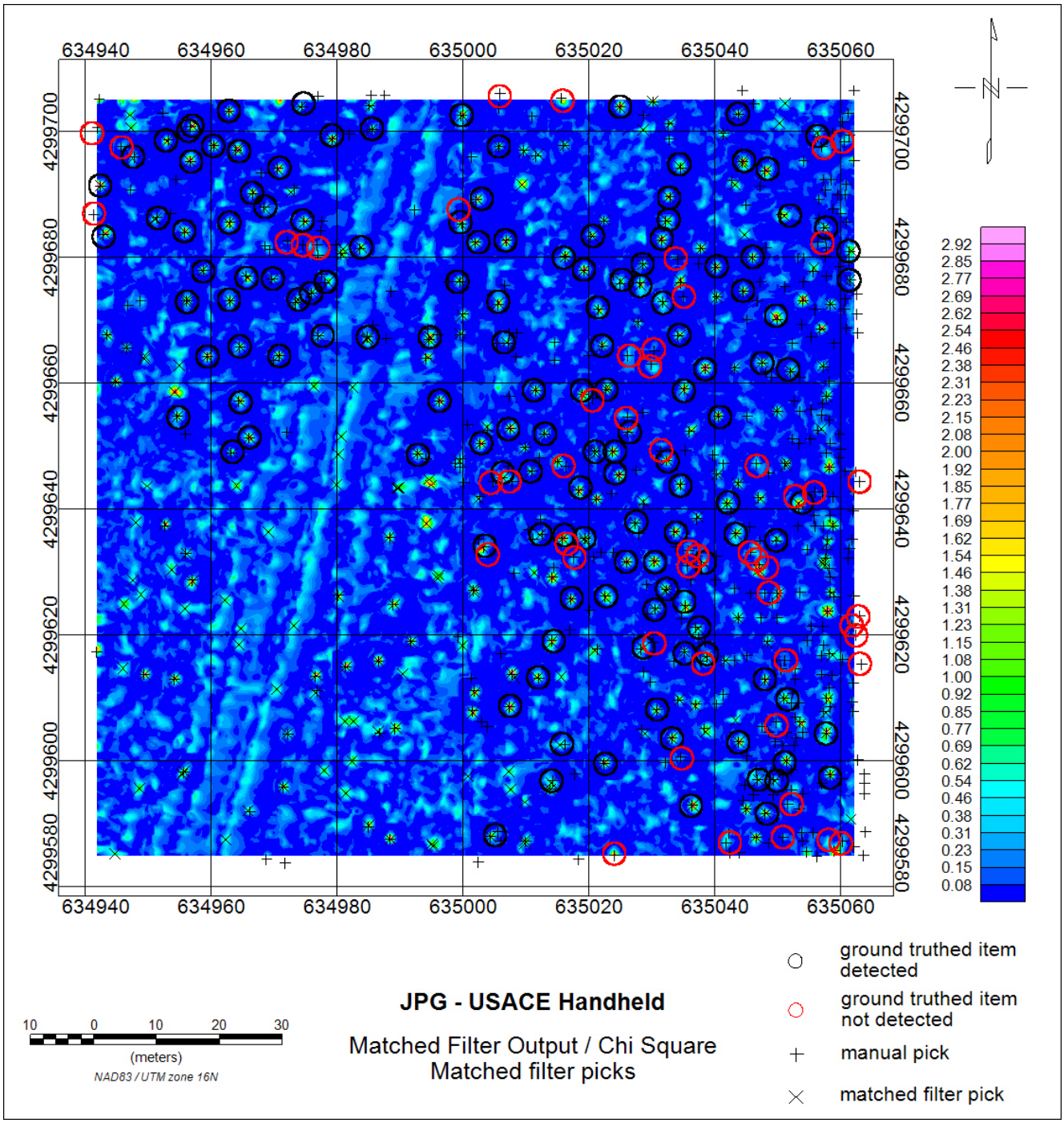

Figure 45. Color-coded map showing the (Matched filter output / Chi square) data overlain by the ground truth, manual picks and anomalies identified by the matched filter method; JPG.

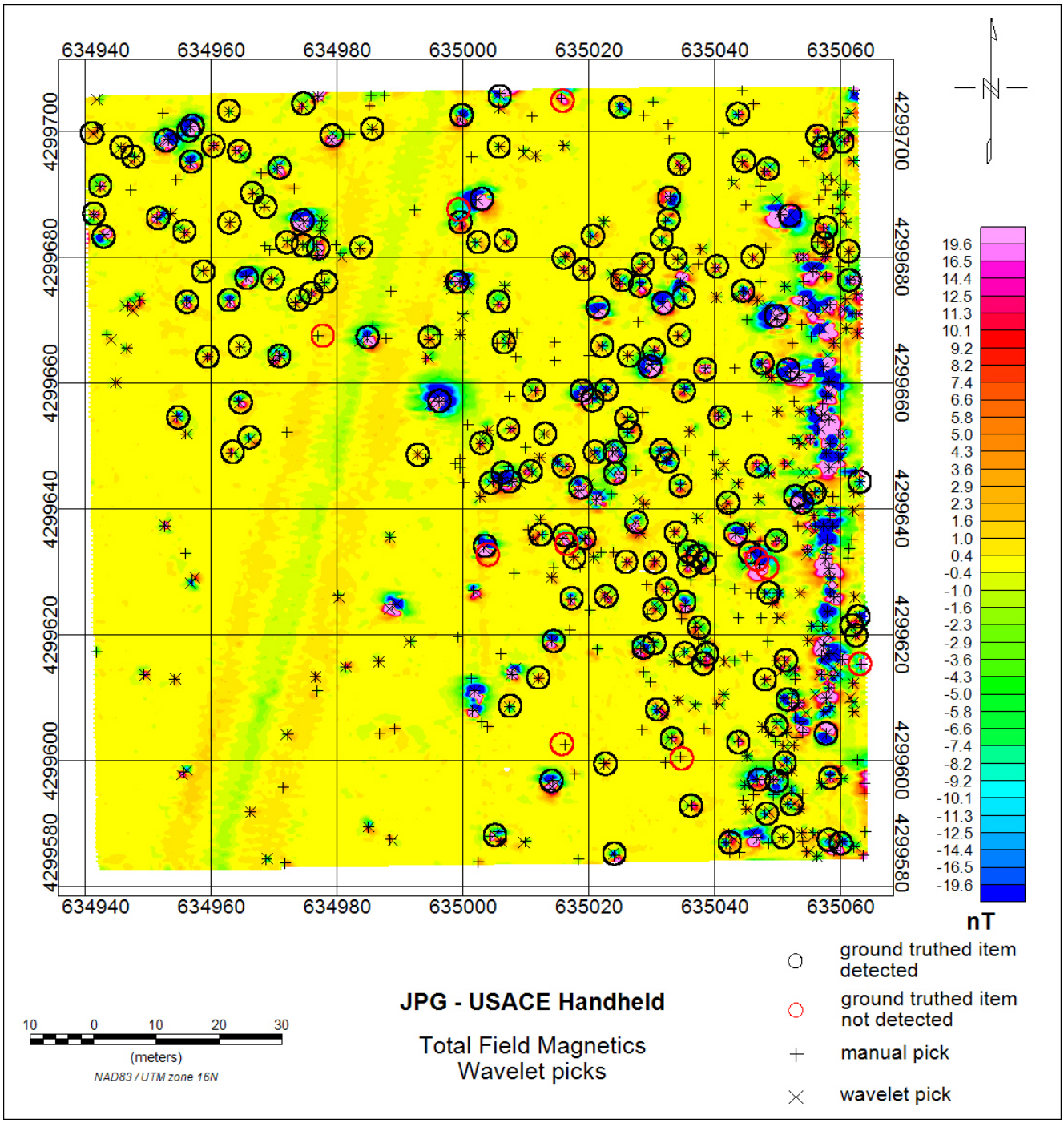

Figure 46. Color-coded map showing the total field magnetic data overlain by the ground truth, manual picks and anomalies identified by the AWD method; JPG.

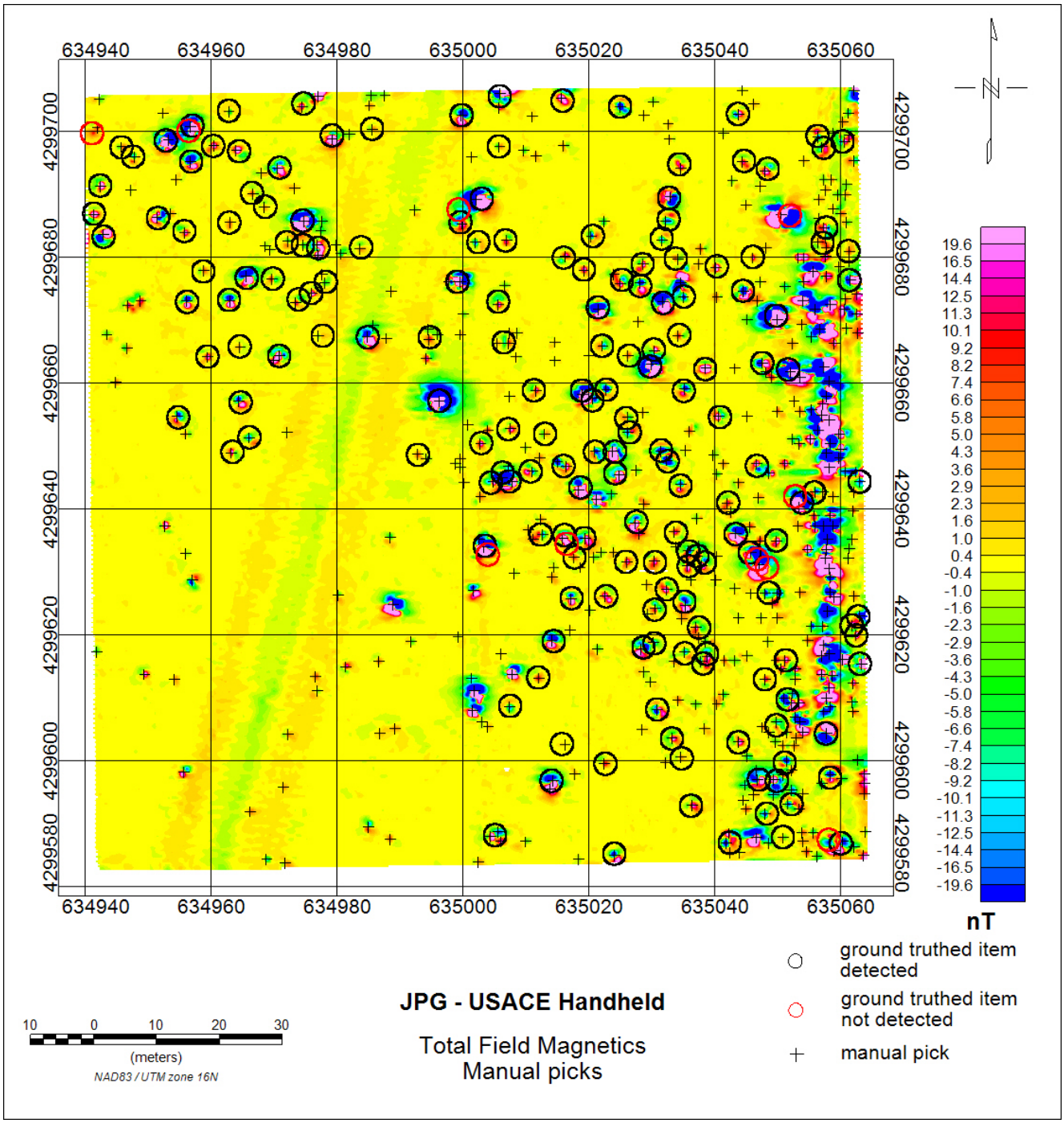

Figure 47. Color-coded map showing the total field magnetic data overlain by the ground truth and anomalies identified manually; JPG.

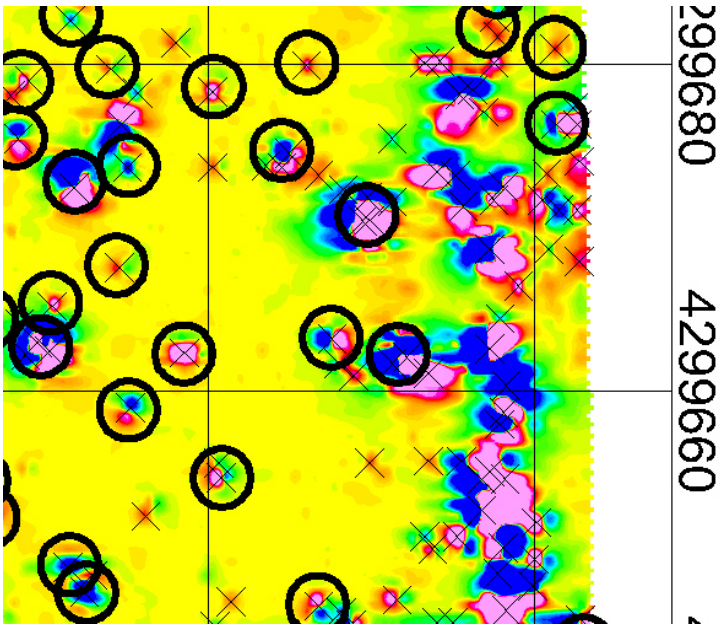

Figure 48. Total field magnetic data over a portion of the eastern edge of the JPG survey area. The X's show the multiple wavelet picks caused by positioning problems. The color scale is the same as in Figure 46.

4.3.2.5 Aberdeen Proving Ground, MD

As previously mentioned, a limited number of ground truth information has been released over the open field area at APG. Therefore our target dig sheets were scored against the emplaced targets by analysts from the Institute for Defense Analyses (IDA). The accurate ground truth information at APG enabled the calculation of Pd and rBAR as well as statistics of the location accuracy of the target declarations for each of the picking methods. The performance of the different target picking methods is summarized in Table 15 and Figure 49 and Figure 50. The numerator for the Pd represents the total number of ferrous ground truth items with no nearest neighbor within 2m (2m flag), AND (for ordnance) not deeper than the 11x depth, AND with an alarm ("suspected target") within the 0.5m scoring halo (radius). No clutter was removed by the diameter to depth filter. For large targets (e.g., 155mm shell), the halo was elongated into an ellipse along the long axis of the shell. The semi-major axis is half the item's length projected onto the ground plane, plus 0.5m. The denominator for the Pd calculation is the total number of true clutter and shallower than 11x ferrous ordnance with no nearest neighbor within 2m. All the calculations were rounded to 5% to protect the truth. The ROC curves in Figure 49 show that the manual and analytic signal methods had the highest Pd with the AWD method close behind. These three methods also had the highest number of background alarms which indicates that parameters were set to pick targets close to the noise background of the data. The last 5% of detections came at the expense of more than doubling the number of background alarms. The location accuracy for the different picking methods was fairly similar with the matched filter method producing the most accurate results. The matched filter method convolves the data with a magnetic dipole signal model which outputs target parameters. This would produce more accurate locations than the other methods that only use the locations and amplitudes of positive and negative peaks in the magnetic data to find the target location.

The following comments on the results were received from IDA.

- Large anomalies caused shadowing of one target over another from 2-6m separation. Ordnance up to 105mm projectiles were missed because of these overlapping signals. In some cases, there was no suspected target (alarm), in others there was a near miss alarm (within a 1m halo however). Note that the 1m halo would only hit more truth targets as onsies, twosies. Near miss was a failure mode, but not the only one.
- The matched filter had trouble with the bomblets and submuntions.
- Some targets were only found by the manual mode; this mode did very well. Several shadowed targets were found with manual.
- All had some trouble with 20mm’s, manual did the best.

We also selected 80 anomalies at APG to submit to the magnetic inversion algorithm found in UX-Analyze (UXO analysis software packaged developed under ESTCP project MM-0210) in order to test the ability of each method to extract the anomalies’ spatial extent. Of the 80 anomalies approximately 80% matched ferrous ground truth within a 0.5m halo with no nearest neighbor within 2m. Table 16, Figure 51 and Figure 52 summarizes the location, depth and size accuracies for the targets that matched a ground truth item. Overall, all the methods produced similar results with the location and depth accuracies being better than the size estimates. As

expected the locations output from the inversion algorithms were more accurate than those output directly from the picking methods (Figure 51). Both location and depth estimates were sufficiently accurate to allow dig teams to easily find the object of interest. Color coded maps showing the different target picking declarations and locations of the 80 anomalies selected for inversion are presented in Figure 53 to Figure 56.

Table 15. APG - Detection and location accuracy

Parameter / Method	*Total # picks*	*Pd*	*rBAR*	*Average miss Distance (m)*
Manual	707	0.9	0.58	.204
Clustering	444	0.8	0.335	.196
Wavelet	743	0.85	0.615	.212
Matched filter	206	0.7	0.105	.171
Analytic signal	620	0.9	0.495	.225

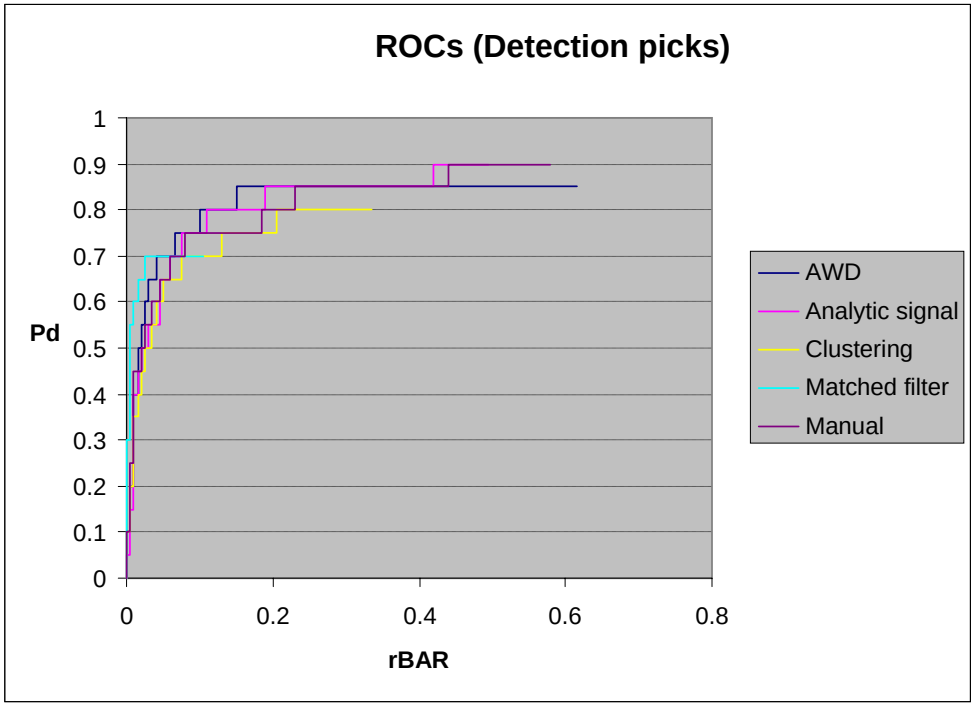

Figure 49. Receiver operating curve showing the number of ground truth objects detected by each method versus Background alarm rate; APG.

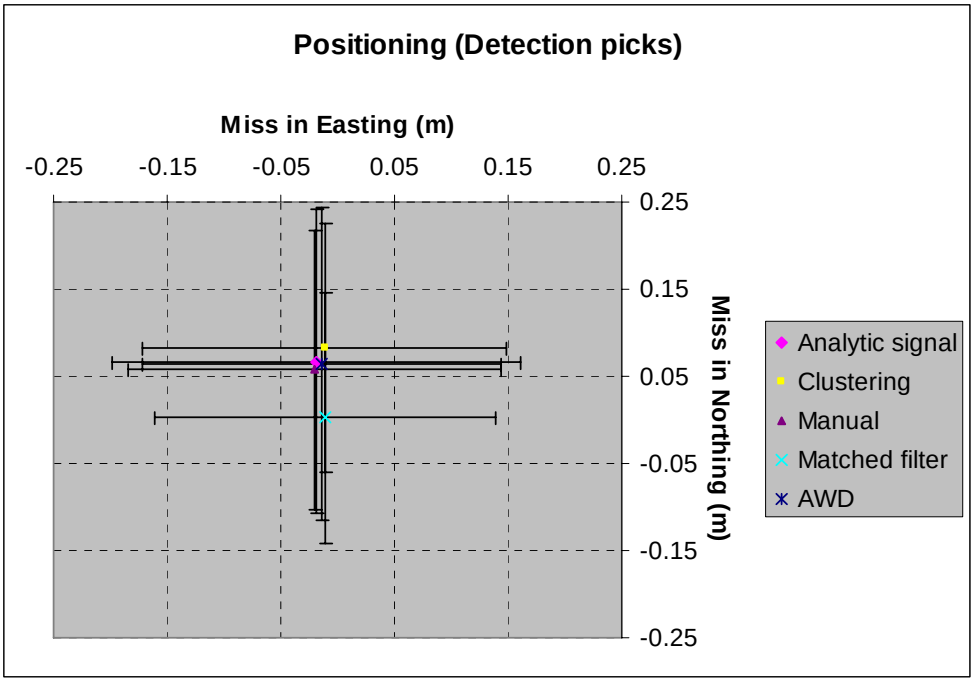

Figure 50. Graph showing the average miss for Easting and Northing (in meters). The range bars are symmetrical standard deviations.

Table 16 APG - Location and size accuracy of the 80 targets selected for inversion.

Method / Parameter	***Analytic signal***	***Clustering***	***Manual***	***Matched filter***	***AWD***
% of UXA targets matched within a 0.5m halo (2m flag) of the ground truth location using the initial XY	79%	77%	81%	81%	81%
% of UXA targets matched to a truth item (2m flag) also within .3m radius using the fitted XY	93%	92%	92%	90%	92%
Average miss distance of initial picks (m)	.217	.177	.193	.156	.196
Average miss distance of fitted picks (m)	.133	.134	.134	.139	.135
% of matched UXA targets within .3m of the ground truth depth.	97%	94%	97%	97%	94%
Average miss depth (m)	-.074	-.057	-.067	-.072	-.082
Standard deviation of depth misses (m)	.157	.181	.148	.151	.162
% of matched UXA targets (only ordnance, 2m flag, 11x flag) with a size factor less than or equal to 0.3. Size factor = ABS(true_size - estimated_size) / true_size. Does not include 500lb Bombs.	47%	39%	44%	44%	44%

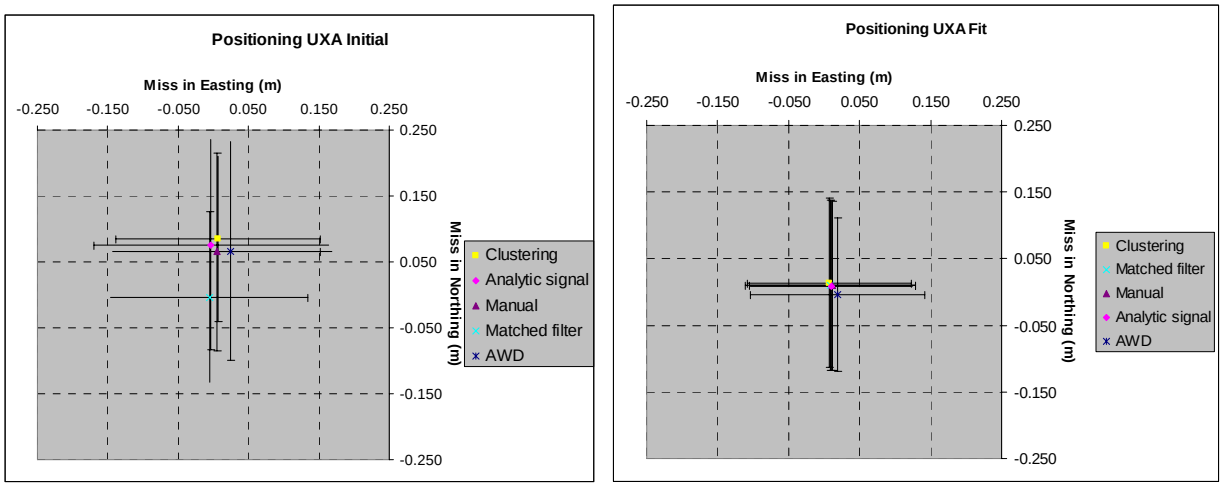

Figure 51. Comparison of the location accuracy of the positions output directly from the different picking methods (left) and the locations output after passing the selected data to the magnetic fitting algorithm in UX-Analyze (right).

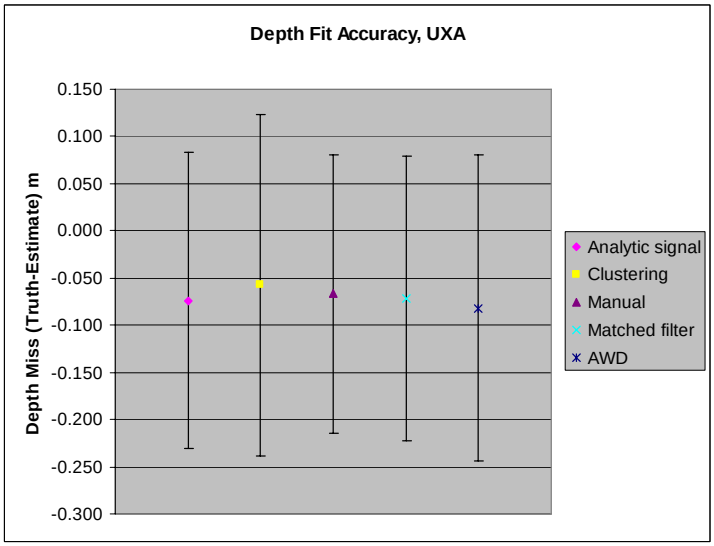

Figure 52. Depth fit accuracy of the different picking methods. Data extracted from each picking method were passed to a magnetic inversion algorithm to estimate the target's depth.

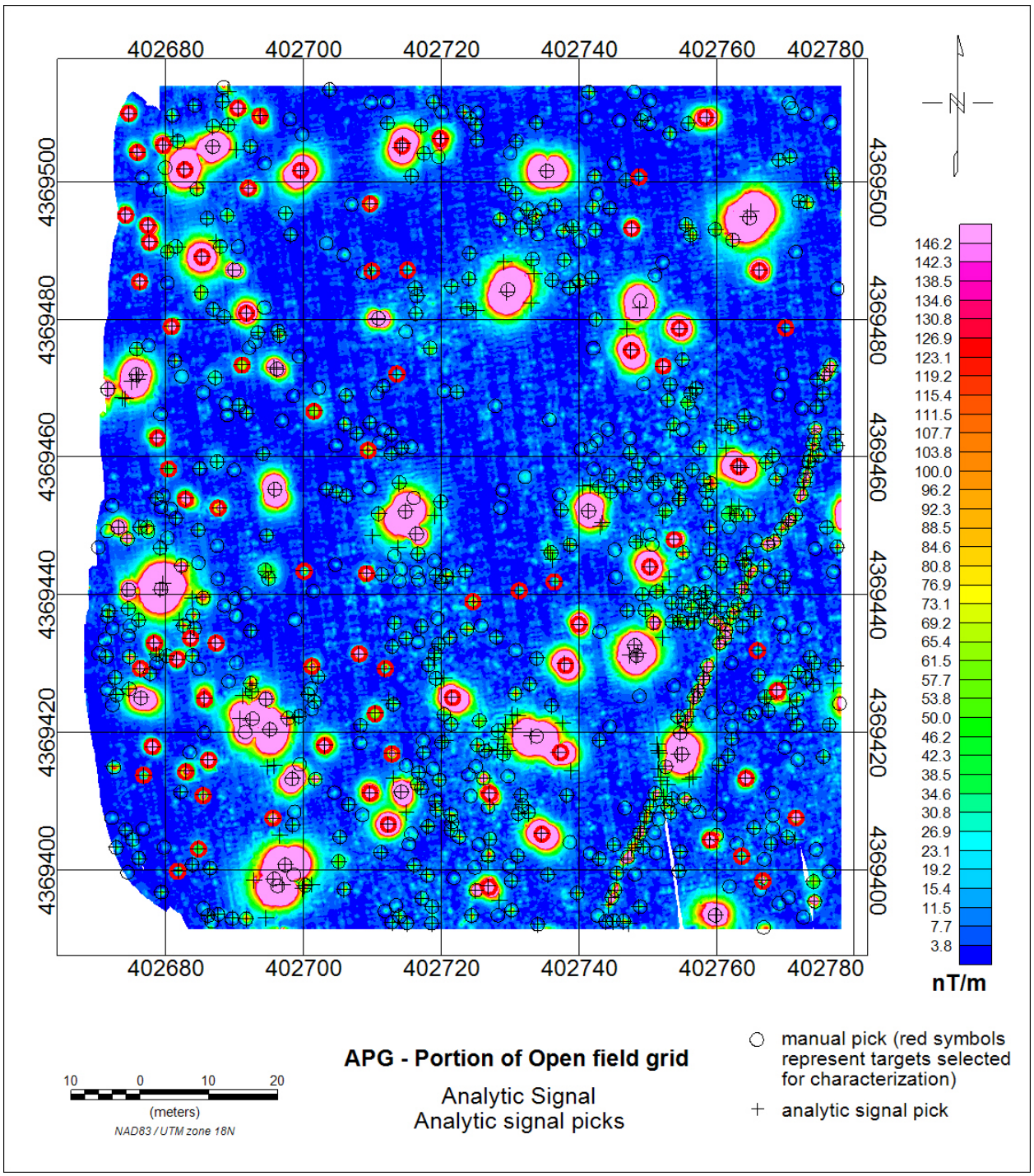

Figure 53. Color-coded map showing the analytic signal data overlain by the manual picks and anomalies identified by the analytic signal method; APG.

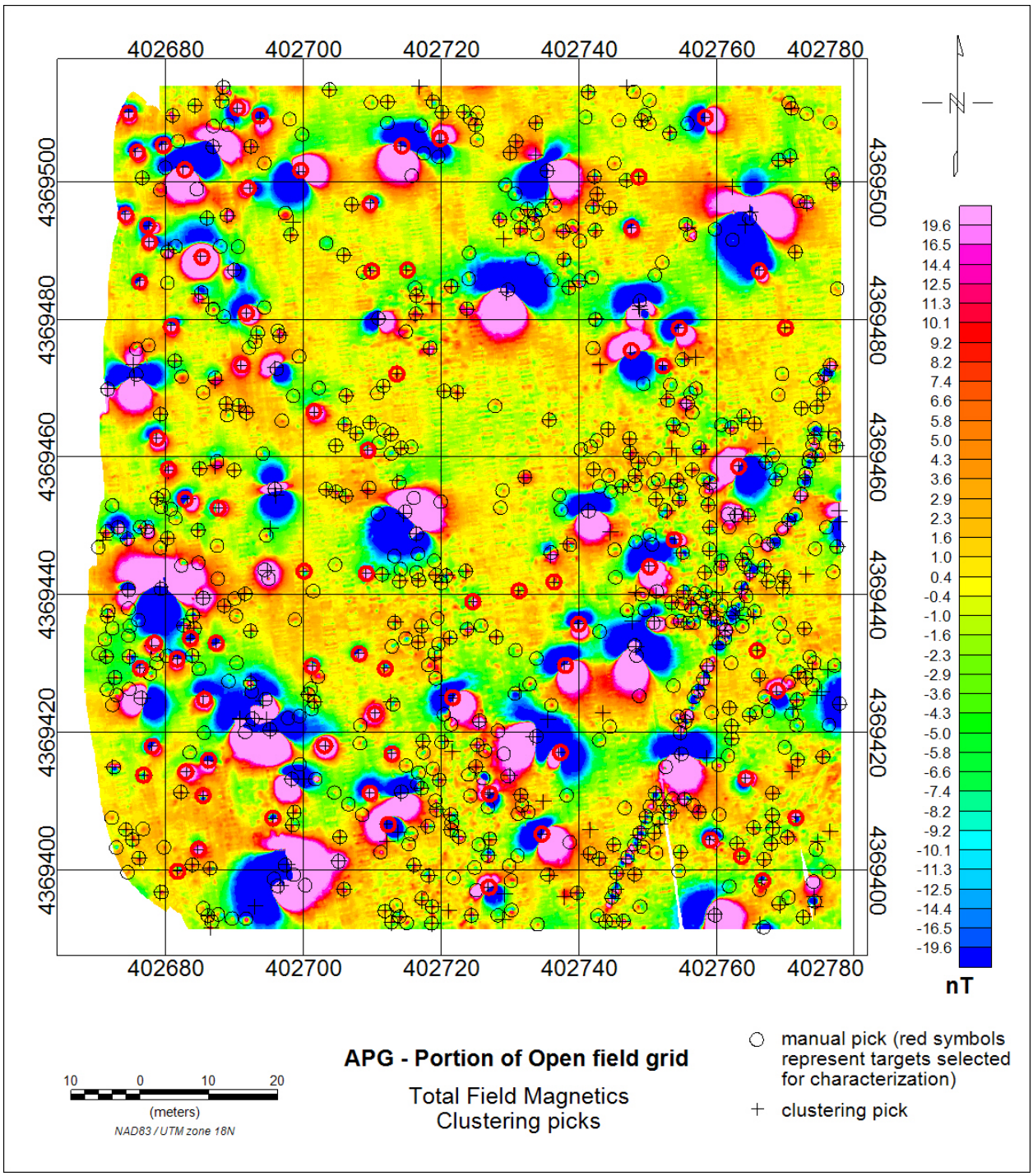

Figure 54. Color-coded map showing the total field magnetic data overlain by the manual picks and anomalies identified by the clustering method; APG.

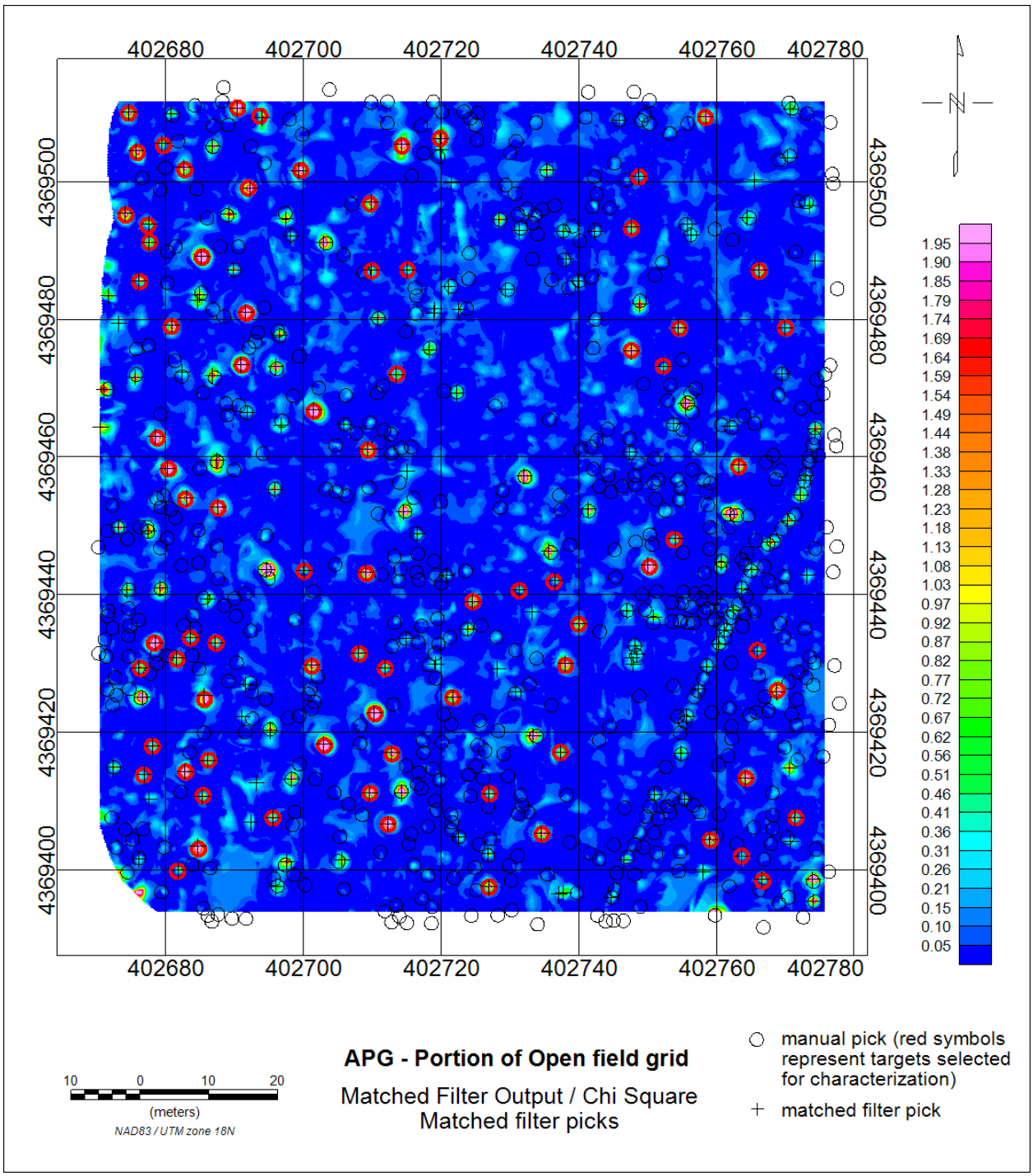

Figure 55. Color-coded map showing the (Matched filter output / Chi square) data overlain by the manual picks and anomalies identified by the matched filter method; APG.

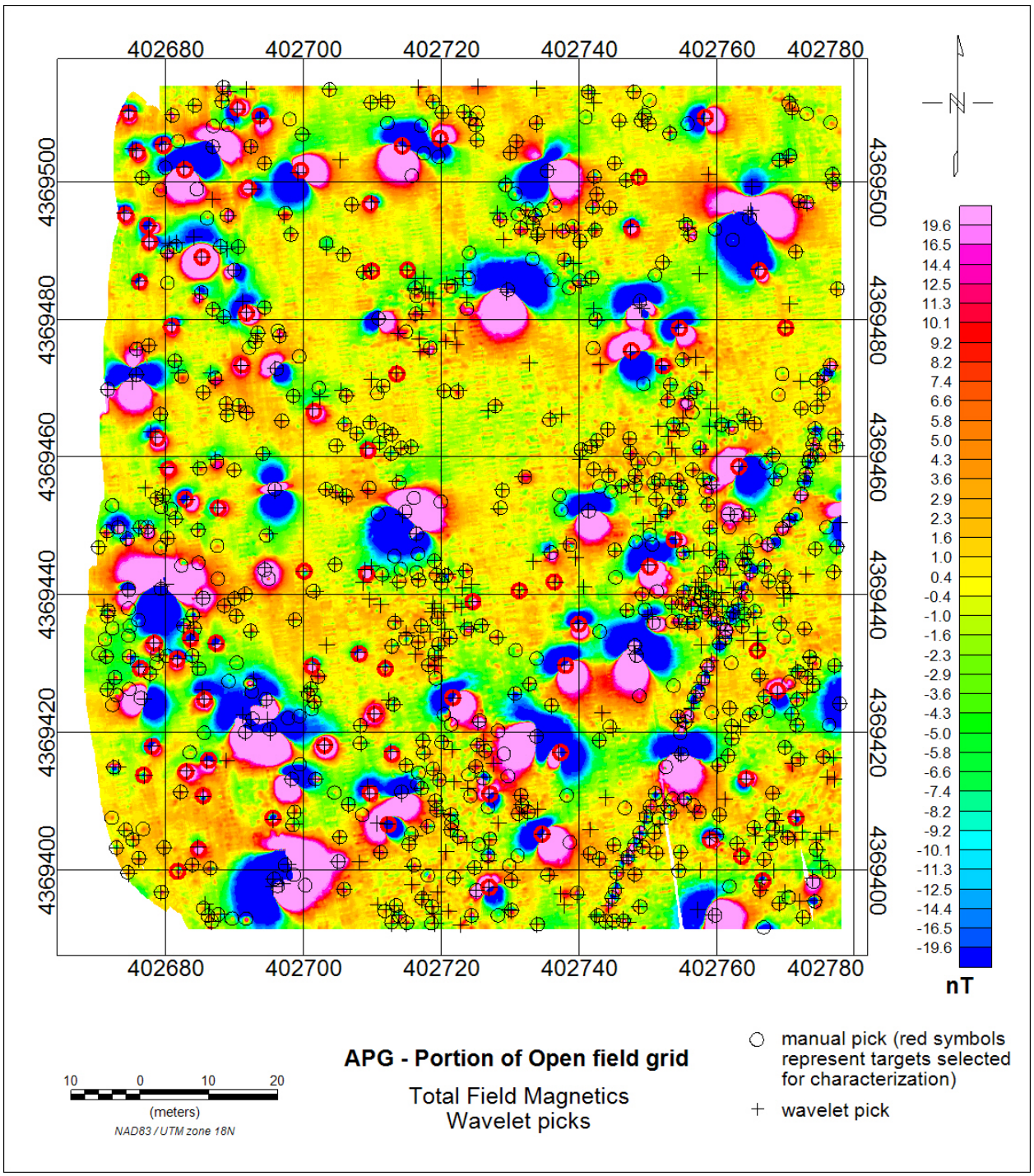

Figure 56. Color-coded map showing the total field magnetic data overlain by the manual picks and anomalies identified by the AWD method; APG.

4.3.2.6 WAA Airborne survey – Pueblo Precision Bombing Range #2, CO

The performance of the different target picking methods is summarized in Table 17 , Figure 57 and Figure 58. Color coded maps showing the different target picking declarations and manual picks overlain on their respective data are presented in Figure 59 to Figure 62. The Pueblo Airborne survey did not have any ground truth so the automatic target picks were compared to the manual picks. The different methods had similarly poor Pd's but a range of Pfa's. The main reason for the poor Pd's was the high background geology throughout the area. Figure 58 shows that all the methods stopped picking targets at roughly the same threshold. The parameters and thresholds for each of the methods were set to maximize the number of targets selected while keeping the number of picks related to geology at a minimum.

Figure 63 shows noise levels at various locations over the survey area. The noise was estimated by calculating the standard deviation of the data contained within each box displayed on the map. The boxes were located in areas that contained various noise levels and were void of any manual picks. The noise ranged from 0.16nT to 2.28nT which is a wide range for these data. The manual method had the advantage of dynamically altering the picking threshold to the surrounding noise levels and thus was able to select targets in the southern portion of the area where the noise levels were lower. In the southern area, the automatic pickers selected few targets because their thresholds could not be set low enough to detect these targets without adding thousands of additional picks due to geology. Conversely, in the northern portion of the survey area where the geologic noise is much greater, many of the automatic pickers selected numerous anomalies that were geology related as shown in Figure 64. This effect is especially seen in the wavelet and analytic signal methods and resulted in their higher Pfa's. On the other hand, the (MFoutput/Chisq) did a good job at reducing the effect of the geology.

Even though the manual method performed well with these data it missed a few obvious strong anomalies that all the automatic methods found as shown in Figure 65. Here we see some anomalies shown by the black squares that were missed by the manual method. It is likely these were missed because of the "human factor". It took the manual analyst 9 hours to pick all the targets in this area. This was a lengthy endeavor and during the systematic process of zooming and scrolling through the data this small section of data was inadvertently missed.

Table 17. WAA Pueblo Airborne - Detection and location accuracy

Parameter / Method	*Total # picks*	*Pd*	*Pfa*	*# within 1m*	*# 1 - 1.5m*	*# 1.5 - 2.0m*	*% within 1.5m*
Manual	383						
Clustering	387	0.55	0.46	153	41	17	92
Wavelet	547	0.53	0.90	138	47	17	92
Matched filter	323	0.50	0.34	140	41	12	94
Analytic signal	397	0.53	0.50	185	17	2	99

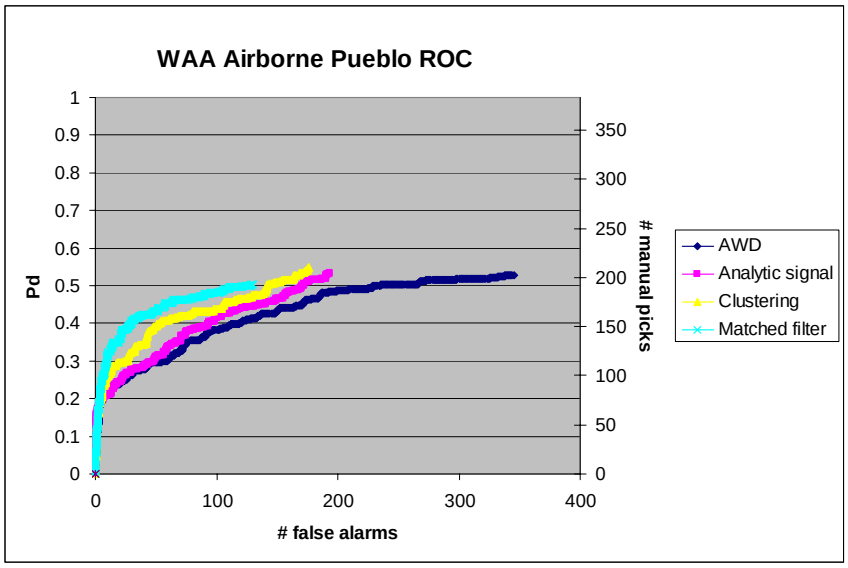

Figure 57. Graph showing Pd versus the number of false alarms (automatic picks not matching a manual picks); Pueblo airborne.

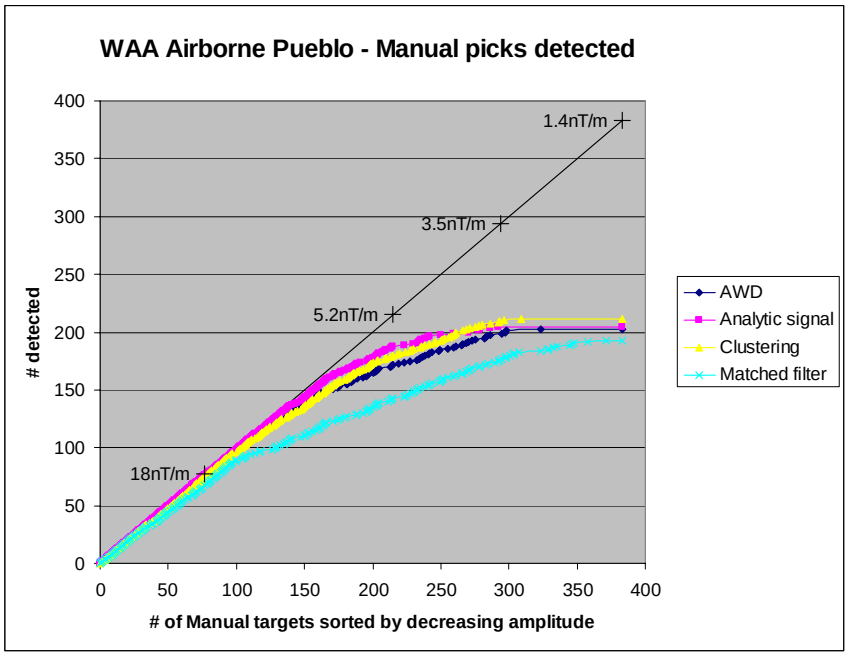

Figure 58. Graph showing the number of manual picks detected by each method as a function of signal amplitude; Pueblo airborne.

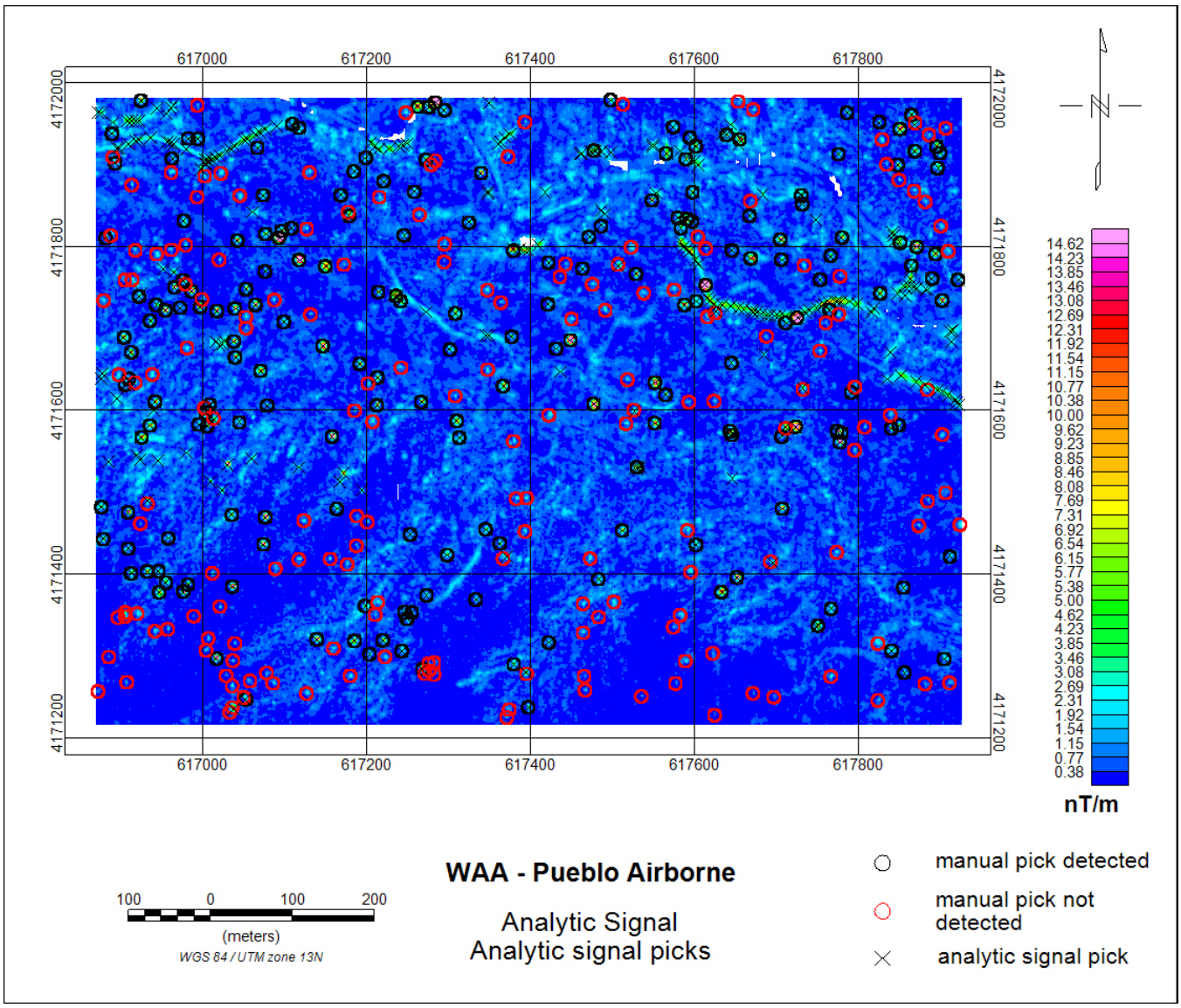

Figure 59. Color-coded map showing the analytic signal data overlain by the manual picks and anomalies identified by the analytic signal method; Pueblo airborne.

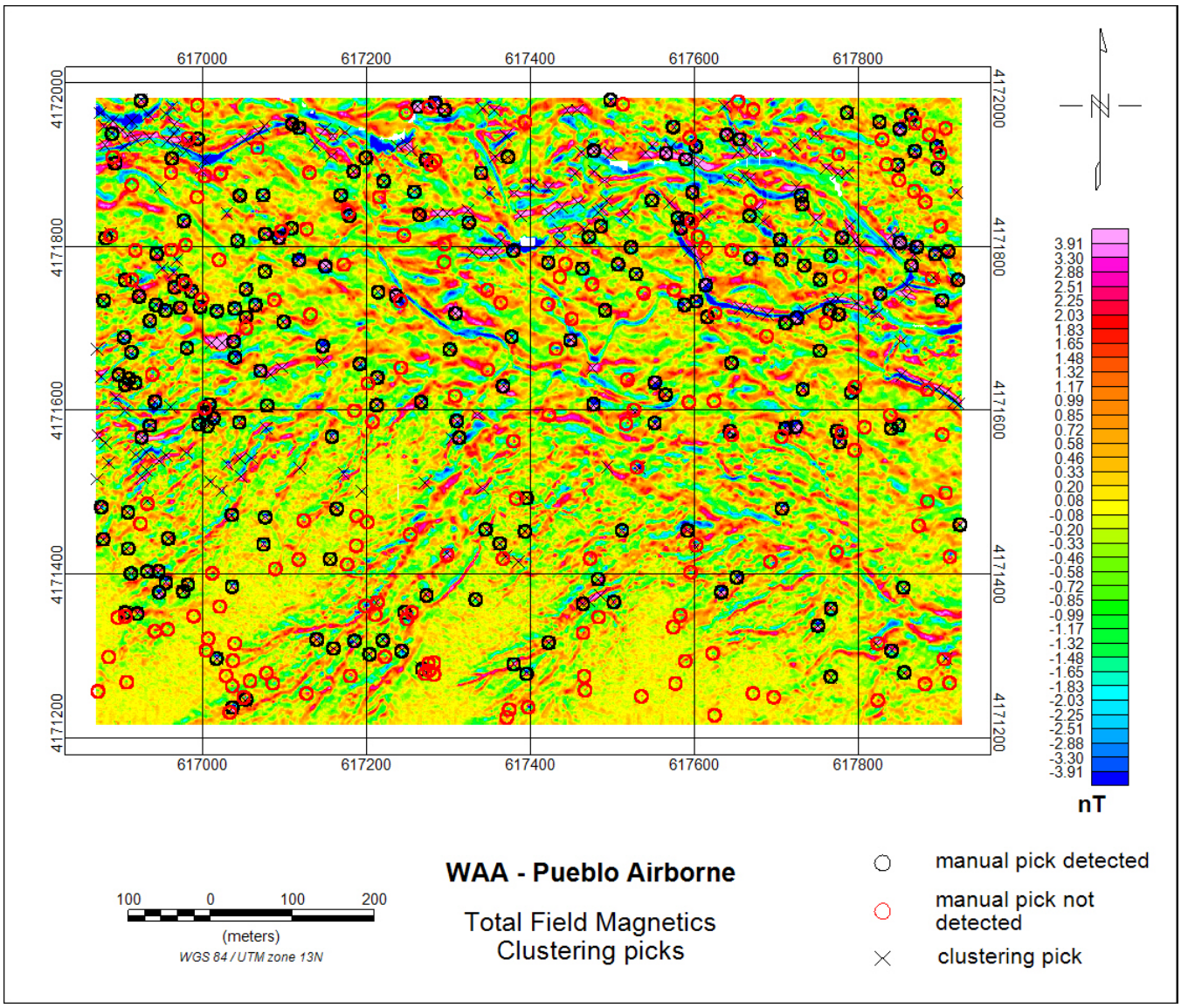

Figure 60. Color-coded map showing the total field magnetic data overlain by the manual picks and anomalies identified by the clustering method; Pueblo airborne.

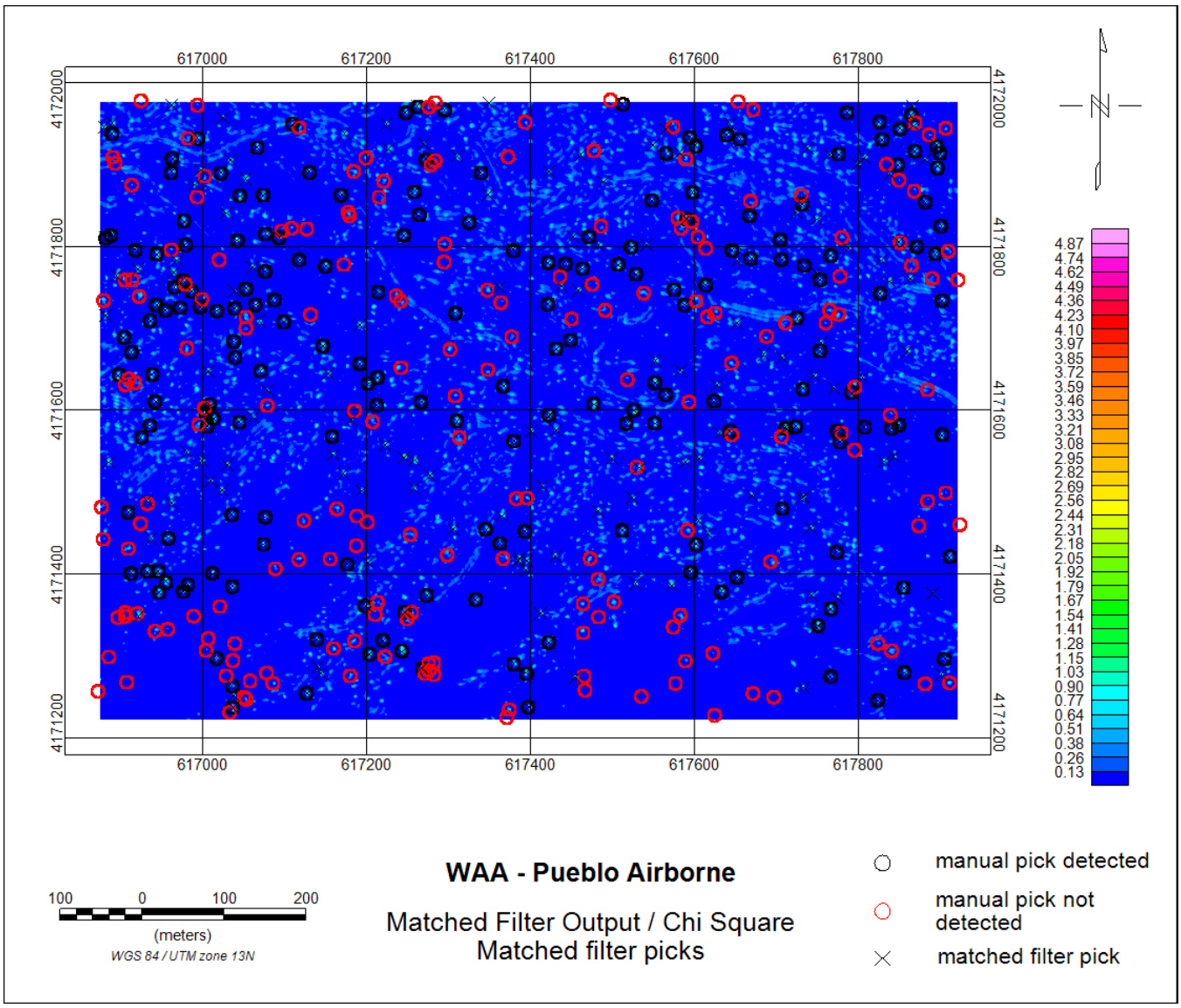

Figure 61. Color-coded map showing the (Matched filter output / Chi square) data overlain by the manual picks and anomalies identified by the matched filter method; Pueblo airborne.

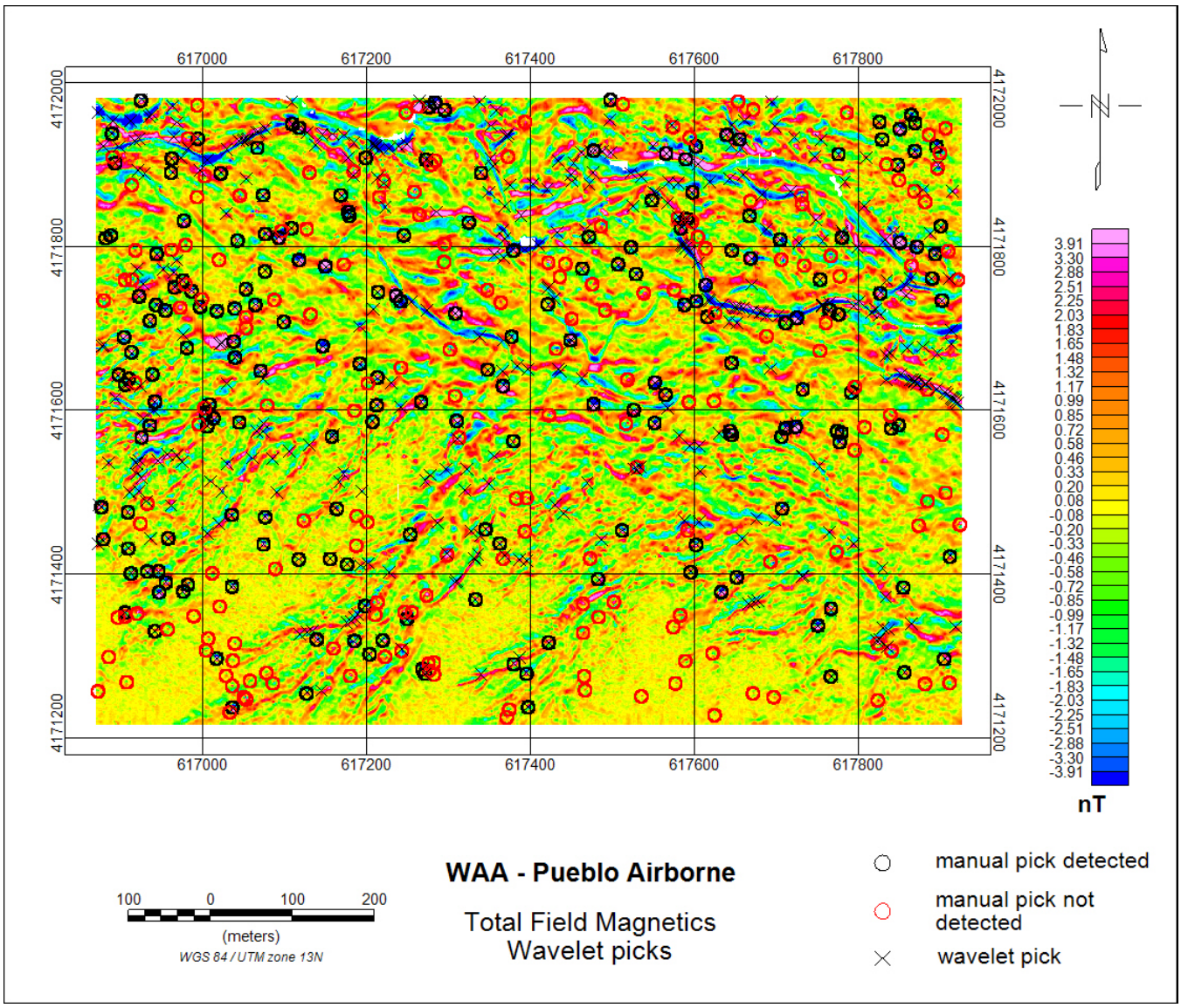

Figure 62. Color-coded map showing the total field magnetic data overlain by the manual picks and anomalies identified by the AWD method; Pueblo airborne.

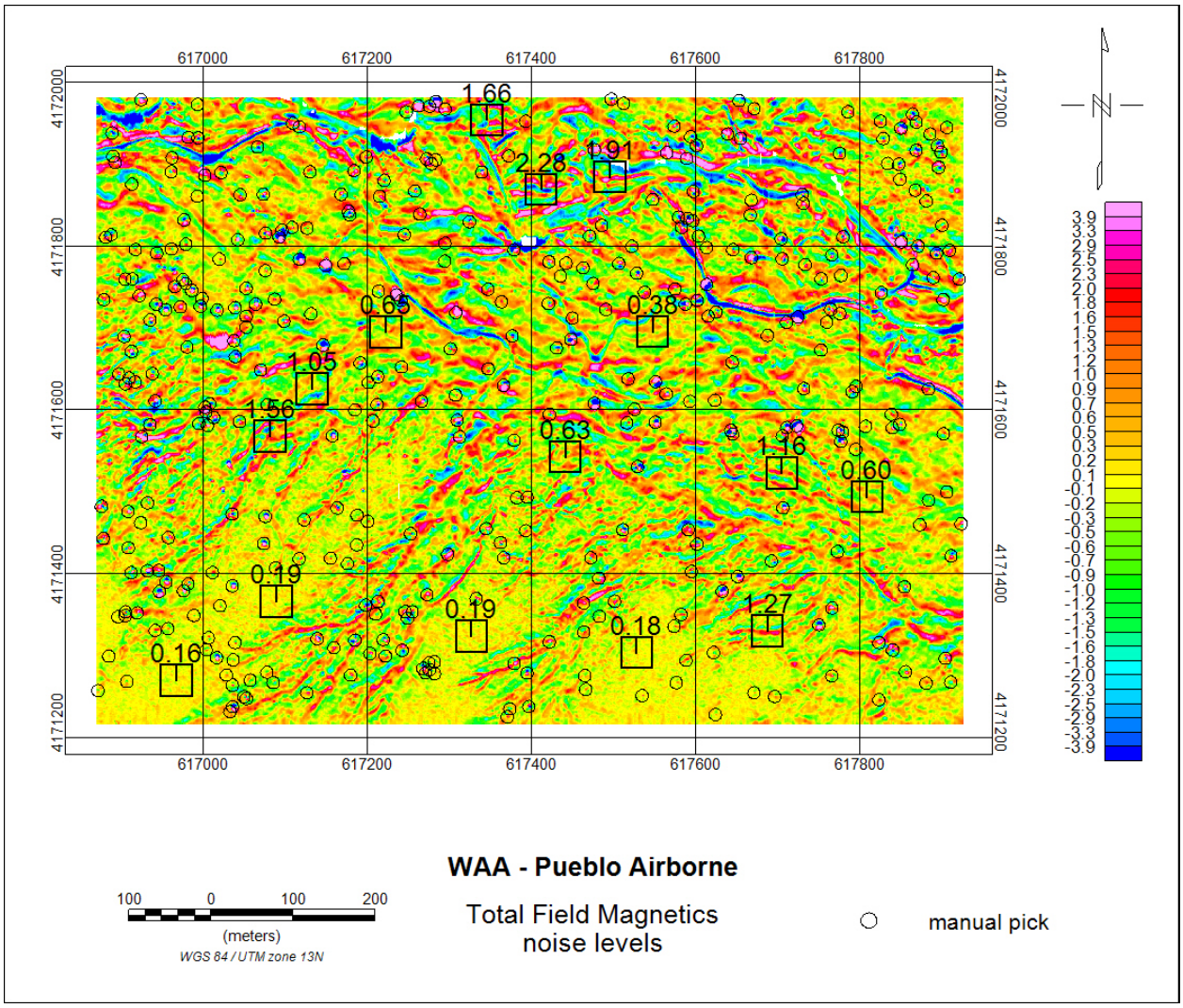

Figure 63. Color coded map of the total field magnetic showing the noise at various locations. The noise was estimated by calculating the standard deviation of the data contained within each box.

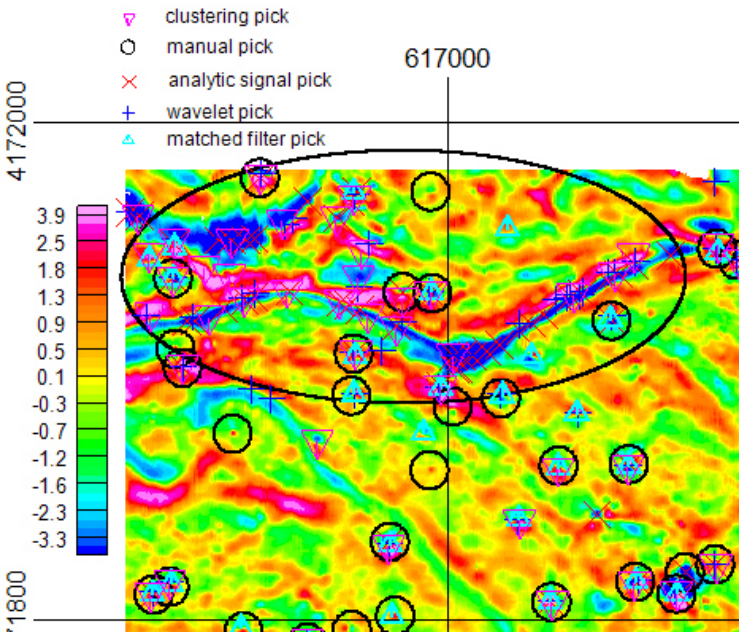

Figure 64. Color coded map of the total field magnetic data showing the numerous picks due to geology by the different target pickers in the northern portion of the Pueblo airborne survey area.

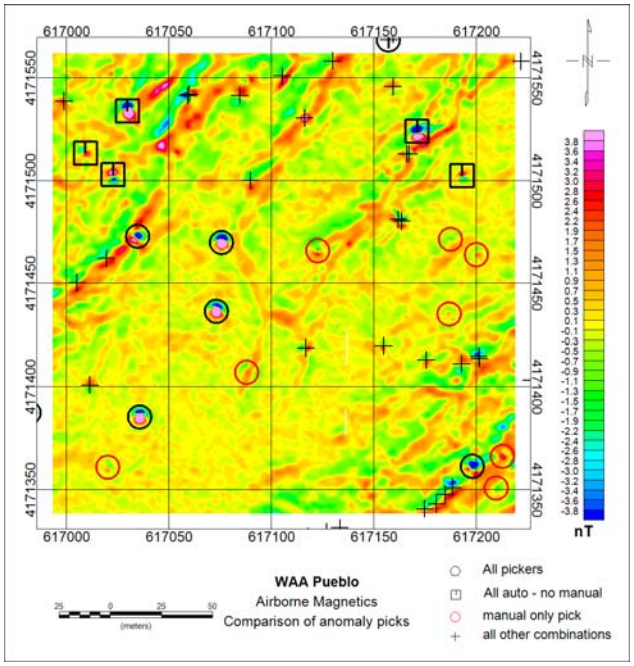

Figure 65. Color coded map of the total field magnetic data showing some targets missed by the manual picker but detected by all the automatic methods.

4.3.2.7 WAA Transect survey – Pueblo Precision Bombing Range #2, CO

The performance of the different target picking methods is summarized in Table 18, Figure 66 and Figure 67. Color coded maps showing a section of the different target picking declarations and manual picks overlain on their respective data are presented in Figure 68. The analyzed transects only covered two anomalies with known ground truth; therefore the automatic target picks were compared to the manual picks. As stated earlier, the matched filter could not be run on this data set because the filter box needed would be larger than the 1.75m width of the transect data. The clustering and analytic signal methods produced similar results for these data. Both methods picked the larger targets with few false alarms when compared to the manual declarations. As Figure 67 shows the thresholds for the two methods were set higher than the wavelet method and the manual method. Because the object of these data was WAA the thresholds were set at reasonable values.

The wavelet method had a higher Pd but at the cost of many more false alarms. 136 of these false alarms are picks that occurred outside the extents of the data. A few examples can be seen in Figure 68. They were caused by extrapolation of the data when creating the input grid to the wavelet algorithm. Most of the remaining false alarms were low amplitude declarations that did not match a manual pick as shown in Figure 69. These additional picks (black crosses) as well as many of the manual picks (black circles) that were not selected by the automatic methods were at amplitudes that were very close to the background noise of the data. Without complete ground truth, we cannot determine if these were valid picks due to a metallic object or caused by noise.

Table 18. WAA Pueblo Transects - Detection and location accuracy

Parameter / Method	***Total # picks***	***Pd***	***Pfa***	***# within 1m***	***# 1 - 1.5m***	***# 1.5 - 2.0m***	***% within 1.5m***
Manual	887						
Clustering	454	0.49	0.02	375	40	24	95
Wavelet	1049	0.76	0.42	506	117	52	92
Analytic signal	505	0.55	0.02	474	9	1	100

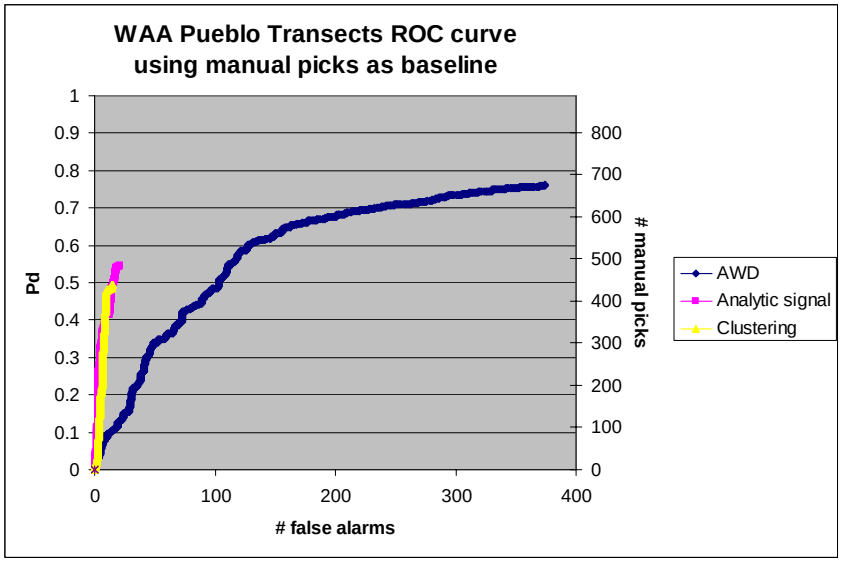

Figure 66. Graph showing the number of ground truth objects detected by each method as a function of signal amplitude; Pueblo transects.

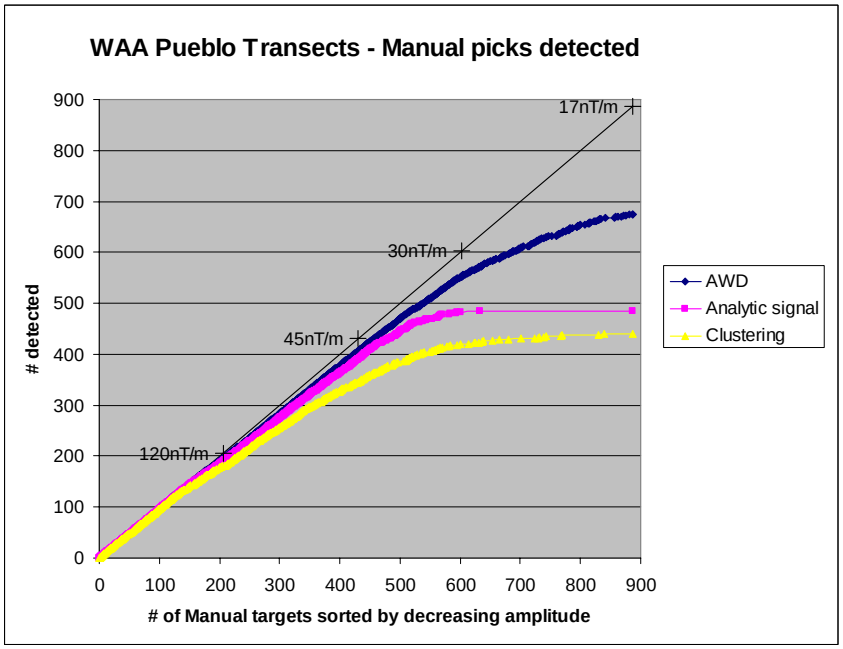

Figure 67. Graph showing the number of ground truth objects detected by each method as a function of signal amplitude; Pueblo transects.

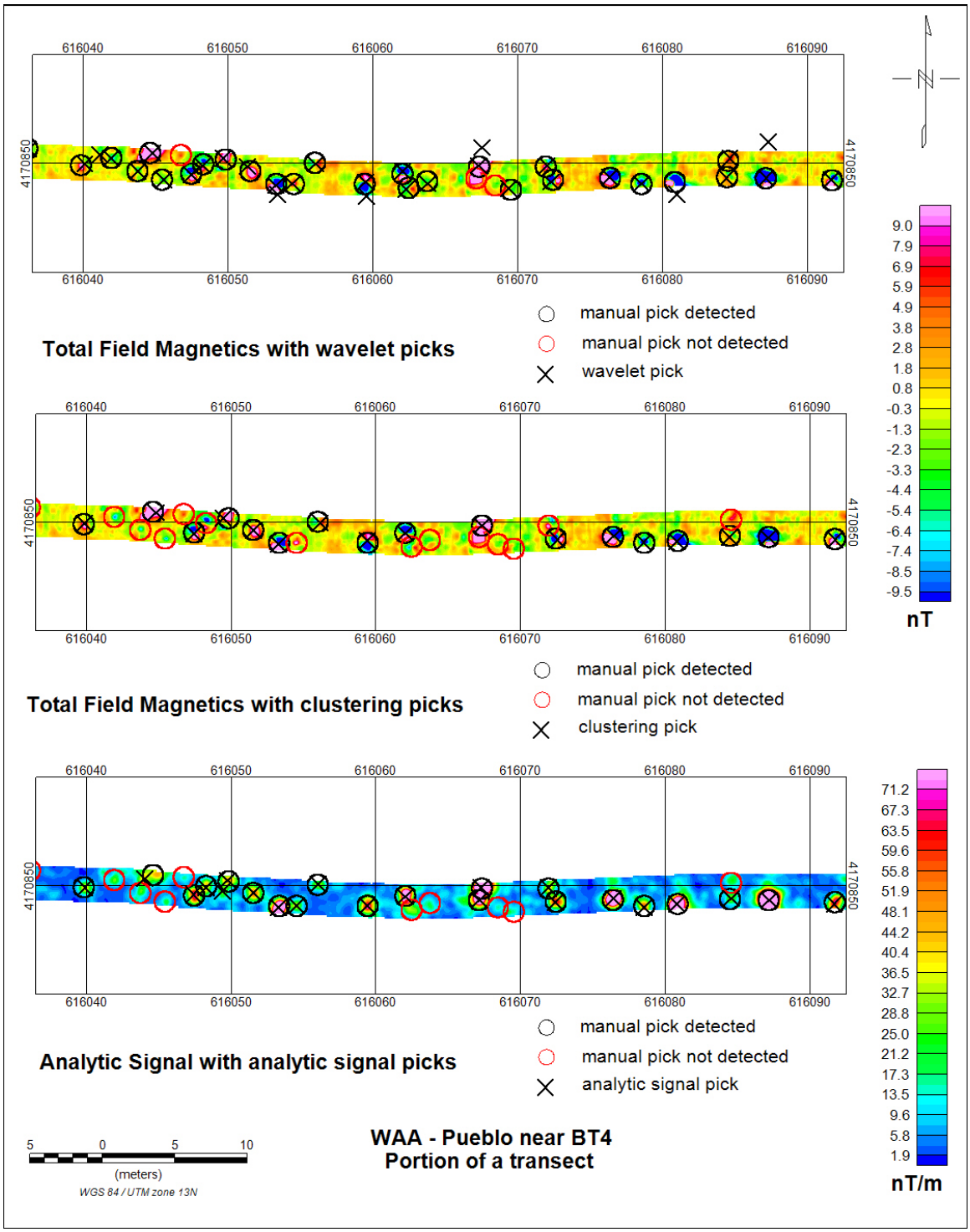

Figure 68. Color-coded map showing the total field magnetic data overlain by the manual picks and anomalies identified by the clustering method; Pueblo transects.

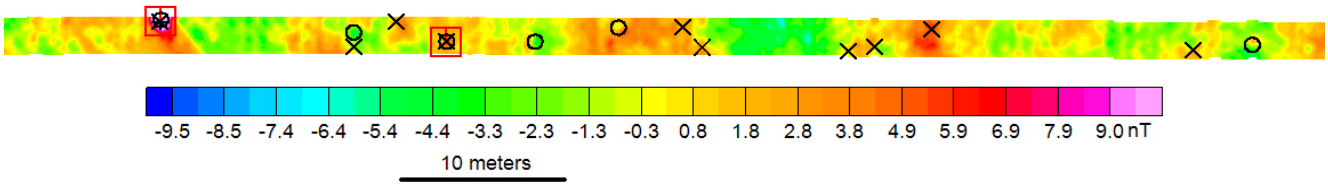

Figure 69. Section of transect magnetic data showing some low amplitude declaration by the different picking methods. The analytic signal, clustering, wavelet and manual picks are plotted as black plus sign, red box, black cross and black circle, respectively.

4.3.3 Target Picking Time

The actual time it took to set up the optimum parameters and run the automatic target pickers were recorded for each algorithm and data set. We also measured the setup time and processing time separately because the setup time will be major component of the total time for the relatively small data sets we used in this demonstration. However, on large data sets that have relatively consistent data characteristics the setup time will be negligible when compared to the overall time to pick all the targets. The total picking time for the different methods is shown in Figure 70. The analytic signal was by far the quickest of the methods followed by the AWD. The matched filter and clustering algorithms gave similar times with the manual picking being the slowest as expected. It was noted that for very small data sets with few anomalies, such as the USACE GPO, the manual picking performed quicker than the clustering and matched filter methods. This was due entirely to the setup time. Figure 71 presents the results if we remove the setup time and only compare the processing times. This graph clearly shows the automatic picking methods are much quicker (4-50 times faster) than the manual method in all cases. We note that for the transect data the speed of the AWD algorithm is greatly affected. This is because of the large spatial extent of the transects and the requirement that the data be gridded at a small (relative to the spatial extent of the data) grid cell size. On the other hand the clustering algorithm works on the actual profile data and not the gridded data so is not affected by spatial extent of the transects.

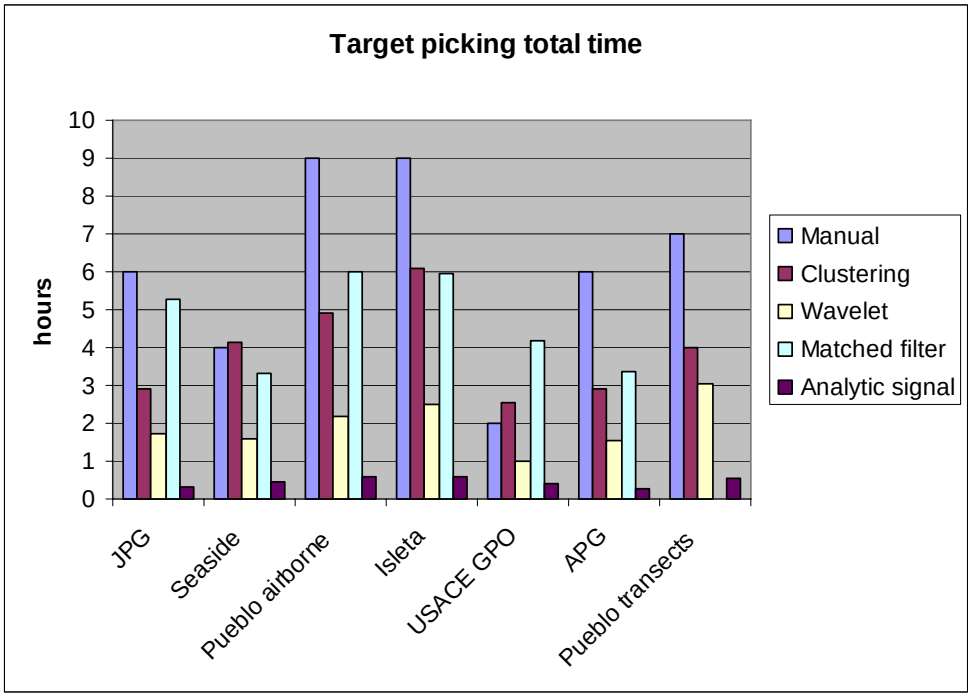

Figure 70. Graph showing the total time to analyze the data sets for the different target picking methods.

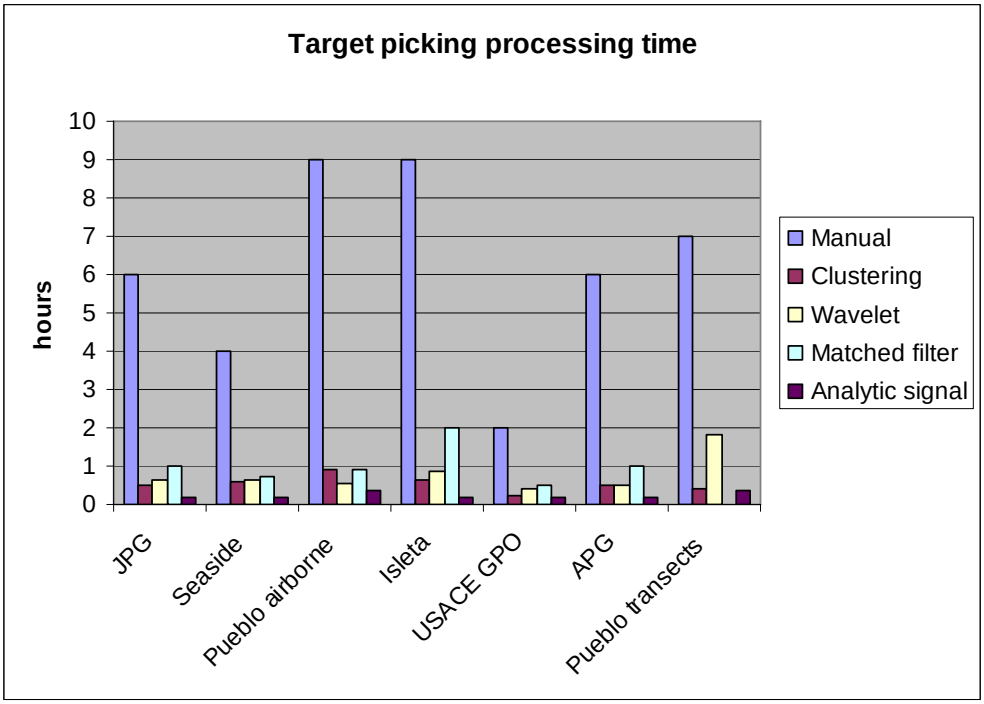

Figure 71. Graph showing the processing time to analyze the data sets for each of the target picking methods.

4.3.4 Qualitative Metrics

All the target picking methods were incorporated into the Oasis montaj™ platform. This made it easy for users experienced in data analysis and Oasis montaj™ to execute the software. The analysts were also able to directly access the graphical presentations and appropriate tools in Oasis montaj™ to assist in their analysis. The input dialogs and basic procedures to run the software are straight forward for all the algorithms but an experienced user would be required to determine which target picking method to use and what how to set the parameters. Currently, the software has limited help for the different algorithms and no user manual to direct the user on the advantages and disadvantages of the different algorithms and how to set the parameters for each of the algorithms. There are few parameters to set for the analytic signal and matched filter algorithms and they are fairly simple to set. Conversely, the AWD and clustering methods have many parameters that require setting to achieve the best results.

During this demonstration, the clustering algorithm encounter a few memory related bugs which have been corrected. As of November 2007, the current Oasis montaj™ release is 6.4 and we do not experience any systematic difficulties or intermittent bugs while using the analytic signal, clustering or matched filter algorithms. The AWD algorithm is also operational but still needs to

be run using Oasis montaj™ V6.2 because of incompatibilities between the .NET versions used in SkyNet and Oasis montaj. This issue is expected to be resolved in the near future as SkyNet is upgraded to .NET version 2.0.

4.3.5 Discussion

Overall, the manual method proved to be the best at picking valid targets especially in areas with varying amounts of geology and background noise. In general, the manual picker was able to set a lower threshold for each data set than the automatic methods because he can screen out the anomalies that are caused by noisy data or geology and pick the small amplitude anomalies located in the quieter areas as seen in the Pueblo airborne data set. This ability is also useful when dealing with poor quality data seen in the JPG data. The manual picker was able to interpret positioning problems that caused some large anomalies to appear to be several small anomalies and only make one declaration whereas some of the automatic picks had multiple declarations. The main drawbacks to the manual method are time, operator bias and operator error. In this demonstration the manual method was 4 to 50 times slower (not including setup time) than the automatic methods depending on the data set. We also saw in the Pueblo airborne data how operator fatigue or error resulted in some missed targets. Although only one manual analyst was used for this demonstration we see signs of operator bias. The manual picking threshold for all the data sets was very close to the background noise level except for the Seaside data which found significantly fewer matches to ground truth objects than the analytic signal and wavelet methods. This bias is likely to be even more pronounced if different analysts are used.

Of the automatic methods the analytic signal and wavelet method gave the best results overall but each of the methods had their own strengths and weaknesses and the best method to use was very data dependent. A general observation for all the automatic pickers is that they should not be run blindly. The analyst should carefully choose their parameters and analyze the results. The process of iteratively changing parameters and visual review of the results was essential in selecting the best parameters.

The analytic signal method was the fastest and simplest method. It worked well on a range of target sizes and densities. It was able to counteract some of the over picking problems due to data quality issues by additional grid filtering passes. Its main weakness was picking targets in areas with a variety of background geology or noise levels. Because a hard threshold is set, it can either be tuned to select the weak anomalies and pick numerous false alarms or set higher with the consequence of missing the weak anomalies but minimizing false alarms.

The wavelet method worked well on a range of target sizes and densities. It performed better than the other methods at picking targets that were clustered. It was fairly quick to run on total coverage surveys but much less efficient when run on transect data. Its main weaknesses were the complexity of the parameters and over picking in areas with geology, noise or poor data quality. The default set of parameters provided an adequate starting point and improvements were easily gained by adjusting the amplitude thresholds. But further improvements in the

detection rate required expertise or at least advanced familiarity with the AWD and the sensitivity of its parameters.

The clustering method performed well detecting isolated targets with similar sizes. When a range of target sizes were encountered and the parameters were set to detect the large anomalies any small anomaly close to the large anomaly tended to be missed. The clustering algorithm also had problems picking anomalies in areas with high geology and noise. Overall, it ran slower than the analytic signal on total survey areas but was more efficient on transect data because it works on the profile data and not a grid. It also took longer to setup because there were multiple parameters that need to be tuned.

The matched filter method performed the worst. It was hindered by its requirement to have total data coverage within the filter box. This would increase geophysical data collection costs because additional data would need to be collected around the perimeter of the survey area. It ran the slowest of the automatic methods but the limited number of parameters helped reduce its complexity. It had difficulty with overlapping targets, range of target sizes and poor data quality. The one area it excelled at was picking targets in areas with a variety of geology.

Implementation of the automatic picking methods used in this demonstration should considerably reduce the time and thus cost required to pick anomalies when compared to the manual method. The amount of cost savings will depend on the data. In areas with isolated anomalies and low background noise or geology the cost savings will be maximized because the automatic pickers are able to detect over 90% of the anomalies in a fraction of the time compared to the manual method. As the geologic noise increases or data quality decreases the cost savings will diminish but still should be significant. Even the toughest data sets in this demonstration will produce cost savings. For example, the airborne WAA data set at Pueblo contained an abundance of geology that resulted in Pd's of around 0.5 for the automatic pickers. The analytic signal required less than an hour to setup and run while the manual method took 9 hours. Even if it takes an additional 5 hours of manual picking to select the other half of the targets, the time savings will be three hours or 33%.

In conclusion, the best use of the automatic target pickers may be to quickly and consistently select all the strong isolated targets by setting the picking parameters to minimize false alarms. The remaining anomalies can then be selected using the manual method. This combines the strengths of each method and will result in a better product than using only the automatic methods and cost savings compared to using only the manual method.

5. Cost Assessment

5.1 Cost Reporting

This demonstration focuses on the detection of anomalies observed in magnetic data. As such, it encompasses only a small subset of costs that are typically associated with full-scale demonstrations. The relevant cost categories and actual costs for this demonstration are shown in Table 19. Time spent during data analysis was logged as described in Section 4.2.

Table 19. Cost categories and details

Cost Category	Details	Sub Category	Time (hours)	Costs* ($)
Data Analysis	Setup parameters for identifying anomalies	Analytic signal	1.5	150
		Wavelet	8.2	820
		Clustering	23.7	2370
		Matched filter**	21.9	2190
		Manual	0	0
Data Analysis	Running automatic target pickers	Analytic signal	1.7	170
		Wavelet	5.4	540
		Clustering	3.8	380
		Matched filter**	6.2	620
		Manual	43	4300
Reporting	Technical Report	--	320	32,000
		TOTAL		43,540

*assumes an fully-loaded labor rate of $100 per hour
** Matched filter hours only includes 6 of the 7 data sets because it could not be run on the WAA Pueblo transect data

5.2 Cost Analysis

The baseline alternative to the automatic target pickers is manual target selection. Implementing the automatic picking methods used in this demonstration should considerably reduce the time and thus cost required to pick anomalies when compared to the manual method. The amount of cost savings will depend on the data which will determine the most efficient automatic method. In areas with isolated anomalies and low background noise or geology the cost savings will be maximized because the automatic pickers are able to detect over 90% of the anomalies in a fraction of the time compared to the manual method. As the geologic noise increases or data quality decreases the cost savings will diminish but still should be significant. Even the toughest data sets in this demonstration will produce cost savings. For example, the airborne WAA data set at Pueblo contained an abundance of geology that resulted in Pd's of around 0.5 for the automatic pickers. The analytic signal required less than an hour to setup and run while the

manual method took 9 hours. Even if it takes an additional 5 hours of manual picking to select the other half of the targets, the time savings will be three hours or 33%.

The parameter setup time represented a large portion of the processing time for the relatively small data sets used in this demonstration. The ground based surveys ranged from 0.3 to 10 acres in size. On the other hand, large scale cleanup efforts are typically hundreds of acres so the setup costs will be a trivial portion of the total costs. Assuming the geology, data quality and data objectives for the survey area are relatively constant; the automatic target picking parameters should need minimal changes. If we compare only the costs to actually run the automatic methods to the manual method, we find the cost of the automatic pickers is roughly 10% of the cost of the manual method. If we factor in a very conservative 40% additional time to fill in missing anomalies using the manual method, there is still a cost savings of 50% achieved by using the automatic picking methods.

6. Implementation Issues

6.1 Environmental Checklist

Not applicable to this demonstration.

6.2 Other Regulatory Issues

Not applicable to this demonstration.

6.3 End-User Issues

The end-users of this data analysis technology include private contractors that conduct geophysical investigations in support of UXO clean up programs and governmental employees that provide technical oversight. This demonstration will introduce the stakeholders and end-users to the applicability of different automatic target pickers to their data. This basic information will help to improve the results of future geophysical investigations conducted by others. The market for this type of guidance document includes all practicing geophysical service firms currently working in the UXO industry. The target picking algorithms would ideally be transitioned to the user community through Geosoft as part of their proposed "UXO System".

7. References

Senate Report 106-50, National Defense Authorization Act for Fiscal Year 2000, May 17, 1999. Research and Development to Support UXO Clearance, Active Range UXO Clearance, and Explosive Ordnance Disposal, pages 291–293.

Department of Defense, Unexploded Ordnance Response: Technology and Cost, Report to Congress, March 2001

Billings, S. D. and Herrmann, F., 2003, Automatic detection of position and depth of potential UXO using a continuous wavelet transform: SPIE Conference on Detection and Remediation Technologies for Mines and Minelike Targets, Orlando, April 21-25.

Moreau, F., Gilbert, D., Holschneider, M. and Saracco, G., 1999, Identication of sources of potential fields with the continuous wavelet transform: Basic theory, *J. Geophys. Res*., 104 (B3), p.5003 –5013.

Hornby, P., Boschetti, F. and Horowitz, F. G., 1999, Analysis of potential field data in the wavelet domain, *Geophys. J. Int*., 137, pp. 175 –196.

Blackhawk Geometrics, Inc., 2000, Model-based data fusion and discrimination of UXO in magnetometry and EM surveys, SERDP CU-1092 Final Report.

Bell, T., Jones, R., Soukup, J., and Puc, B., 2001, "Matched Filter Processor for Detection and Discrimination of Unexploded Ordnance", ESTCP Report for Project 199918, AETC Report VA-095-050-TR-01, November.

AETC Incorporated, 2002, "Matched Filter Processor for Detection and Discrimination of Unexploded Ordnance: OASIS Montaj™ Integration", ESTCP Final Report for Project 199918, AETC Report VA-3499-009-02-TR, November.

Barrow, B, 1998, "Report on MTADS Automatic Processor", AETC Report VA-074-075-TR, January 12.

Blakely, Richard J.and Simpson, Robert W., 1986,"Approximating edges of source bodies from magnetic or gravity anomalies", Geophysics, v.51, p.1494-1498.

Briggs, I, 1974,"Machine contouring using Minimum Curvature" Geophysics, v.39, No. 1, p.39-48.

Swain, C., 1976," A Fortran IV Program for interpolating irregularly spaced data using the difference equations for minimum curvature", Computer & Geosciences, v. 1, p. 231-240.

8. Points of Contact

ESTCP

Jeff Marqusee	ESTCP 901 North Stuart Street Suite 303 Arlington, VA 22203	Tel: 703-696-2120 Fax: 703-696-2114 Jeffrey.Marqusee@osd.mil	ESTCP Director
Anne Andrews	ESTCP 901 North Stuart Street Suite 303 Arlington, VA 22203	Tel: 703-696-3826 Fax: 703-696-2114 Anne.Andrews@osd.mil	Program Manager UXO Thrust Area

SAIC

Tom Furuya	SAIC 120 Quade Drive Cary, NC 27513	Tel: 919-653-0215 Fax: 919-653-0219 tom.n.furuya@saic.com	PI
Jim Kingdon	SAIC 1225 Jefferson Davis Highway Suite 800 Arlington, VA 22202	Tel: 703-413-0500 Fax: 703-413-0512 james.b.kingdon@saic.com	Data Analyst

Sky Research

Stephen Billings	Sky Research 445 Dead Indian Memorial Road Ashland, OR 97520	Tel: 604-822-1819 Fax: 604-822-6088 stephen.billings@skyresearch.com	Co-PI